8-2015

A Study Model Predictive Control for Spark Ignition Engine Management and Testing

Qilun Zhu
Clemson University

A STUDY OF MODEL PREDICTIVE CONTROL FOR SPARK IGNITION ENGINE MANAGEMENT AND TESTING

A Dissertation
Presented to
the Graduate School of
Clemson University

In Partial Fulfillment
of the Requirements for the Degree
Doctor of Philosophy
Automotive Engineering.

---

by
Qilun Zhu
August 2015

Accepted by:
Dr. Robert Prucka, Committee Chair
Dr. Hussein Dourra
Dr. Zoran Filipi
Dr. Simona Onori

ABSTRACT

Pressure to improve spark-ignition (SI) engine fuel economy has driven the development and integration of many control actuators, creating complex control systems. Integration of a high number of control actuators into traditional map based controllers creates tremendous challenges since each actuator exponentially increases calibration time and investment. Model Predictive Control (MPC) strategies have the potential to better manage this high complexity since they provide near-optimal control actions based on system models. This research work focuses on investigating some practical issues of applying MPC with SI engine control and testing.

Starting from one dimensional combustion phasing control using spark timing (SPKT), this dissertation discusses challenges of computing the optimal control actions with complex engine models. A nonlinear optimization is formulated to compute the desired spark timing in real time, while considering knock and combustion variation constraints. Three numerical approaches are proposed to directly utilize complex high-fidelity combustion models to find the optimal SPKT. A model based combustion phasing estimator that considers the influence of cycle-by-cycle combustion variations is also integrated into the control system, making feedback and adaption functions possible.

An MPC based engine management system with a higher number of control dimensions is also investigated. The control objective is manipulating throttle, external EGR valve and SPKT to provide demanded torque (IMEP) output with minimum fuel consumption. A cascaded control structure is introduced to simplify the formulation and

solution of the MPC problem that solves for desired control actions. Sequential quadratic programming (SQP) MPC is applied to solve the nonlinear optimization problem in real time. A real-time linearization technique is used to formulate the sub-QP problems with the complex high dimensional engine system. Techniques to simplify the formulation of SQP and improve its convergence performance are also discussed in the context of tracking MPC.

Strategies to accelerate online quadratic programming (QP) are explored. It is proposed to use pattern recognition techniques to "warm-start" active set QP algorithms for general linear MPC applications. The proposed linear time varying (LTV) MPC is used in Engine-in-Loop (EIL) testing to mimic the pedal actuations of human drivers who foresee the incoming traffic conditions. For SQP applications, the MPC is initialized with optimal control actions predicted by an ANN. Both proposed MPC methods significantly reduce execution time with minimal additional memory requirement.

ACKNOWLEDGMENTS

This dissertation would not be possible without the contribution and support from many people. Their efforts cannot be completely credited for with one page of document. First, I would like to acknowledge Professor Robert Prucka, Professor Simona Onori and Professor Zoran Filipi of the Clemson University. Their guidance and support have transformed this research work into a foundation of career, for which I am more than grateful. I also want to thank my fellow colleagues of the powertrain team for their support of my lab work and countless brainstorming moments.

This research work is funded by Fiat Chrysler Automobiles. I would like to express my special thanks to Dr. Hussein Dourra, Michael Prucka and their colleagues for their technical support and guidance. More importantly, I am grateful for their effort of establishing such an efficient and encouraging academic – industry environment.

It has been said that all PhD graduate students have a motivating and understanding family behind them. And I am very gratefully for mine. For Lujia, the love of my life, I am grateful for the 31 dinners and 26 dish washings during the preparation of this dissertation. And I thank my parents for their unconditional support for my entire time at the states. Home is 7500 miles away, yet it never felt this close.

TABLE OF CONTENTS

Page

Table of Contents (Continued) Page

Table of Contents (Continued) Page

LIST OF TABLES

LIST OF FIGURES

CHAPTER ONE

INTRODUCTION

1.1 Motivation

1.1.1 Landscape of Internal Combustion Engine Control

More than 95% of production vehicles are and will be powered by IC engines, with the consideration of Hybrid Electric Vehicles (HEVs) and Alternative Fuel Vehicles (AFVs), for the foreseeable future (*International Energy Agency*). The reasons for the dominating role of IC engines include low cost (around $25/kW), high power density (> 60 kW/L) and high overall energy conversion efficiency (compare to electricity generation from fossil fuel). The efficiency of IC engines is still improving with new technologies like Variable Valve Timing (VVT), Direct Injection (DI), Homogeneous Charge Compression Ignition (HCCI) (*Stanglmaier et al. 1999*), downsizing and turbocharging (*Yi et al. 2009*) and external Exhaust Gas Recirculation (EGR) (*Pfeifer et al. 2003*). In addition to the improvement of IC engine design, other renewable fuel sources have been explored to replace gasoline and diesel. Some OEMs have been developing IC engines that can automatically adapt to multiple types of fuel (*Nakajima et al. 2007*). All these technologies increase the degrees of freedom, and therefore significantly complicate the design and calibration of the engine control algorithms. It is realized that traditional map and Single Input Single Output (SISO) feedback based engine control structures can no longer efficiently provide good enough performance

because of the exponentially increased calibration time and cost. In response to this challenging situation, OEMs are forced to transfer effort from calibration of simple control algorithms to execution of complex model-based feedback control algorithms. Recently, Model Predictive Control (MPC) has drawn strong attention in the IC engine control field for its constraints handling capability, superior transient performance and low calibration effort.

1.1.2 Advantages of Model Predictive IC Engine Control

The term Model Predictive Control (MPC) refers to a range of control methods that explicitly use mathematical models of the controlled systems to predict future response. Control laws are generated to optimize the tracking performance, control effort and other interested factors for the future horizon with respect to actuators and system constraints.

The most important advantage of MPC engine control is that it can save significant calibration and tuning resources compared to traditional map based engine controllers, particularly for transient operation conditions. Any new actuator added to the engine could easily increase the map calibration time of traditional engine controllers by an order of magnitude. In the case of MPC, only minor updates of the objective function and constraints are needed along with the new system model that has been integrated with the new actuator dynamics. Although it is not realistic to construct a system model capable of perfectly describing behavior of an IC engine, MPC is able to keep the model prediction error from growing with feedback of system states at each step. Therefore, it can tolerate a certain amount of modeling error. Tracking performance during transient

state scenarios is one of the many reasons for considering MPC in the first place. Provided with future references, the MPCs can optimize control sequence for the entire prediction horizon instead of only responding to the current and prior tracking error, which is the concept of traditional feedback control. Therefore, it can compensate for most of system delays and overshoots, making it desirable to control systems with high order and non-minimum phase dynamics. During the optimization process, constraints can be imposed to the control actions and system states. This grants MPCs the ability to compensate for actuator saturations ahead of time. This is a beneficial factor in engine control applications, where control actions are constantly restricted with mechanical limitations and complex combustion phenomena.

1.1.3 Challenges of Applying MPC to IC Engine Control

Although MPC has great potential for modern IC engine control, its computational complexity is still a barrier keeping it from being accepted by the automotive industry. In particular, the additional cost of faster ECUs with large memory is the most challenging one. The MPC based engine controller has to be comprehensively superior to the traditional map based engine controllers in order to justify the extra cost. After implementing MPC into the ECU, there will not be many computation and memory resources left for other control tasks. Therefore, the MPC has to work in all engine operation conditions including idling, tipping-in, coasting and many other transient and steady state scenarios. Furthermore, this situation requires the MPC to handle comprehensive control objectives, including fuel economy, torque delivery, emissions and drivability. These demands lead to complicated optimization algorithms with

nonlinear system models. Few articles about MPC engine control focus on comprehensive control objectives over a wide engine operation range. *Vermillion et al. (2010)* proposed a MPC engine control strategy considering fuel economy, emission and drivability in the objective function. The control scheme was evaluated under comprehensive operation conditions with a driver-in-the-loop simulation. Unfortunately, the MPC strategy was not implemented with prototype engine controllers due to its complex optimization algorithm.

The prediction model of the controlled system plays an important role during the design and execution of the MPC algorithm. Most control applications have nonlinearities in the system models. The original Linear Time Invariant (LTI) model based MPC has certain tolerance for model nonlinearities and inaccuracy due to the states feedback. Therefore, they are the most commonly used MPC strategies for IC engine control applications (e.g. *Li et al. 2010*). For systems with high nonlinearities, the approximated linearized model diverges quickly from the original nonlinear dynamics when the optimal control actions strays away from the nominal point, reducing the optimality and feasibility of the calculated control actions. There were two general ways to treat systems with high nonlinearities. One group focuses on directly solving nonlinear programming with improved versions of Nonlinear Programming (NLP) algorithms (*Vermillion et al. 2010, Lee et al. 2011, Murayama et al. 2009* and *Zhou et al. 2001*). However, most of these algorithms take too many iterations to find the optimal solutions, making them not realistic for real time implementation. The other set of literature tries to modify the parameters of the linear MPC formulation so that some nonlinearities of the

original models could be captured. These MPCs are referred to as the Linear Time Varying (LTV) or Linear Parameter Varying (LPV) MPCs, with some literature discussing their applications with engine control (e.g. *Sharma et al. 2010*). These "suboptimal" approaches are proven to be more feasible with current engine ECUs. However, they require real time linearization of the system dynamics. For IC engine applications, the control oriented models with decent accuracy are extremely complex. The modeling of some engine dynamics, like the turbulent combustion related systems, are very ad hoc for specific engine designs. Linearizing these models costs a significant amount of execution time in addition to the solving of MPCs.

MPC controllers are essentially discrete event controllers with units as "steps". The most instinctive way to formulate a MPC engine controller is letting each step represent an engine cycle. This was the case for MPC applications with HCCI combustion phasing control (*Widd et al. 2013* and *Bengtsson et al. 2006*), in which cyclic dynamics have to be considered. However, the computational time is too short to complete the online optimization during engine operation, especially for high speed operation. Therefore, most MPC engine control researchers discretize their system model by fixed sampling time, which is commonly from 10 to 50 Hz. This large time scale arouses many application issues with engine systems. The most obvious one is waste of actuation bandwidth. A very representative example is Spark Timing (SPKT) control, which can be updated for every engine cycle. Therefore, it has the capability to stabilize cyclic dynamics providing better Covariance (COV) of Indicated Mean Effective Pressure (IMEP) performance and avoidance of knock and misfire.

Even with complicated nonlinear prediction models, it is still not possible to capture all the detailed engine dynamics with explicit mathematical equations. The traditional map based controller has the capability to fine tune the control actions experimentally to account for these detailed factors(e.g. different pressure wave tuning and coolant temperature for each cylinder). It is possible, yet very difficult, to consider these factors in the MPC algorithms. *Li et al. (2010)* demonstrated the possibility of using MPC to control Air-to-Fuel Ratio (AFR) of a SI multiple-cylinder engine with focus on different delay of individual cylinders. The engine model used in this application has a high number of dimensions to account for discrepancy of different cylinder dynamics.

Some of the MPC application issues discussed above were addressed by previous research work. A detailed literature review is presented later in this dissertation. It is an important finding of this research that most MPC application issues can be solved by properly designed control hierarchy in the first place. The advantage of this methodology is that it reduces the model complexity for the upper level controllers by transferring the tasks of managing the high frequency dynamics to the lower level controllers. As a result of this frequency separation, the upper level controller has more execution time to run more advanced control algorithms generating reference/target signals for the faster controllers to track with the lower level control loops. However, the interface between the two layers should be explicitly addressed. Ample amount of MPC researchers have exploited the benefits from cascaded control strategies. *Zhu et al. (2014)* designed an active suspension control system with a low speed MPC vehicle body motion control and a high speed LQG wheel motion control, utilizing the time scale separation between these

two dynamics. *Raffo et al.(2009)* presented a multi-layer MPC based control structure of autonomous vehicles. The control levels (from high to low) included route planning, vehicle guidance, dynamics and subunits control. The higher level controller had slower update frequency and more complicated control algorithms compared to lower level controllers. There are only two research publications focused on MPC engine control that discuss control cascade organization for IC engine applications, which is far from sufficient. The control structure proposed by *Vermillion et al. (2010)* included a MPC upper level controller manipulating AFR, Air Mass Flow (AMF), VVT and SPKT, while two lower level controllers tracked the AFR and AMF reference generated by the MPC manipulating fuel Injection Pulse Width (IPW) and throttle respectively. *Huang et al. (2013)* applied MPC to control diesel engines with external EGR and a Variable Geometry Turbocharger (VGT). By applying lower level controllers for the EGR valve and VGT position with a partial inversion technique, a significant amount of nonlinearities were removed from the MPC loop. Experimental results indicated considerable improvement of MPC calculation efficiency.

1.1.4 Research Scope

The previous section summarized the challenges of applying MPC to IC engine control application from previous literature. This research work focuses on investigating three fundamental issues of applying MPC with SI engine control: 1) a new SI engine control framework that can maximize the MPC's potential to optimize engine performance and exploit the control bandwidth of actuators; 2) optimization algorithms that are able to utilize complex engine models to compute optimal control actions; 3)

strategies to reduce the computation, calibration and memory demand of the MPC controllers.

1.2 Dissertation Outline

Chapter two of this dissertation introduces the engine that is used for this research work. Experimental setup is also discussed in this chapter including data acquisition and the prototype engine control system. Starting from the simple one dimensional combustion phasing control with SPKT in chapter 3, challenges from the complexity of IC engine modeling are discussed. The control objective is to find the SPKT of next engine cycle that can generate close to reference combustion phasing without inducing knock and excessive cycle-by-cycle combustion variation. The models to predict combustion phasing, knock and combustion stability are semi-physical in nature. After the analysis of these models, Section 3.2 introduces three optimization approaches that are able to directly use these complex models to find the optimal SPKT for the next engine cycle with several iterations. The final section of chapter 3 introduces a model based combustion phasing estimation technique to improve the quality of cylinder pressure sensor measurement, making the feedback and adaption functions possible for the proposed combustion phasing controller.

Chapter four expands the number of control dimension of the MPC based engine management system by including the air-path dynamics of a SI engine with external EGR. The control objective is to provide demanded torque output while minimizing fuel consumption. The control actions are constrained by knock, combustion stability,

actuator operation range and air-path dynamics. Section 4.2 discussed the cascaded control structure, which is identified as the first issue of applying MPC to engine control. Some models used in the one-dimensional combustion phasing control are transferred into the model predictive IMEP control framework. Section 4.3 investigates MPC strategies that are able to find the optimal control actions with the complex high dimensional system.

Chapter five focuses on the third MPC application issue with engine control by discussing the strategies to solve the optimization problems in real time. Specifically, methods to accelerate online quadratic programming (QP) are explored, since QP is the most common optimization problem faced by MPC applications. Chapter six introduces an Engine-in-Loop (EIL) testing method that can evaluate engine performance with realistic driver actuation and powertrain behavior. The proposed MPC strategy is implemented as the "driver" of the EIL test. The MPC is able to mimic the actual human drivers who foresees the incoming speed profile. Finally, chapter seven summarizes the contributions of the dissertation and lists possible future extension of this research work.

1.3 Literature Review of MPC Application in IC Engine Control

Developed in late 1970s, MPC was firstly applied to chemical plants for slow processes control (*Richalet et al. 1976* and *Richalet et al. 1978*). As microprocessors became faster, MPCs were widely applied to robots, autonomous vehicles and other systems with fast dynamics (e.g.*Raffo et al. 2009*). The earliest attempt of applying MPC to engine control can be traced back to the early 1990s (*Garcia et al. 1989*). However, only simulation results were presented in most research works by then since the engine ECUs at that time were not fast enough to meet with the computational requirements of MPCs. The processor situation of automotive industry was significantly improved since 2000s. Numerous attempts were made to exploit possibilities of using MPCs to solve control challenges facing various vehicle systems, including IC engine (*Hrovat et al. 2012*) and other powertrain and chassis control systems, like HEV energy management (*Yan et al. 2012*) and active suspension (*Zhu et al. 2014*).

Idle Speed Control (ISC) is the most fundamental engine control problem (*Hrovat et al. 1997*). OEMs pay considerable amount of attention to ISC since vehicles consume significant amount of time and fuel on idle operation. In order to reduce Friction Mean Effective Pressure (FMEP) and fuel consumption, the idle speed should be controlled as low as possible without losing stability and stall the engine. Strict constraints are imposed to actuators for ISC to avoid nonlinear dynamics and combustion instability. *Sharma et al. (2010)* applied MPC to regulate idle speed of a hydrogen IC engine with throttle, Spark Timing (SPKT) and Air-to-Fuel Ratio (AFR). The nonlinear effect was considered

through the approximation of Linear Time Varying (LTV) state space model, which requires update for every step along the prediction horizon. Stability of this approach was proved using Lyapunov method. Simulation results showed remarkable performance of speed reference tracking. *Di Cairano et al. (2012)* and *Hrovat et al. (1996)* focused on ISC of conventional gasoline SI engine with by-pass valve and SPKT. The prediction model used in MPC is a Linear Time Invariant (LTI) state space model. Piecewise Affine (PWA) equivalence of the original MPC was applied in the experiment. Both simulation and test results indicated superior disturbance rejection performance with less actuation effort compared to original Proportional Derivative (PD) and Proportional Integral (PI) ISC controller. It was also concluded by these research works that preview of known torque disturbance, e.g. power steering and air conditioner could greatly improve the MPC based ISC performance. With these preview information, it could be possible to maintain engine speed without altering SPKT.

AFR control of SI engine is another basic yet challenging control problem that needs to be considered for all engine operation conditions. The dead time delay between actuators and lambda sensor feedback leads to difficulties of modeling and design of traditional feedback controller. Another challenge of AFR control is the coordination of multiple actuators (usually throttle, injectors and VVT) with different bandwidth, which causes large amount of time on calibration of maps and tuning of SISO feedback controllers (*Cristofaro et al. 2003*). *Li et al. (2010)* discussed possibility of using LTI MPC for controlling AFR of multi-cylinder SI engine during steady state. The focus of this research work was on balancing different dynamics of each cylinder caused by the

location of lambda sensor. *Zhai et al. (2011)* and *Sardarmehni et al. (2013)* proposed to model the AFR dynamics using ANN. Secant Method (*Rao 1996*) was applied to find the optimal solution in (*Zhai et al. 2011*). Experiment results are available. *Sardarmehni et al. (2013)* recommended using Multi-Layer Perceptron Neural Network (MLPN) directly to calculate optimal solution instead of optimizing objective function online. Only simulation results were available for this research work.

Torque delivery is the main function of IC engine. In spite of the difficulties associating coordination of various actuators, feedback control on torque output is challenging because real time measurement of engine torque output is difficult and expensive. *Ali et al.(2006)* demonstrated potential of using LTI MPC to track torque reference with simulation results. *Lee et al. (2011)* applied Nonlinear MPC (NMPC) on SI engine with VVT to track torque reference and reduce NO_x emission. Simulation results were presented. Both of these research works did not include further discussion of torque measurement. Using an empirical model to map engine torque to MAP (or AMF) and SPKT can generate reasonably good estimation of torque output (*Livshiz et al. 2004*), until recent powertrain technologies, like torque vectoring (*Thang Truong et al. 2013*) and transmission with dog clutch (*Gaetner et al. 2013*), rise the demand. *Grünbacher et al. (2005)* suggested using Extended Kalman Filter (EKF) to estimate diesel engine torque with measurement of engine speed, injection fuel rate, injection timing and air/fuel ratio. Experiment results are promising. Market available cylinder pressure sensor for SI engines makes direct measurement of IMEP possible. Using IMEP as feedback can significantly improve the torque tracking performance of MPC engine control.

Constructing explicit Mean Value Model (MVM) of engines with VVT actuation is a very challenging topic. The existing publications were often focused on dual equal variable cam timing technology with highly nonlinear coupled dynamics model (*Stefanopoulou et al. 1998*). These factors make the MPC design even more difficult. The independent VVT model of (*Vermillion et al. 2010*) is from Toyota, and classified to be presented in the paper. Nonlinear programing with 1 dimensional search was used to find optimal solution. *Colin et al. (2005)* and *Lee et al. (2011)* used ANN model to capture effects of VVT. Nonlinear programming with terminal penalty was applied in by *Lee et al. (2011). Colin et al.(2007)* formulated a QP scheme by linearizing the ANN model at specific operation point. Experiment results were provided in this paper. More recently, *Feru et al. (2012)* suggested using MPC with Lyapunov based constraint to control engine with dual equal variable cam timing. The VVT model was still highly nonlinear, though it is greatly simplified from (*Stefanopoulou et al. 1998*). The LP optimization was formulated using $\infty - \infty$ norm technique to improve robustness and reduce computation effort. Flexible Control Lyapunov function (CLF) constraint was added to guarantee system stability. Simulation results shows better settling time along with other performances compared to traditional controllers.

Down size turbo charged engine has been proven to be more fuel economic compared to natural aspirated engine with similar power. Considering its potential in MPG boosting, many research works demonstrated that turbo charged engine control could be a great application for MPC for its unique non-minimum phase, nonlinear and unstable dynamics (*Karnik et al 2012*). There are two reasons causing the difficulties of

controlling non-minimum phase systems with conventional linear or nonlinear feedback controller. The first reason is that there are positive zeroes of non-minimum phase dynamics, leading to unstable controllers based on the inversion of the system dynamics. The second reason of the difficulty is high frequency manipulation of actuators will lead to negative response of the system. In comparison to the extensive discussion of non-minimum phase dynamics control found in literatures about traditional feedback control of turbocharged engine, most research works of MPC based controller did not specifically address this issue since the negative response was predicted by the system model and compensated ahead of time. Therefore, the MPC controller could significantly reduce turbo lag during transient scenarios. For SI turbo charged engine control, *Colin et al. (2007)* and *Santillo et al. (2013)* suggested using LTI MPC based on QP with linearized model at specific operation point. There were more research papers focused on MPC based turbo charged CI engine control with external EGR device, since it is a very good demonstration of multi-actuators coordination ability and reference tracking performance of MPC. LTI MPC with QP is applied in the following articles. *Ortner et al. (2006)*, *Langthaler et al. (2007)* and *Ferreau et al. (2007)* simplified the MPC execution with Piecewise Affine approximation, making it possible to run on prototype engine controllers. Experimental results were available. *Maruyama et al. (2012)* explicitly addressed issues with dead time modeling and steady state offset compensation. However, the necessity of the offset compensation was questionable since the references of most real application are smoothed continuous signal instead of a step function.

There are some other published applications of MPC in engine control field. *Giorgetti et al.(2006)* proposed using MPC to control Direct Injection Stratified Charge (DISC) engines. The switch dynamics of two different operation modes required Mixed Integer Quadratic Programming (MIQP) to calculate optimal solution. *Murayama et al. (2009)* discussed application of NMPC to control engine speed with variable valve lift. Controlling engine speed during coast down scenario with LTI MPC was the focus of *Di Cairano et al. (2012)*. Application of MPC in HCCI combustion phasing control was discussed by *Widd et al. (2013)* and *Bengtsson et al. (2006)*. *Caruntu et al. (2011)* and *Balau et al. (2011)* suggested driveline oscillation damping control with 1 step horizon $\infty - \infty$ norm MPC. Flexible CLF constraint was imposed on the LP formulation. *Caruntu et al. (2011)* approximate the control law with PWA technique, and conducted test bench validation.

CHAPTER TWO

TEST ENGINE AND EXPERIMENTAL SETUP

2.1 Test Engine Description

The test engine is a naturally-aspirated 3.6 L port fuel injected V-6 with two intake valves and two exhaust valves per cylinder and a pent-roof shaped combustion chamber (see Figure 2.1). The engine is equipped with oil-driven dual-independent valve phasing on both banks. A special flywheel (see Figure 4) was designed at Clemson University to connect the engine to the dynamometer driveshaft as to hold the crank angle encoder disk (AVL 365X). A summary of basic engine geometry is given in Table 2.1.

Table 2.1: Engine parameters

Fuel	Gasoline (87 Pump Octane)
Max Engine Speed	6400 RPM
Bore	96 mm
Stroke	83 mm
Compression Ratio	10.2
Connecting Rod Length	156.5 mm
Intake Valve Diameter	39 mm
Exhaust Valve Diameter	30 mm

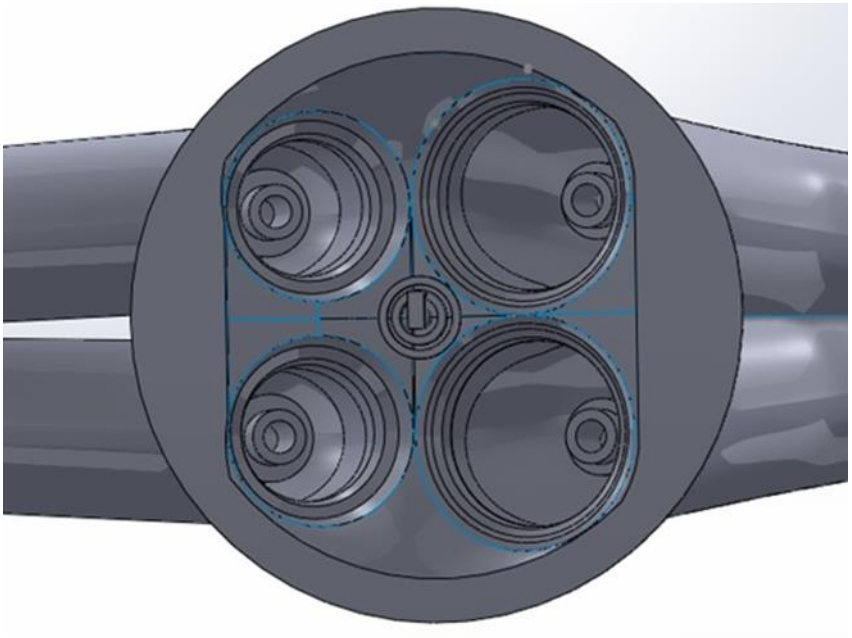

Figure 2.1: Approximate CAD drawing of the combustion chamber

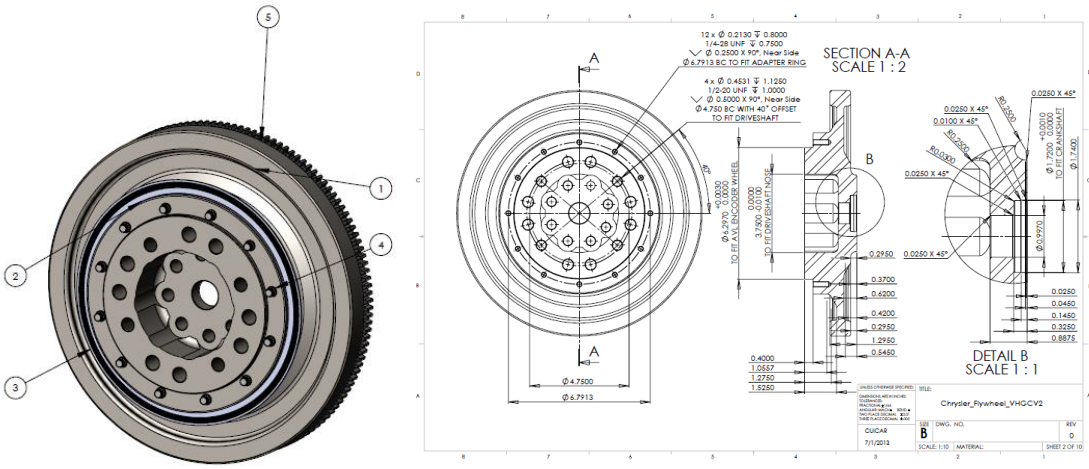

Figure 2.2: A custom flywheel was designed and built to connect the engine to the dynamometer driveshaft a hold the crank encoder disk.

2.2 Data Acquisition Setup

Combustion and gas exchange processes are the primary focus of experimental data collection to aid control model/algorithm development. Combustion analysis will be performed using a 32 channel AVL 671 crank-angle resolved data acquisition system and AVL GH12D piezoelectric cylinder pressure sensors. The sensors were located in the cylinder head to maximize accuracy according to *Patterson et al. (2009)*, and were equipped with flame guards to minimize thermal shock errors. The system is capable of sampling data in 0.25 crank angle degree intervals to properly capture all relevant combustion characteristics. Piezoresistive Kulite sensors are used for both intake and exhaust pressure measurements. The exhaust sensors are cooled using a Miller TIG torch cooling system to minimize signal drift when exposed to high temperatures. AVL Indicom® software is used to monitor measured sensor signals from the data acquisition system cycle-by-cycle and record measured data. AVL Concerto® software is used for combustion data analysis to provide in-cylinder temperatures, rate of heat release and other parameters. Crank angle resolved measurements of intake and exhaust port pressures are used with cylinder pressure for gas exchange analysis. A one-dimensional gas dynamic model of the combustion chamber, intake, and exhaust ports was built using AVL BOOST®. This model was then imported into AVL Gas Exchange and Combustion Analysis® (GCA) software for mass flow calculations across the intake and exhaust valves. The GCA software uses the experimentally measured intake and exhaust

pressures as boundary conditions and calculates many difficult to measure gas exchange characteristics, such as internal residual gas fraction, and total in-cylinder mass.

2.3 Engine Control

INTECRIO® system is used to override the stock GPEC2 control system on an as-needed. The system allows for adjustment of engine actuators and is programmed using MATLAB/Simulink®. The prototype controller is ETAS ES910 system. The cylinder pressure measurement was sent to a Cylinder Pressure Development Controller (CPDC) unit to compute CA50 and IMEP (*Schten et al. 2007*). The communication between the CPDC and ES910 was established via a CAN communications link.

CHAPTER THREE

ONE DIMENSIONAL COMBUSTION PHASING OPTIMAL CONTROL

The combustion phasing of Spark Ignition (SI) engines is traditionally regulated with map-based spark timing (SPKT) control. The calibration of these maps consumes tremendous amount of time and resources making it less favorable for SI engines with a high number of control actuators. This chapter of the dissertation introduces a model based optimal combustion phasing control strategy for SI engines. The entire combustion phasing optimal control system is described in Figure 3.1.

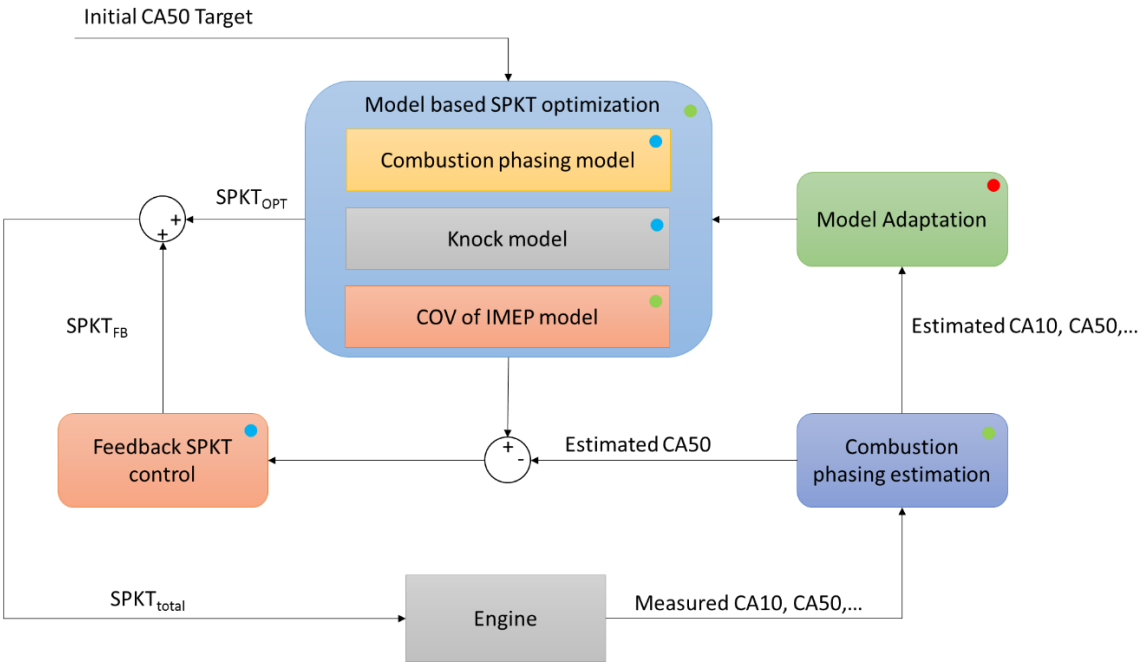

Figure 3.1: Block diagram of the entire model based combustion phasing control system. Green dot indicates the models that will be extensively discussed in this chapter. Models with blue dot will be briefly introduced. Model adaptation with red dot is not discussed in this document.

The first section of this chapter introduces a high-fidelity combustion stability model. Since the combustion stability model requires the information of the combustion

states at TDC, it must be accompanied with a crank resolution combustion model. Section 3.2 discussed approaches to find the optimal SPKT that can generate close to target combustion phasing without violating the knock and COV of IMEP constraints. Since these high-fidelity combustion models are very complex in nature, the conventional gradient based search methods cannot be implemented with this application. This research analyzes the characteristics of the SPKT optimization problem and provides three efficient optimization strategies, which are validated with extensive dynamometer and proving ground tests. The final section introduces a model based estimation technique that is able to significantly improve the combustion phasing feedback signal quality. This combustion phasing estimator makes it possible for feedback SPKT control and combustion models adaptation.

3.1 Covariance of IMEP Model

Engine cycle-by-cycle combustion variation is a potential source of emissions and drivability issues in automobiles, and has become an important concern for engine control engineers. This research proposes a control oriented approach for estimating the Covariance of Indicated Mean Effective Pressure (COV of IMEP). One fundamental cause of COV of IMEP is turbulent combustion variation, which is analyzed with flame regime analysis in this research. In-cylinder thermodynamics are then evaluated to reveal how the changes of heat release transform into the variation of cylinder pressure, producing COV of IMEP. A range of model input parameters are assessed to determine the set that produces the most accurate prediction of IMEP variation with minimal

computational requirements. An Artificial Neural Network is applied to capture the nonlinear coupled correlations between COV of IMEP and model inputs. The ANN is combined with a regression pretreatment to reduce network size and improve extrapolation stability. The single-layer three-neuron ANN that is computationally efficient achieved a 99% R^2 for COV of IMEP. Dynamometer tests shows that the model performs well outside the training region.

3.1.1 Introduction

Combustion variations in Internal Combustion (IC) engines induce mechanical design and control issues. These variations shift the combustion phasing and increase the chance of the engine running outside of the designated operation range. Covariance of Indicated Mean Effective Pressure (IMEP) is commonly used to indicate the level of combustion variation in the IC engine field. For spark-ignition (SI) engines, the risk of knock and misfire are critical issues related to combustion variation. Most knock control considers this effect and further retards the spark timing to reduce the chance of knock (*Bozza et al. 2014*) .This also results in lower thermal efficiency of the engine. A high-fidelity prediction of combustion variation can reduce the conservativeness of spark retard during knock limited operation. Unintentionally late combustion phasing can lead to reduction in torque output, risk of misfire and increased CO and HC emissions. Finally, IMEP variation leads to engine speed fluctuation and powertrain vibrations, worsening vehicle NVH (Noise, Vibration and Harshness) performance and causing engagement issues in modern transmissions with interlocking mechanisms.

The nature of turbulent combustion in IC engines means that COV of IMEP cannot be eliminated completely. Furthermore, it is inevitable for the engine to run at conditions with high combustion variations in most vehicle applications. For example, during gear shifts spark timing can be changed dramatically to help track the fast transitions of torque demand, often resulting in high COV of IMEP. Under these circumstances, the control engineers have to weigh between combustion variation and other performance demands (i.e. fast torque tracking). An accurate online estimation of COV of IMEP can be beneficial to this process. A calibrated map of COV of IMEP versus engine operating conditions can be an option for engines with few control actuators. As the number of control actuators is increased, physics based models of combustion variation becomes favorable due to their potential for reduced calibration effort.

Most previous research investigating the cause of IMEP variation is founded upon the theories of turbulent combustion stability. It can be summarized that the cyclic combustion variation is caused by charge composition variation (*Aleiferis et al. 2004*) and in cylinder flow variation (*Le Coz et al. 1992*) . Some of these researchers concluded that stochastic properties of the flame kernel development stage affect the rest of the combustion propagation significantly, so it should be the primary consideration for investigation of COV of IMEP (*Lee et al. 2001, Mantel 1992 and Galloni 2009*). The reasoning and logic of these approaches are without questions. However, most of these works explain the cause of COV of IMEP at a concept level without giving an accurate prediction model for COV of IMEP. This situation is a result of modeling COV of IMEP,

a stochastic value, with other stochastic variables (e.g. in-cylinder charge motion, fuel-air distribution, etc.). Available measurements are for experiments where the engine can be controlled to run at steady states for multiple cycles, which is not a common situation for actual driving scenarios.

Research has been published relating combustion variations to deterministic properties. High Speed Particle Image Velocimetry (HSPIV) was applied by *Long et al. (2008)* to capture real time turbulence levels in cylinder. It was concluded that high frequency turbulent motion contributed to the COV (Covariance) of IMEP. *Abdi Aghdam et al. (1989)* incorporated this concept to his quasi-dimensional combustion model by adding a cyclic random factor K to the calculation of turbulence intensity. The simulation results showed cylinder pressure variations close to experimental observation. Without further discussion that correlated the random factor K to measureable engine parameters, extending this concept to other engine platforms may be limited. Furthermore, relating the IMEP variation to only one contributing factor, turbulence intensity, is considered an over-simplification of the issue. *Galloni (2009)* proposed to estimate the COV of IMEP with laminar flame speed (S_L), turbulence intensity (u') and magnitude of the mean flow velocity in the spark region. These three variables were calculated at the spark timing. CFD methods were applied to estimate U making this method unlikely to be applied online for real-time applications.

Combustion regime diagrams are generally utilized to categorize flame propagation of premixed turbulent flames (*Abdel-Gayer et al.1989, Abraham et al. 1985, Peters 1986* and *Russ et al. 1999*). These diagrams show that different time scale

combinations of turbulent motion and flame propagation can significantly affect combustion stability. These diagrams are separated into several zones with different flame patterns. Zones with continuous laminar flame sheets tend to have stable combustion, while others indicates possible combustion instability (flame quench). *Russ et al. (1999)* related the COV of IMEP to the Leeds diagram inputs, u'/S_L and L/δ_L (turbulent integral length scale/laminar flame thickness). Results of this work indicated that COV of IMEP is high when the engine is operated close to the "flame quench" zone. Another important conclusion that can be drawn from this research is that the beginning of combustion is the most unstable phase of the entire reaction process. Once the flame kernel is developed inside the cylinder, the combustion is going to become more stable because of the formulation of a continuous laminar flame sheet. *Dai et al. (1998)* stated similar conclusions with slightly different explanations. Even though combustion stability is the fundamental reason of IMEP variation, treating COV of IMEP as an extension topic of combustion stability does not yield reasonably good prediction of its exact value over a wide range of engine operating conditions.

Although COV of IMEP is used as an indicator of combustion variation, these two concepts are not equivalent to each other. It is not reasonable to use models and variables directly from studies of turbulent combustion variation to predict COV of IMEP without considering how combustion affects cylinder pressure. The exact quantification of combustion variation is ambiguous to some extent since combustion can be considered as a series of heat release events in the crank angle or time domains. For each event, the released heat is then transformed into cylinder pressure corresponding to the current in-

cylinder air states (e.g. volume and pressure). This synchronization between piston motion and the combustion process significantly affects how sensitive the COV of IMEP is to the combustion variation. *Lee et al. (2009)* suggested that the COV of IMEP has strong correlation with combustion phasing. By regression analysis, this research work identified clear ascending tendency of COV of IMEP as the duration between CA10 and CA90 increases. The significance of combustion phasing on COV of IMEP is discussed in this document.

Many methods were proposed to capture combustion variation by adding randomness to the combustion model (*Brehob et al. 1992, Matthews et al. 1991* and *Sjeric et al. 2014*). These models are designed to regenerate the stochastic behavior of the IC engines through Monte Carlo simulations instead of estimate the COV of IMEP directly. Few researchers demonstrated models with COV of IMEP as an output. *Young (1980)* applied linear regression methods to predict COV of IMEP. A polynomial model was proposed by *Dai et al (1998).* By introducing combustion phasing as an input, the model demonstrates good performance. However, the reasoning and physics for selecting the model inputs were minimally discussed. *Galloni (2009)* employed a nonlinear regression model to predict COV of IMEP. Although the accuracy is satisfying for all the test points, validation results shows that the model can captures only the tendency of COV change with different engine operation conditions.

This research proposes a prediction model for COV of IMEP that combines combustion phasing information and premixed turbulent combustion stability theory. The 3.1.2 and 3.1.3 section discuss the effects of combustion phasing and turbulent

combustion parameters on the IMEP variation. Then, this information is utilized to construct a COV of IMEP prediction model that can be executed in ECUs. Finally, results of both offline and online validations are presented and conclusions are drawn.

3.1.2 Effects of Combustion Phasing on IMEP variation

To derive the relationship between cylinder pressure and heat release the open thermodynamics of the cylinder are evaluated. From the ideal gas law:

$$PV = mRT \tag{3.1}$$

Considering p, V, m and T as time-variant variables, differentiate Equation (3.1) and rearrange:

$$\dot{P} = -\frac{P}{V}\dot{V} + \frac{RT}{V}\dot{m} + \frac{mR}{V}\dot{T} \tag{3.2}$$

Internal energy of the gas is:

$$E = mc_V T \tag{3.3}$$

Differentiate Equation (3.3):

$$\dot{E} = \dot{m}c_V T + mc_V \dot{T} \tag{3.4}$$

From conservation of energy:

$$\dot{E} = \dot{m}_i c_P T_i - \dot{m}_o c_P T + \dot{Q} - P\dot{V} \tag{3.5}$$

Equalize Equation (3.3) and Equation (3.4), and rearrange:

$$\dot{T} = \frac{1}{m}\left[\dot{m}_i(\gamma T_i - T) + \dot{m}_o T(1-\gamma) + \frac{\dot{Q}}{c_V} - \dot{V}\frac{P}{c_V}\right] \tag{3.6}$$

$$c_V = \frac{R}{\gamma - 1}$$

Substitute Equation (3.6) into Equation (3.2):

$$\dot{P} = -\frac{\gamma P}{V}\dot{V} + \frac{\gamma - 1}{V}\dot{Q} + \frac{R\gamma}{V}(\dot{m}_i T_i - \dot{m}_o T) \tag{3.7}$$

Equation (3.7) is the ODE for cylinder pressure dynamics. During the combustion process, the in cylinder mass change is small and neglected. It is important to observe that variation in heat release rate ($\dot{Q}$) propagates to the cylinder pressure. During this process, the cylinder volume determines how much of pressure variation is produced. Figure 3.2 shows the IMEP change after adding 100 J/CA deg energy from -20 to 50 deg CA to a typical engine cycle. It can be seen that the IMEP is more sensitive to the heat release at TDC than other CA due that location having the minimum cylinder volume. Therefore, it can be inferred that high variation of heat release around TDC will result in increased COV of IMEP.

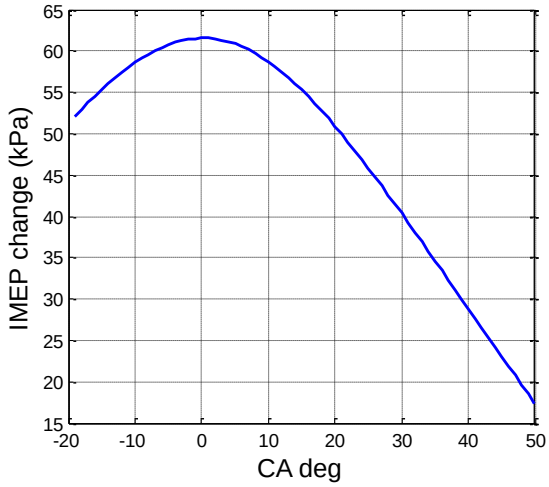

Figure 3.2: IMEP change after adding 100 J/CA deg energy from -20 to 50 deg CA to a typical engine cycle

Late combustion phasing can affect IMEP variation by enhancing cycle-by-cycle coupling. For instance, a late combustion engine cycle increases the exhaust temperature and reduces IMEP. According to ideal gas law (Equation 3.1), the Residual Gas Mass (RGM) for next engine cycle is reduced (for the same volume fraction). This leads to a faster combustion and increase of IMEP. The cycle-by-cycle return plot of IMEP can show this phenomenon clearly with the off-diagonal points.

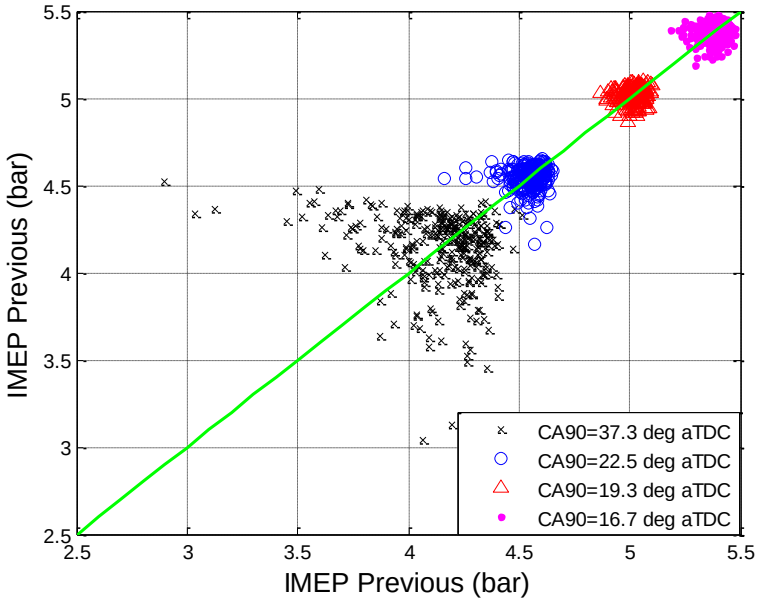

Figure 3.3: IMEP return plot showing cycle-by-cycle coupling at late combustion phasing. RPM=1000. MAP=70 kPa.

Although it is reasonable to argue that the cyclic coupling induced IMEP variations are no longer stochastic and does not agree with a normal distribution, most current engine research and tests do not consider this effect separately and include it in the computation of COV of IMEP. Therefore, it can be concluded that retarding combustion phasing also leads to higher COV of IMEP.

3.1.3 Effects of Turbulent Combustion Parameters on IMEP Variation

The interaction between flame propagation and turbulent motion (visualized in Figure 3.4) creates many different combustion characteristics. The flame propagates from right to left in this figure, creating a pre-heated zone ahead of the flame front. At the meantime, the turbulent motion of the unburnt gas, characterized as a rotating eddy ball, feeds low temperature reactants into the reaction zone while taking pre-heated mass away. When the flame thickness (δ_L) is thin or the laminar flame speed (S_L) is high, the

reaction zone has a higher energy. In this case, the turbulent motion accelerates the combustion process by transporting unburnt mixture to the flame front. On the other hand, the turbulent motion may "blow out" the flame if it takes away too much energy before the flame can prorogate through the reaction zone and feed in more energy. This phenomenon causes instability of combustion.

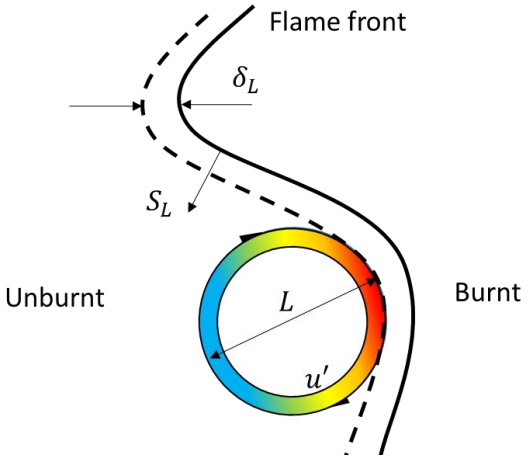

Figure 3.4: Visualization of flame front.

Combustion regimes that produce high variability are often characterized on a Leed's diagram (*Abdel-Gayer et al. 1989*). The diagram contains $\log_{10}\left(\frac{u'}{S_L}\right)$ on the y-axis and $\log_{10}\left(\frac{L}{\delta_L}\right)$ on the x-axis (Figure 3.5). The shaded area is identified regimes of the normal operation of the 3.6L engine under this research.

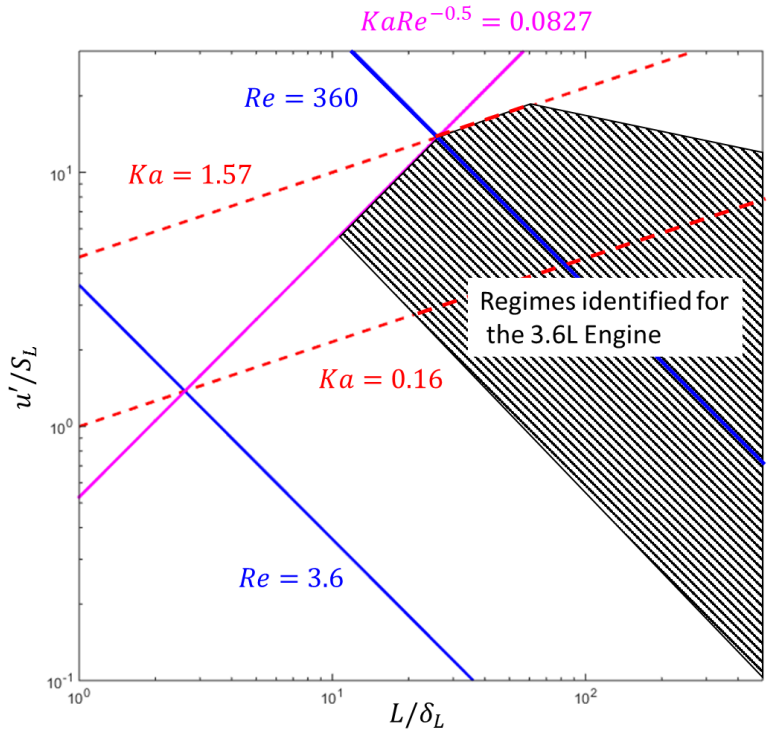

Figure 3.5: Leed's diagram with identified regimes for the 3.6L engine.

The following briefly discusses the important boundaries between regimes.

Letting $x = L/\delta_L$ and $y = u'/S_L$, the constant turbulent Reynolds number (Re) results in a straight line with slope -1 since:

$$Re = \frac{u'L}{v} = \frac{u'L}{\delta_L S_L} = xy \tag{3.8}$$

Where:

Kinematic viscosity $v = \delta_L/S_L$

The constant Karlovitz number also leads to a straight line, whose slope is 1/3.

$$Ka = \frac{\delta_L u'}{S_L \lambda} = 0.157 \left(\frac{u'}{S_L}\right)^2 Re^{-0.5} = 0.157 x^{-0.5} y^{1.5} \quad (3.9)$$

Taylor micro-scale for gasoline engines is approximated with

$$\lambda = \left(\frac{15}{0.371}\right)^{-0.5} Re^{0.5} L$$

For constant $KaRe^{-0.5}$:

$$KaRe^{-0.5} = 0.157 x^{-1} y \quad (3.10)$$

The risk of misfire is high when the engine is operated near the flame quench region. A continuous laminar flame sheet is developed toward the bottom right corner of the Leed's diagram, leading to stabilized combustion. It is expected that combustion stability is closely related to the variation of heat release ($\dot{Q}$). Considering the practicality and computational burden of the combustion stability model, it is critical to choose a point of the entire combustion process to analyze the relationship between Leeds diagram inputs and heat release. The instantaneous heat release rate can be calculated from the measured mass fraction burnt profile $x_b(\theta)$:

$$Q(\theta) = LHV \cdot m_{fuel} \frac{dx_b}{d\theta} \quad (3.11)$$

In order to investigate at which point of the combustion the heat release rate has the largest variation, heat release data for 354 unique engine operation points were analyzed, with 300 consecutive engine cycles recorded for each point. Figure 3.6 shows the standard deviation of normalized heat release per CA through the entire combustion process. The four curves have the same engine speed and load, but different combustion

phasing. It can be observed from this plot that the maximum amount of heat release variation happens close to TDC at crank domain. After changing the x-axis into MFB, the maximum heat release variation occurs at the point where about 20% of fuel is burnt. In fact, retarding the SPKT moves the peak heat release variation closer to the TDC. Therefore in addition to the conclusion from previous section, the heat release analysis reveals another reason suggesting the important correlation between COV of IMEP and heat release variation at TDC.

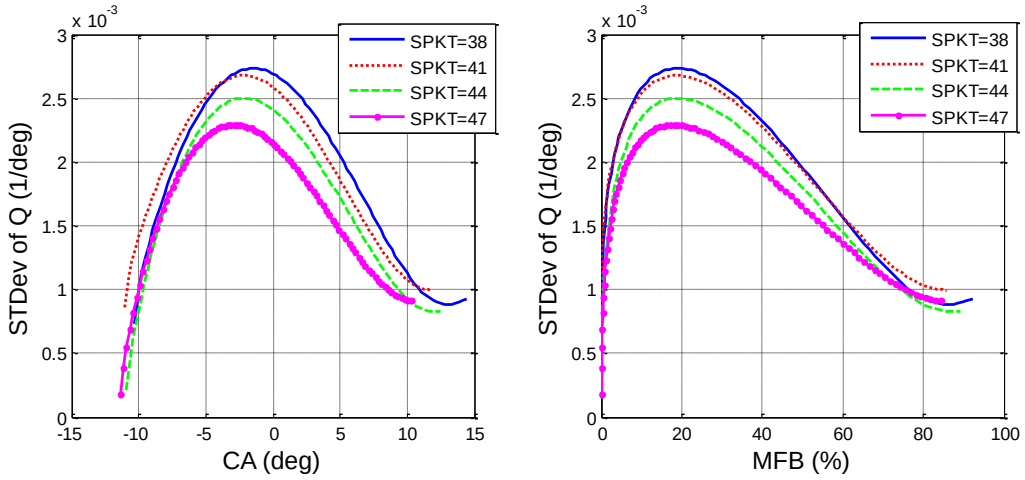

Figure 3.6: Standard deviation of normalized heat release per CA. RPM=1000, MAP=70 kPa

The standard deviation of normalized heat release at TDC is superimposed as a contour plot on the Leed's diagram in Figure 3.7. The Leed's diagram inputs, u', S_L, L and δ_L, are also calculated at TDC. It can be observed that variation of heat release agrees with the tendency of combustion stability. Therefore, it can be inferred that the inputs of Leed's diagram can be used to estimate the magnitude of heat release variation.

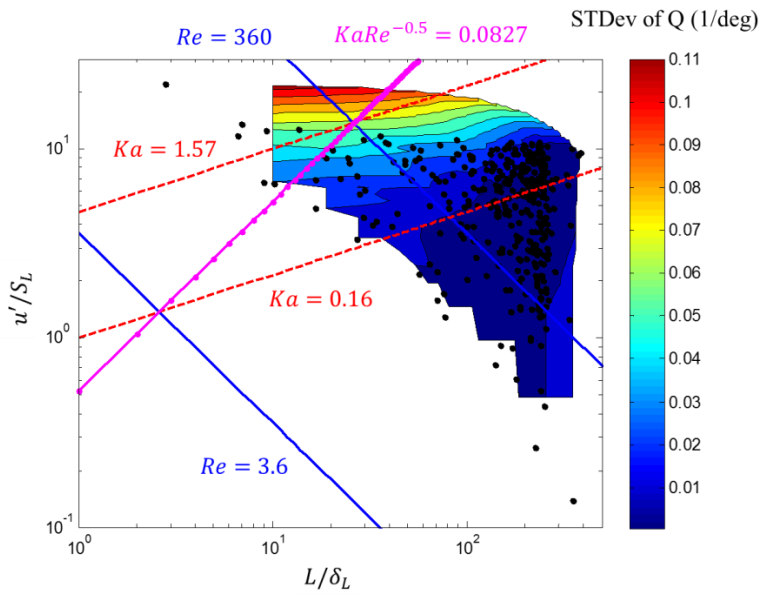

Figure 3.7: Leed's diagram with standard deviation of normalized heat release at TDC.

3.1.4 Modeling of the IMEP Covariance

It can be concluded from previous sections that the COV of IMEP is strongly related to the heat release variation at TDC and combustion phasing. Selecting the inputs to the COV of IMEP model should consider which variables are available for the application. In the proposed combustion phasing control framework, the COV of IMEP model is used together with a crank angle resolution semi-physical combustion model. The combustion model is used to compute CA50 with given SPKT. Thus, COV of IMEP model inputs that reflect the impact for combustion phasing is selected as the SPKT and CA50. The combustion model is also able to provide the u' and S_L at TDC, which are used to estimate the heat release variation at TDC. The inputs of Leed's diagram also requires the turbulent integral length scale, which can be approximated as the distance between cylinder head piston (*Filipi et al. 2000*) at TDC. The laminar flame thickness (δ_L) can be calculated with laminar flame speed (S_L) and the gas kinematic viscosity (v)

(Equation 3.8). For gasoline engines, the viscosity is sensitive to temperature but not to the gas composition (*Heywood 1988*). A simple nonlinear regression model is applied to calculate the viscosity according to unburnt gas temperature:

$$v(kg/m \cdot s) = 3.3 \times 10^{-7} \times T^{0.7} \tag{3.12}$$

The unburnt gas temperature at TDC is determined by the cylinder gas temperature at IVC and the energy balance between IVC and TDC. The residual gas dominates the mixture's temperature at IVC. The energy input during this period include the mechanical work done by the upward motion of piston and the portion of combustion. The energy output is the heat transfer to coolant. The manifold pressure (MAP) affects the compression work of the piston. It also determines the amount of fuel inside the cylinder since the SI engines mostly operates at stoich AFR conditions. SPKT also influences both the energy input sources. Advancing SPKT increases the cylinder pressure and heat release between IVC and TDC. Thus it results in higher unburnt gas temperature. Figure 3.8 shows the effects of residual gas fraction and SPKT on the unburnt gas temperature at TDC.

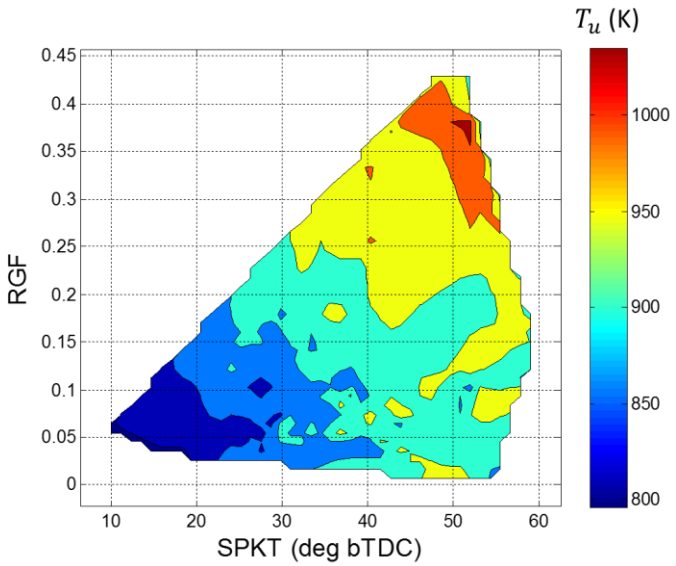

Figure 3.8: Contour plot of unburnt gas temperature vs. residual gas fraction (RGF) and spark timing (SPKT). Unburned gas temperatures increase as SPKT is advanced and internal RGF increases.

The heat transferred to coolant between IVC and TDC is determined by the engine speed. Higher speed results in less time for heat transfer, leading to higher unburnt gas temperature. However, the engine speed is included as an model input because of its almost linear relationship with u'. Figure 3.9 plots the RPM against u' at TDC of the 3.6L engine in this research. The model output makes no noticeable difference after removing the RPM from the model inputs. The mean value of IMEP has significant impact the COV of IMEP, which is calculated as the standard deviation of IMEP divided by the mean value. The mean value of IMEP is determined by many variables like MAP, RPM and CA50. Most of these variables are already included as the model inputs.

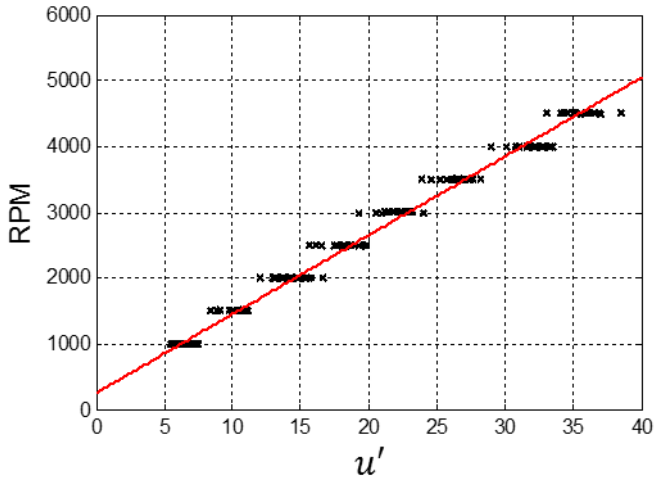

Figure 3.9: Linear relationship between turbulence intensity at TDC and RPM.

The above analysis shows that the correlations between COV of IMEP and other measureable (or estimated in a model-based control architecture) engine operating parameters are highly nonlinear and coupled. Artificial Neural Networks (ANNs) are an efficient "black box" modeling method for systems with nonlinear inter-correlation characteristics. However, the robustness of ANN prediction outside the training region is not guaranteed. Although it is difficult to find techniques to ensure extrapolation stability with strict mathematical proof, it has been acknowledged that decreasing number of hidden layers and neurons can improve the stability of ANN outside the training region. The inevitable cost of reducing neural network size is loss of accuracy in terms of capturing nonlinear correlations. To simplify the ANN structure in this case polynomial regression based nonlinear conversion is applied to the original model inputs, transforming them into intermediate variables. These variables are then used as inputs to the ANN, which only has 1 hidden layer and 3 neurons (Figure 3.10).

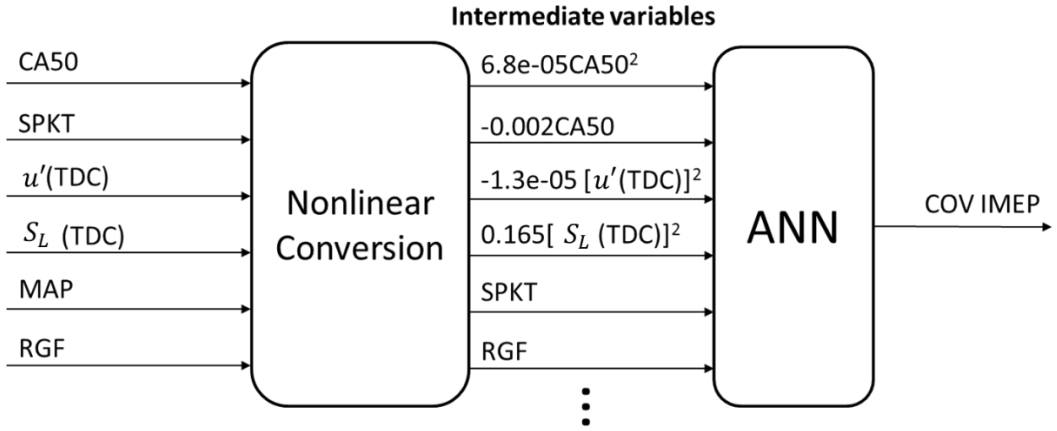

Figure 3.10: Block diagram of the proposed COV of IMEP model.

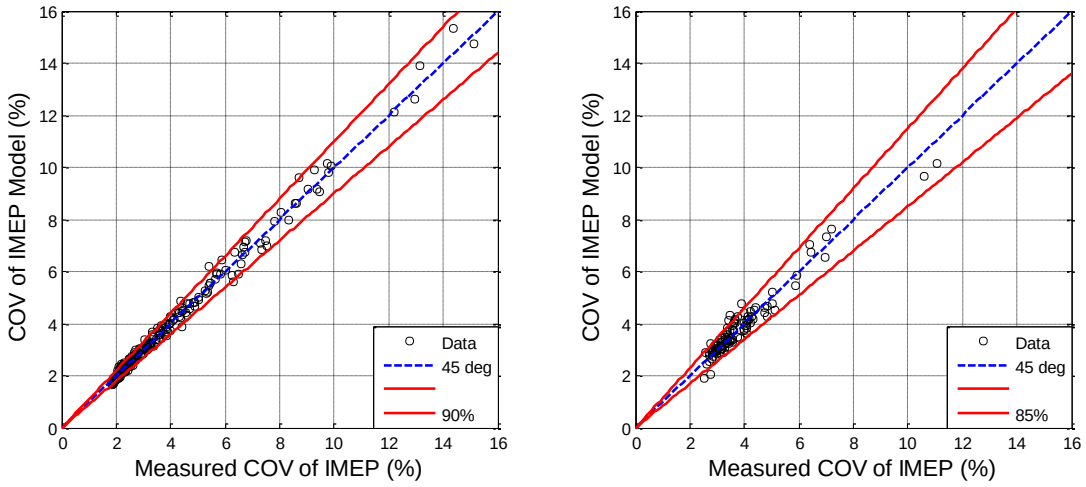

Figure 3.11: Comparison between measured COV of IMEP and ANN. Left is training data and right is validation with different data set.

The ANN is trained and validated with 248 and 106 data points correspondingly. It can be observed from Figure 3.11 that the model performs well with data other than the training set with RSME of 0.35%, 0.14% more than the training data. This model was implemented within a prototype ECU and tested over a FTP drive cycle, during which the engine operates frequently outside the training region of the ANN. Figure 3.12 shows that the predicted COV of IMEP from the model is within a reasonable range. Figure 3.13

plots the contour of the predicted COV of IMEP on top of CA50 and MAP. It shows that the high COV of IMEP occurs at low MAP and late combustion phasing situations.

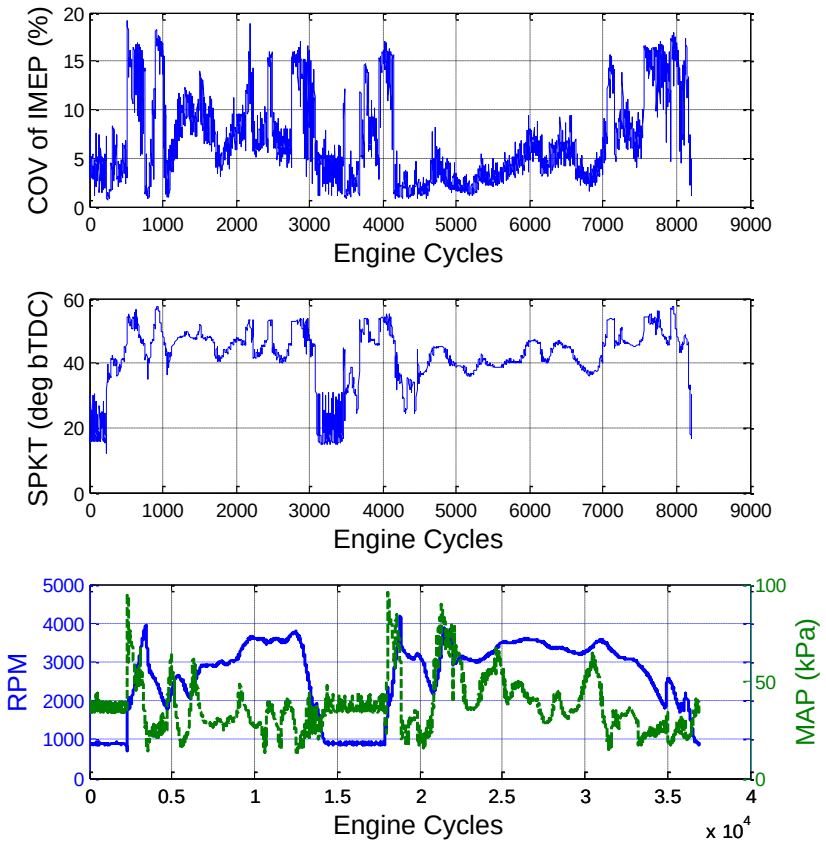

Figure 3.12: COV of IMEP model predictions from real-time dynamometer testing over a section of the FTP drive cycle.

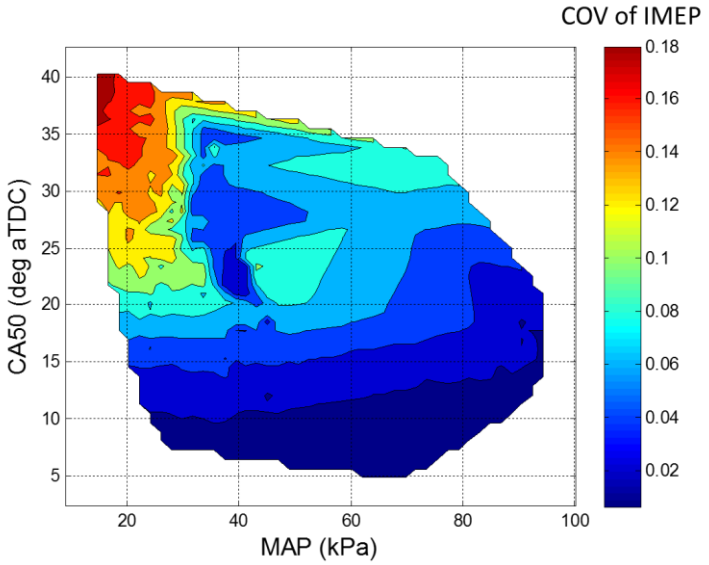

Figure 3.13: A contour plot of COV of IMEP vs. CA50 and MAP from test data during the FTP drive cycle.

The COV of IMEP is essentially a statistical quantity that is computed from certain amount of consecutive engine cycles with the same operation conditions. Thus validating the model in terms of transient engine operation conditions are not possible. However, the COV of IMEP is treated as an indication of combustion stability for most automotive OEMs, making the representation of this statistical quantity to have exact physical meaning. Similar to the proposed model based combustion phasing control framework, the COV of IMEP is treated as the limit for combustion phasing retard to avoid misfire and worse emission quality. This fact makes the cyclic prediction of COV of IMEP has significant importance.

3.1.5 Conclusions

This section of the dissertation provides a pragmatic modeling method for the COV of IMEP based on flame regime analysis of combustion stability and the thermodynamics of in-cylinder mass. Although variation of turbulent combustion is the

cause of COV of IMEP, these two concepts are not equivalent to each other. This paper illustrates that the combustion variation can be considered as the heat release variation. The synchronization between heat release variation and cylinder volume determines how much of the variation propagates to cylinder pressure resulting in COV of IMEP. It is concluded that the combustion variation at TDC has significant influence of COV of IMEP since the cylinder volume is the smallest. Furthermore, the highest heat release variation is usually close to TDC. The heat release variation of the entire combustion process can be inferred by examining the combustion stability at TDC. The analysis of correlations between different engine operation parameters was used to narrow the COV of IMEP model inputs into combustion phasing related terms (SPKT and CA50), combustion stability terms (TI at TDC, LFS at TDC and RGF) and IMEP terms (MAP and RGF). The inputs are treated with nonlinear regression polynomial functions to convert them into intermediate variables. This process allows an ANN with few hidden layers and neurons to accurately predict the COV of IMEP. Furthermore, the simple structure of the ANN improves the robustness of the model in untrained regions. Although this model is implicit, it is proven to be fast enough to run within one engine cycle. Its computational efficiency makes it favorable for use with control applications.

3.2 Cycle-by-cycle Model Predictive Spark Timing Control

The combustion phasing of Spark Ignition (SI) engines is traditionally regulated with map-based spark timing (SPKT) control. The calibration of these maps consumes tremendous amounts of time and resources making it less favorable for SI engines with a high number of control actuators. This paper proposes three online SPKT optimization algorithms that can utilize control oriented physics based combustion models making the SPKT control algorithm more adaptive to different engine designs. Model inversion and derivative information are not required by these three SPKT optimizers considering the complex nature of physics based combustion models. These methods also preserve the dependence between combustion phasing, knock and COV of IMEP models to avoid evaluating combustion models multiple times within one iteration. The 2-Phase and constraint relaxation methods are derived from direct search optimization theories. The Recursive Least Square (RLS) polynomial fitting method can be considered as a virtual Extreme Seeking process that converts the original "black" box nonlinear constrained optimization into the solution of three low order polynomial equations. Although these three online SPKT optimization approaches have unique properties making them preferable with certain types of combustion models, simulation and test results show that all of them can find the optimal SPKT with less than 10 evaluations of the combustion model. This fact makes it possible to implement the proposed model based SPKT control strategy in future engine ECUs.

3.2.1 Introduction

Calibration time and effort has become an important limiting factor to further increasing the number of control degrees of freedom of modern IC engines. Model based engine controllers that can more easily adapt to different engine designs and are becoming favorable as the cost of calibration increases and the online computation load shrinks with the development of faster micro-processors. Controlling Spark Timing (SPKT) to achieve optimal combustion phasing without violating the constraints of normal combustion is critical for SI engines to improve efficiency while maintaining stable operation. Many computationally efficient control oriented combustion models have been proposed to potentially replace the mapping process of SPKT calibration (*Ghojel 2010, Bonatesia et al. 2010, Hall et al. 2012, Lee et al. 2010* and *Bougrine et al. 2009*). The fundamental challenge of computing SPKT online using these models is that the SPKT is mostly an input to the combustion model rather than an output. The complex structure of these high-fidelity physics based models makes them difficult to invert and compute SPKT based on target combustion phasing. This paper proposes to employ iterative optimization techniques to find the optimal SPKT with control-oriented combustion models. This approach exploits the computational efficiency of these models while avoiding the necessity to invert them.

Before the existence of control oriented combustion models, optimization routines for SPKT were researched in the context of Extreme Seeking (ES) control (*Hellström et al. 2013, Popovic et al. 2006, Scotson et al. 1990, Dorey et al. 1994, Larsson et al. 2008, Haskara et al. 2006 and Draper et al. 1954*). ES control is an important class of adaptive

optimal controllers that consists of model identification and optimization processes (*Teel et al. 2001, Wellstead et al. 1990, Blackman 1962* and *Krstić et al. 2000*). The optimization process searches for the extreme value of a specific cost function. Although dependence of the cost function on the control variables is unknown, the relationship is required to be convex to avoid local minimum issues that could terminate the search for the global optimum. The cost functions were often defined as fuel consumption (*Hellström et al. 2013, Popovic et al. 2006* and *Haskara et al. 2006*), torque output (*Larsson et al. 2008* and *Draper et al. 1954*) or combustion phasing (*Dorey et al. 1994*) when the ES approach was applied to SPKT control. It has been observed from several previous researchers that the relationship between most engine performance parameters and spark timing can be approximated with a quadratic function while the engine operating conditions are fixed. However, if the engine operating condition changes, ES methods must update this quadratic dependency using online identification methods based on real time measurement feedback. Therefore, cylinder pressure sensors are usually necessary if the control objectives are to track a combustion phasing reference and/or maximize IMEP. The coefficients of the quadratic dependence are estimated iteratively with Recursive Least Square (RLS) methods (*Ljung, 1999*). In order to maximize the potential of the optimal solution to improve engine performance, the identification process should be converged before the engine operating conditions change significantly. RLS algorithms can be altered with forgetting factors and exponential weighting to accelerate this identification process (*Scotson et al. 1990*). Both of these methods make the RLS estimation sensitive to measurement noise, leading to instability

of ES based engine controllers. Regardless of the quadratic dependence assumption, non-parametric ES algorithms (*Blackman 1962*) have been applied to control SPKT for flex-fuel engines (*Hellström et al. 2013*). This method required the constant addition of SPKT perturbations to identify its relationship with the proposed cost function. The magnitude of these perturbations is critical to the operation of this SPKT controller. Small perturbation results in slow convergence rates while large perturbation induces drivability issues and degenerated stability.

ES SPKT control algorithms have also been extended to include other actuators such as Exhaust Gas Recirculation (EGR) (*Haskara et al. 2006*), flex-fuel (*Hellström et al. 2013*), Variable Valve Timing (VVT) (*Popovic et al. 2006*) and Air-to-Fuel Ratio (AFR) (*Scotson et al. 1990*). Although results indicated that the optimization converged after certain intervals of engine cycles, rigorous proof of the global optimum was not addressed extensively. Most of these previous research publications indicated that the slow convergence rate of an ES SPKT control approach made it more suitable for steady state calibration or adaptation rather than completely replacing the map based SPKT control.

This paper focuses on manipulating SPKT to track a designated combustion phasing reference, specifically CA50, from an upper level controller. Instead of measuring the CA50 with cylinder pressure sensors, many control oriented combustion phasing models have been proposed to estimate the combustion phasing with other sensors (*Ghojel 2010, Bonatesia et al. 2010, Hall et al. 2012, Lee et al. 2010* and *Bougrine et al 2009*). These methods were proven to be reasonably accurate with

acceptable complexity for online computation. The combustion phasing models can be categorized into Wiebe Function based models (*Ghojel 2010* and *Bonatesia et al. 2010*) and simplified flame entrainment models (*Hall et al. 2012, Lee et al. 2010* and *Bougrine et al 2009*). The common trait of these models is that they are required to be computationally efficient so they can be carried out one or more times within one engine cycle. However, the drawback is that most of these models are difficult to invert, making them difficult to use to compute SPKT with a given combustion phasing target. Since these models are constructed to be computationally efficient, iterative optimization methods can be applied to search for the SPKT that generates the desired combustion phasing. This strategy can be considered as a virtual ES process. Unlike the traditional ES SPKT control that applies these SPKTs to the engine through many engine cycles and measures the response with cylinder pressure sensors, the proposed SPKT control employs combustion models to simulate the CA50s for multiple SPKTs within one engine cycle. The mathematical tools used in ES SPKT control literature can be transferred to this application. Cylinder pressure sensing is not required for this SPKT control approach since it is feed forward based. However, it does not exclude the possibility of model adaptation if combustion phasing feedback information is available. The most important advantage compared to the traditional ES method based methods is that the proposed method can generate the optimal SPKT within one engine cycle. Therefore, it is capable of handling highly transient engine operating conditions.

It is challenging for the traditional ES SPKT control algorithms to account for combustion constraints like auto-ignition (or knock), COV of IMEP and misfire. This

issue is caused by the dilemma that the algorithms require the engine to run at, or close to, the unstable conditions to identify limits, which is usually not allowed during normal engine operation. As for the proposed "virtual" ES method that completes the seeking process virtually with combustion models, it is possible to incorporate high-fidelity control oriented knock and COV of IMEP models to guarantee the optimal SPKT solution will not violate combustion constraints. Previous researchers have proposed that engine knock can be accurately predicted by integrating the Arrhenius function output for the end gases (*Livengood et al. 1955* and *Xiao et al. 2013*). Misfire is often considered as a more relaxed constraint compared to the COV of IMEP requirement. The limit for SPKT retard is determined by the COV of IMEP, which is considered as an indicator of combustion stability. The extreme case of instable combustion corresponds to the misfire phenomenon. Researchers have illustrated that combustion variation is the main cause of COV of IMEP (*Ozdor et al. 1994* and *Lacour et al 2011*). *Lee et al. (2009)* suggested that the COV of IMEP has strong correlation with combustion phasing. Finally, regression models of COV of IMEP have been proposed by (*Young 1980, Dai et al. 2000* and *Galloni 2009*). Most of these models are computationally efficient and implicit, making them ideal for implementation as constraints of non-gradient based direct search optimization algorithms.

As a general class of optimization solvers, the direct search methods can find the optimal solution utilizing only the information of each numeric evaluation of objective and constraint functions. Compared to the gradient based algorithms, direct search methods do not require first and second derivatives of both objective functions and

constraints. This unique property makes the direct search methods favorable for SPKT optimization with complex combustion models. Many powerful direct search solvers were developed for different types of applications, including Hook Jeeves (*Hooke et al. 1961*), Cyclic Heuristic Direct (*Li et al. 1995*), Leapfrogging (*Rhinehart et al. 2012*), Particle Swarm (*Banks et al. 2007*) and genetic algorithm. The analysis of the SPKT optimization problem reveals that not all of these algorithms are efficient for this application.

Considering the short computation time of engine cycle based SPKT control, modifications are added to the real-time versions of the selected solvers to reduce iteration number and improve stability considering some practical issues in this research. One of these issues is handling infeasible start scenarios. Some direct search algorithms cannot find feasible search directions when the start point is infeasible and the improving direction of the objective function furthers this violation. This research discusses solutions to this dilemma. Inspired by ES SPKT control, the complex combustion phasing model and constraints can be approximated by simple polynomial functions, which are constantly updated with the RLS algorithm. The optimal solution can be explicitly computed with these approximated functions. This "virtual" ES approach is explored in this research and compared with the direct search methods.

This research proposes a SPKT control method based on online optimization with combustion constraints. The optimization iteration process is able to finish within one engine cycle utilizing control oriented high-fidelity combustion phasing, auto-ignition and COV of IMEP models. The next section discusses the optimization problem

formulation and convexity analysis of SPKT control. The third, fourth and fifth sections illustrate three different optimization approaches to solve this optimization problem, including direct search, constraint relaxation and RLS polynomial fitting. Finally, simulation and experimental results are presented and discussed.

3.2.2 Optimization Problem Formulation and Analysis

3.2.2.1 Semi-physics Based Combustion Model

The objective of this optimization is to find the SPKT that will generate the desired combustion phasing (CA50) without inducing knock and excessive COV of IMEP. The combustion phasing is modelled by a quasi-dimensional flame entrainment combustion model. The combustion model was originally proposed by *Blizard et al. (1974)* and then refined by *Tabaczynski et al (1980)*. This turbulent flame entrainment based combustion model assumes that the fresh mixture at the flame front is; (1) entrained into small eddies, and then (2) burned up in a characteristic time. Based on these assumptions, the flame entrainment and burned up processes are shown below as Equation (3.13) and (3.14) respectively.

$$\frac{dm_e}{dt} = \rho_{unburned} A_{flame} \left(u' + S_L \right) \tag{3.13}$$

$$\frac{dm_b}{dt} = \frac{m_e - m_b}{\tau} + \rho_{unburned} A_{flame} S_L \tag{3.14}$$

Equation (3.13) describes the unburned mass entrainment rate at the flame front. It is assumed the flame propagates through unburned charge along Kolmogorov scale

vortices entraining turbulent eddies. The unburned mass entrainment rate is determined by unburned mixture density, flame front area, laminar flame speed and turbulence intensity. After unburned mixture entrainment, mass burn-up occurs at a rate described by Equation (3.14). Burn-up occurs at a characteristic time, τ, which is defined as the time to burn up an eddy at laminar flame speed. The eddy size is assumed to be Taylor microscale (λ) (*Tabaczynski et al. 1977*).

3.2.2.2 Knock Constraint Model

Knock in an SI engine occurs as the unburned end gases auto-ignite before the spark ignited flame reaches them. This occurs from the expanded burned gas compressing the unburned end gas to auto-ignition. Knock is likely when cylinder pressures and temperatures are high (combustion phasing is advanced). Varieties of auto-ignition characteristic modeling methods are available, from comprehensive chemical kinetic based simulations (*Westbrook et al. 1988*), to a global single step Arrhenius function describing all hydrocarbon oxidation reactions (*Livengood et al. 1955*). Reduced chemical kinetics descriptions are available (*Glassman 1977*) as well. Among the methods above, the single step Arrhenius function is recognized as a practical way of predicting the ignition delay for control purposes due to its simplicity and relatively good physical representation (*Kasseris 2011*). It is widely studied based on experimental data for auto-ignition prediction in constant volume bombs, steady flow reactors, rapid compression machines and IC engines (*Assanis et al. 2003* and *Douaud et al. 1978*). Phenomena for ignition delay are observed both experimentally, in rapid compression

machines (RCM) (*Wo 1998*) and in detailed chemical kinetics simulations (*Kee et al. 1989*).

A typical commercial automotive gasoline contains approximately seven hundred types of molecules (*Viljoen et al. 2005*). For highly detailed chemical kinetic modeling ignition characteristics of each individual molecule in the temperature and pressure domain is required. This information is rarely available and time consuming to calculate, so a global reaction that describes all the hydrocarbon oxidation processes in a single-step Arrhenius function is favored in this research. The equation relates the rate of reaction of an auto-ignition process as a function of pressure and temperature, assuming single-step chemical kinetics:

$$\frac{d[x]}{dt} = A'_G[x]p^n \exp(-\frac{B_G}{T}) \tag{3.15}$$

The ignition delay, in milliseconds, can be expressed as the inverse of the reaction rate of the global single-step mechanism:

$$\tau_G = A_G p^{-n} \exp(\frac{B_G}{T}) \tag{3.16}$$

Equation (3.16) is developed to represent the ignition delay in a RCM with coefficients extracted from experimental data. In a RCM, the pressure is assumed approximately constant until combustion occurs. However, for a spark-ignited engine, the end gas is compressed by the propagating flame and the temperature rises following a polytropic process. *Livengood et al. (1955)* proposed that the end gas auto-ignition chemistry is cumulative and can be predicted by integrating the reaction rate of the end

gas at discretized pressure and temperature time steps until the critical time when the integral value is equal to one (L-W knock integral).

3.2.2.3 Optimization Problem Analysis

The real time optimization of SPKT is finished within a single engine cycle. The other engine actuators and states are assumed to be constant during this period of time (e.g. RPM, MAP and VVT). Therefore, the CA50, L-W knock integral and COV_{IMEP} models described in previous sections can be expressed as $(SPKT)$,$g(SPKT)$ and $h(SPKT)$. The optimization problem can be written as the following:

$$\begin{aligned} &\min_{SPKT} \left| f(SPKT) - CA50_{target} \right| \\ &s.t. \quad g(SPKT) \leq KI_{max} \\ &h(SPKT) \leq COV_{max} \end{aligned} \tag{3.17}$$

Where:

KI_{max} : specified upper bound of L-W knock integral.

COV_{max}: specified upper bound of COV of IMEP.

It is commonly acknowledged that advancing SPKT will advance CA50 and increase the knock integral. Therefore, the objective function and the first constraint are convex if the combustion and knock models are reasonably accurate. Although the relationship between COV of IMEP and SPKT is not monotonic, it is observed that $h(SPKT)$ takes a quadratic like shape for the admissible SPKT range. Thus the second constraint can be considered as convex. Table 3.1 illustrates the engine operation condition ranges that are used to generate the combustion phasing, knock and COV of

IMEP models. Figure 3.14 to 3.16 show some examples of $f(SPKT)$, $g(SPKT)$ and $h(SPKT)$ from the recorded data.

Table 3.1: Range of test data

	Min	Max
RPM	900	4500
MAP (kPa)	30	100
ICL (deg aTDC intake)	78	128
ECL(deg bTDC intake)	69	117
CA50 (deg aTDC spark)	0	39
RGF	0.02	0.44

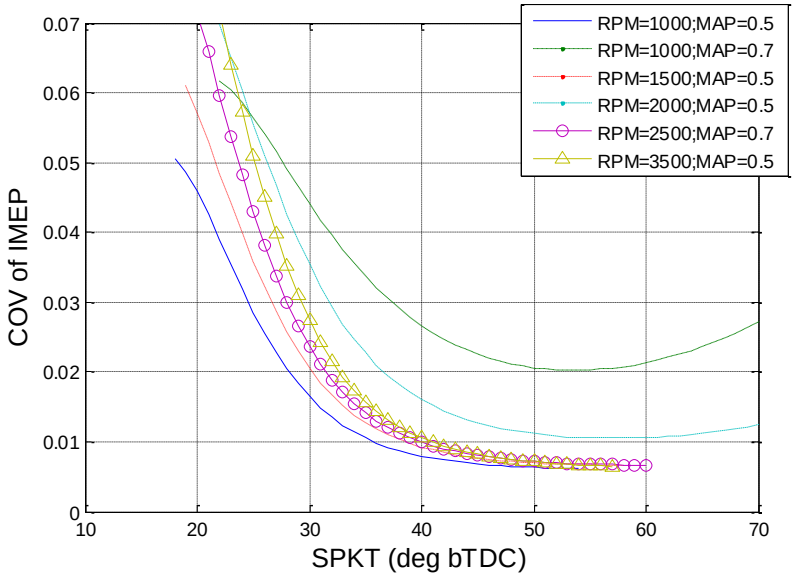

Figure 3.14: Relationship between COV of IMEP and SPKT for various engine operation conditions. This relationship is mostly convex.

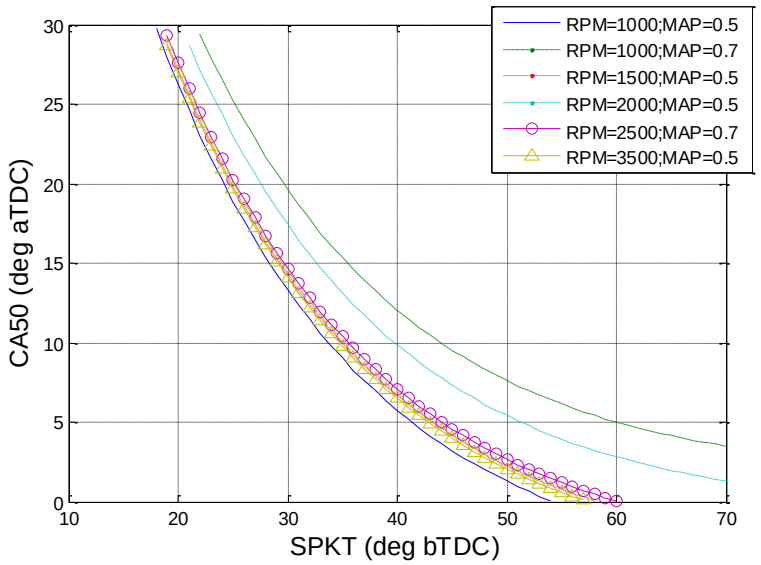

Figure 3.15: Relationship between CA50 and SPKT for various engine operation conditions. This relationship is mostly convex.

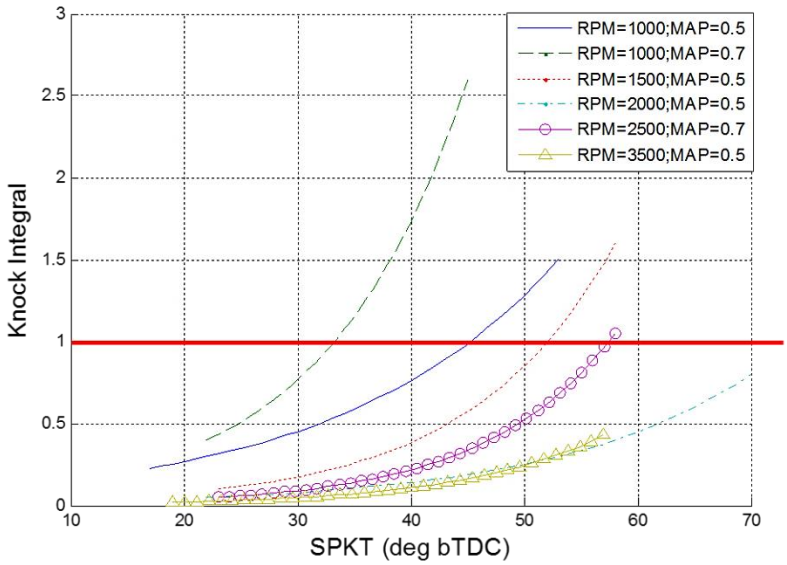

Figure 3.16: $g(SPKT)$ for various engine operation conditions. The engine is very likely to knock if KI is greater 1. This relationship is mostly convex. Knock is likely to happen when the knock integral is larger than 1 (red horizontal line).

The above analysis indicates that there is a unique solution to the optimization problem (3.17). Thus algorithms designed to solve local optimum issues, like genetic algorithm and particle swarm, are less favorable for this application. The physics based

combustion model is computationally intensive for online applications, so iterations should be minimized. The ES910 system is able to compute the proposed combustion model 10 times per engine cycle on average when the engine speed at 2000 RPM. Production engine ECUs are slower than the ES910 system currently and occupied with many other computation tasks. Therefore, each function evaluation is considered extremely "expensive". This fact leads to another consideration of the algorithm selection that it should evaluate both the objective function and constraints together within each iteration since the COV of IMEP and knock models are dependent on the intermediate outputs of the combustion phasing model. Handling constraints and objective functions separately will increase the number of evaluations of the combustion phasing model. This research proposes three approaches to solve this optimization problem. Each approach has unique advantages for certain types of applications.

3.2.3 2-Phase Direct Search Method

The problem described in Equation (3.17) is a single dimension constrained optimization. Since the objective function and constraints are complex and implicit, direct search methods provide the most straightforward solutions. Gradient based methods utilize first and second order derivatives of the objective and constraint functions to compute searching directions, whereas direct search methods rely only on the evaluation of these functions to find the feasible descending directions (for minimization problems) of the manipulated variables. Many existing algorithms can be employed directly to this application (e.g. *Hooke et al. 1961* and *Rhinehart et al. 2012*).

However, some knowledge about the combustion models can be utilized to improve algorithm performance.

A feasible initial guess of the SPKT enables interior point methods that keep the search point confined in the feasible region and guarantees decreasing objective function values. This method can significantly reduce the number of iterations. Another advantage of the interior point method is that the solution will always be feasible and better than the starting point even if the optimization is terminated prematurely due to the lack of computation time. The feasible initial guess can be generated with calibration and stored as a map in the ECU. Since this initial guess only requires the SPKT to be feasible instead of optimal, this calibration process should be much faster than that of generating the traditional SPKT control map. The feasible initial guess can also be generated using a phase 1 optimization program. The added phase of optimization only needs to evaluate the constraint functions (knock and COV of IMEP). However, since these functions are correlated with the combustion phasing model, the 2-phase solution will significantly increase computation load.

After a feasible start point is acquired, the second phase of the optimization will start. The descending direction of the SPKT optimization problem (Equation (3.17)) is easily decided due to the monotonic relationship between CA50 and SPKT. The search step size is computed iteratively after every objective and constraint function is evaluated. The following is the pseudo code of the proposed 2-phase direct search approach:

Run physics based combustion phasing model;

Calculate objective function value;

Calculate constraint function value;

If iteration=1

Assume the "previous iteration" is in phase 1;

STEP=-STEP if violate knock constraint; // the initial STEP is positive

feval = sufficiently large initial value;

End if;

If violate constraints and previous iteration is in phase 1 // phase 1

If the violated constraint is the same as previous iteration

$STEP=k_1STEP$;

Else

$STEP=-k_2STEP$;

End if;

$SPKT_i=SPKT_{i-1}+STEP$

feval=feval;

Else // phase 2

If objective function < feval and no violation of constraints

$STEP=k_3(CA50_i-CA50_{i-1})$;

$SPKT_i=SPKT_{i-1}+STEP$;

feval=objective function value;

Else

$SPKT_i=SPKT_{i-1}-STEP+k_4STEP$;

$STEP=k_4STEP$;

feval=feval;

End if;

End if;

Go to the beginning;

Terminate the loop **if** 1) reach maximum number of iterations; or 2) STEP is less than α ; or 3) feval is less than β and no violation of constraints.

The step multipliers k_1, k_2, k_3 and k_4 are critical to the efficiency and stability of the algorithm. In order to accelerate the program to recover from an infeasible start point, k_1 is greater than 1. However, the step size should decrease ($0 < k_2 < 1$) once the search point has left the original infeasible region. Otherwise, it is possible that the algorithm will cycle between knock and COV limits without finding the feasible region between them. Traditional direct search algorithms usually increase search step size if the previous iteration is feasible and objective function decreases. This method could cause issues near the optimal solution. It is likely that a large step size will overshoot the optimal point, increasing the number of iterations. Figure 3.15 shows that the relationship between CA50 and SPKT are very similar for different engine operation conditions. The slopes of these curves are almost identical. Therefore, the adjustment of SPKT of each iteration can be approximated with the difference of CA50 (i.e. a one-to-one SPKT to CA50 relationship is assumed). The multiplier k_3 is added to fine tune this approximation. The step size shrinks by the factor of k_4 if the last iteration results in an increase of objective function or violation of constraints during phase 2.

This method generates an overall decreasing tendency of the search step sizes as the searching point converges to the optimal solution. This characteristic reduces error to

the optimal solution. Another advantage of this approach is that the step size can serve as an indication of convergence. Thus the optimization process can be terminated once the step size is smaller than a certain threshold. The 2-phase SPKT optimization approach does not require the objective and constraint functions to be continuous. This could make this approach favorable for applications with low resolution models. For instance, the 2-phase approach can utilize a misfire model as a constraint.

3.2.4 Constraint Relaxation Method

It is acknowledged that constraint handling can the most challenging aspect of optimization algorithms. Constraint relaxation methods modify the original objective function to approximate the effects of constraints. Thus the algorithm will not have to handle the constraints explicitly. The converted objective function is not unique. It is proposed here that the optimization problem described in Equation (3.17) can be approximated with the following problem:

$$\min_{SPKT}\Big[\big|f(SPKT)-CA50_{target}\big|+\max\big(0,c_1(g(SPKT)-KI_{max})\big) + \max\big(0,c_2(h(SPKT)-COV_{max})\big)\Big] \tag{3.18}$$

It is easy to prove that the new objective function in Equation (3.18) is convex, resulting in a unique optimal solution. However, parameters c_1 and c_2 have to be sufficiently large to penalize the violation of the original constraints for Equation (3.18) to generate similar results as Equation (3.17). Solving Equation (3.18) is much easier than Equation (3.17) since it does not have any explicit constraints. The algorithm used to solve the phase 2 problem described in last section can be directly applied to solve

Equation (3.18). The disadvantage of the constraint relaxation method is that the solution may slightly violate the constraints if the target CA50 is not feasible.

3.2.5 RLS Polynomial Fitting Method

Both the 2-phase and constraint relaxation methods are non-gradient based optimization. They are chosen for this application since the objective and constraints functions are implicit and complex. Although these functions cannot be solved analytically, they can be approximated with low order polynomial functions whose solutions can be calculated easily. The optimization can be considered as a simple process that compares the SPKT solution for the target CA50, COV limit and knock limit.

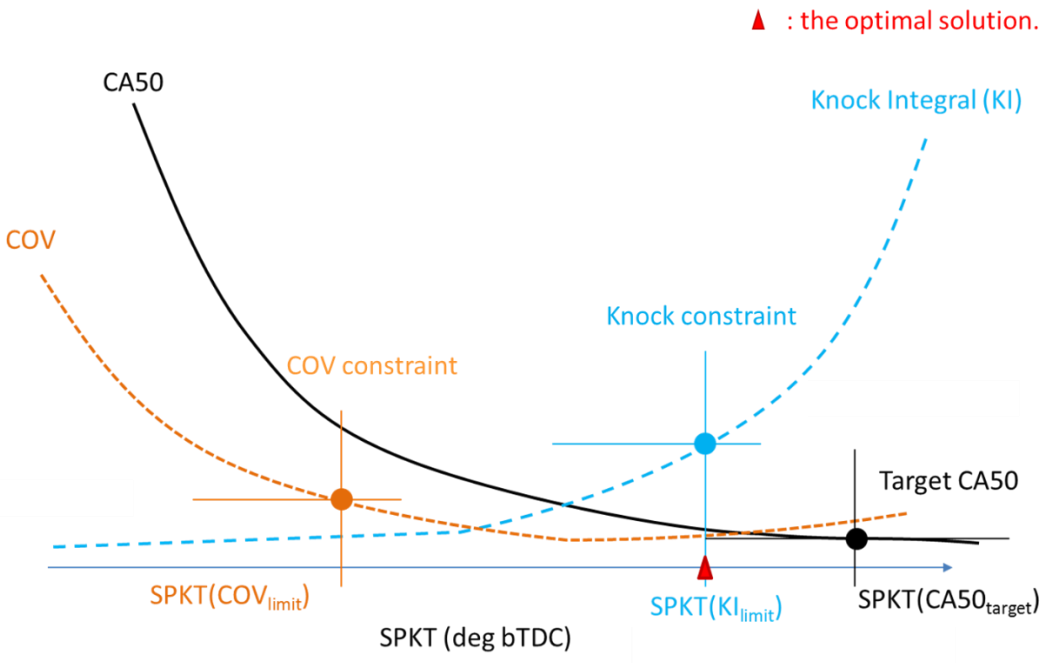

Figure 3.17: Demonstration of SPKT optimization process. The optimal SPKT can be identified if SPKT(COV$_{limit}$), SPKT(KI$_{limit}$) and SPKT(CA50$_{target}$) can be solved.

However, Figure 3.14 and Figure 3.15 show that the effects of SPKT on CA50, COV of IMEP and knock integral vary with engine operation conditions. Furthermore, the linear and quadratic approximation of some curves are only valid for a narrow range of SPKT. Therefore, the low order polynomial approximation needs to be adapted for each iteration during the optimization.

The Recursive Least Square (RLS) method is selected to fit these polynomial functions since it can update the estimation results iteratively during the optimization process. Another advantage of the RLS algorithm is that it is very robust under the influence of noise. For this application, the source of noise is from model inaccuracy. The combustion phasing and knock integral models discussed previously are essentially numerical integration processes. The integration step size (i.e. model resolution) can create discontinuity in the model outputs. The RLS is still capable of fitting the polynomial functions in this situation with a minimum number of additional iterations. Figure 3.18 shows the information flow for the RLS SPKT optimization algorithm.

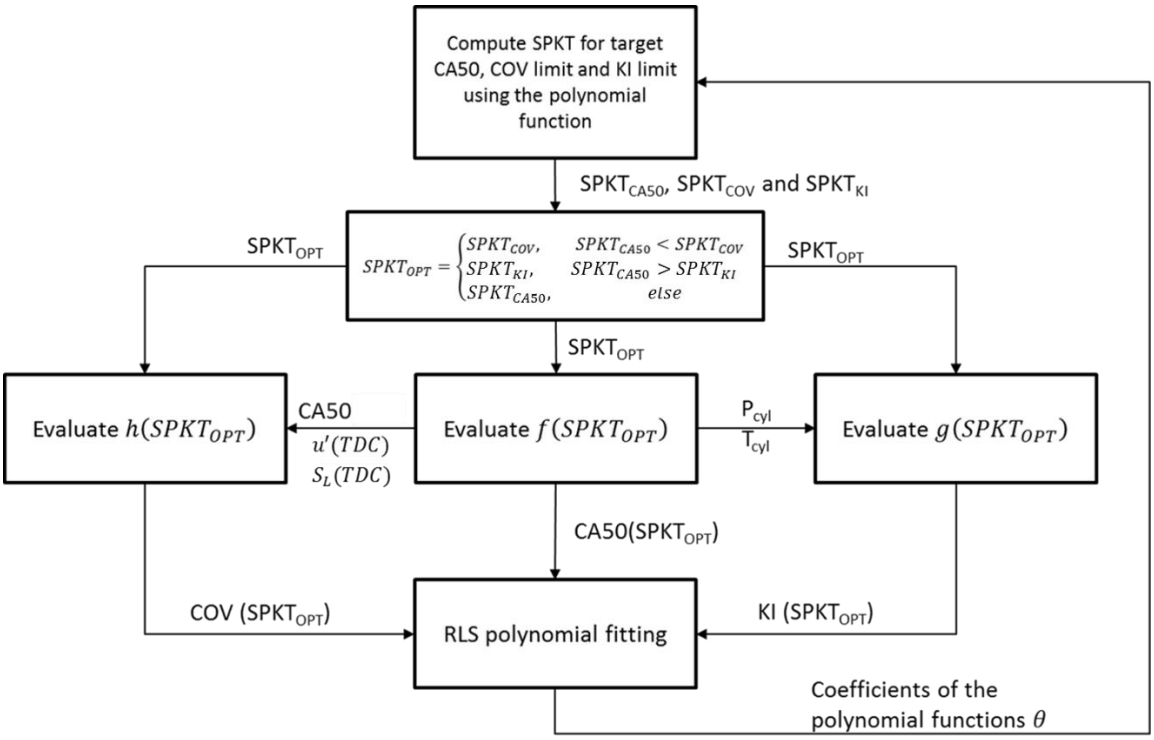

Figure 3.18: Block diagram of the RLS polynomial fitting based SPKT optimization algorithm.

The $SPKT_{OPT}$ converges to the actual optimal value as the polynomial approximation improves with more iterations. The original nonlinear function $f(SPKT)$, $g(SPKT)$ and $h(SPKT)$ may not be perfectly fitted with a low order polynomial. However, this assumption becomes more reasonable as the optimization converges to a small region around the optimal solution. The objective and constraint functions have small curvature in this region, and can be approximated with linear or quadratic functions. Furthermore, this SPKT optimization approach preserves the dependence of the COV and knock constraints on the combustion model. Therefore, each iteration only requires a single execution of the combustion model. The algorithm can be terminated when the variation of $SPKT_{OPT}$ or the coefficient estimation covariance P is smaller than

a certain threshold which can be determined by the available computation power of the ECU.

The polynomial functions that approximate the original $f(SPKT)$, $g(SPKT)$ and $h(SPKT)$ are parameterized as:

$$Y = X^T\theta \tag{3.19}$$

Where:

$Y \in \mathbb{R}^{1\times1}$ is the output CA50, COV of IMEP or knock integral.

$X \in \mathbb{R}^{m\times1}$is the input vector

$[SPKT^0, SPKT^1, SPKT^2 \dots SPKT^m]$

$\theta \in \mathbb{R}^{m\times1}$ is the coefficient vector to be estimated.

Define positive definite covariance matrix $P \in \mathbb{R}^{m\times m}$ as:

$$P_k = \sum_{i=1}^{k} X(i)X^T(i) \tag{3.20}$$

Where:

k is the current number of iterations.

Then:

$$P_k^{-1} = P_{k-1}^{-1} + X(k)X^T(k) \tag{3.21}$$

Using the Matrix Inversion Lemma and rearrange:

$$P_k = P_{k-1} - \frac{P_{k-1}X(k)X^T(k)P_{k-1}}{1 + X^T(k)P_{k-1}X(k)} \tag{3.22}$$

The estimation is recursively updated with new output $Y(k)$ and input data $X(k)$ after evaluating $f(SPKT_{OPT})$, $g(SPKT_{OPT})$ and $h(SPKT_{OPT})$ during each iteration.

$$\theta(k) = \theta(k-1) - K_k[Y(k) - X^T(k)\theta(k-1)] \tag{3.23}$$

Where the estimation gain K_k can be calculated as:

$$K_k = \frac{P_{k-1}X(k)}{1 + X^T(k)P_{k-1}X(k)} \tag{3.24}$$

It was proven by previous researchers that the estimation results of the RLS algorithm minimizes the sum of accumulated squared estimation error and weighted squared distance from the initial guess, $\theta(0)$.

$$\theta(k) = \arg\min_{\theta} \frac{1}{2}\left\{\sum_{i=1}^{k}[Y(k) - X^T(k)\theta(k-1)]^2 + [\theta - \theta(0)]^T P_0^{-1}[\theta - \theta(0)]\right\} \tag{3.25}$$

A good initial guess of θ will no doubt reduce the number of iterations over which the RLS algorithm and the entire optimization program converges. Therefore, $\theta(0)$ can be calibrated and tabulated under various engine operation conditions to reduce online computational burden. This will also result in a smaller P_0, which represents a higher confidence level of the initial guess.

The order of the polynomial functions can be freely chosen. Linear or quadratic functions are recommended for the simplicity. It is also possible to parameterize other forms of nonlinear functions to fit the original $f(SPKT)$, $g(SPKT)$ and $h(SPKT)$. However, similar to high order polynomial functions, some parameters may have high

sensitivity leading to robustness and stability issues. This issue can be observed even with quadratic fitting since the shape of the quadratic curve is much more sensitive to the second order term than the other two. While the RLS algorithm does not weight these parameters separately, noise (model inaccuracy) can significantly alter quadratic coefficient estimation and impact the performance of the first few iterations. One solution to the sensitivity issues caused by model quality is to apply linear fitting. However, a forgetting factor technique is recommended since the original $f(SPKT)$, $g(SPKT)$ and $h(SPKT)$ are nonlinear. RLS with a forgetting factor minimizes the exponentially decaying weighted squared error.

$$\theta(k) = \arg\min_{\theta} \frac{1}{2}\left\{\sum_{i=1}^{k} \alpha^{k-1}[Y(k) - X^T(k)\theta(k-1)]^2 + [\theta - \theta(0)]^T P_0^{-1}[\theta - \theta(0)]\right\}, \quad 0 < \alpha \leq 1 \tag{3.26}$$

The estimation gain and error covariance matrix can be calculated as:

$$K_k = \frac{P_{k-1}X(k)}{\alpha + X^T(k)P_{(k-1)}X(k)} \tag{3.27}$$

$$P_k = \frac{1}{\alpha}\left[P_{k-1} - \frac{P_{k-1}X(k)X^T(k)P_{k-1}}{\alpha + X^T(k)P_{(k-1)}X(k)}\right] \tag{3.28}$$

α is the forgetting factor in this equation. Asmaller α results in less impact from the historic data. Equation (3.26) returns to the original RLS algorithm when $\alpha = 1$. Figure 3.19 shows the effect of the forgetting factor on fitting $f(SPKT)$ with a linear

function $CA50 = aSPKT + b$. It can be seen that the convergence rate is much faster with $\alpha = 0.5$ than $\alpha = 1$.

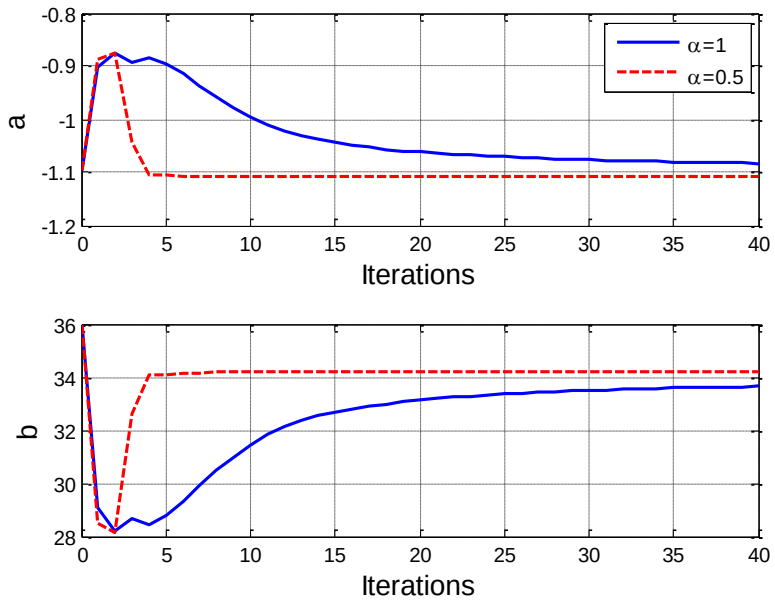

Figure 3.19: RLS fitting the function CA50 (SPKT) with linear functions. The forgetting factor significantly accelerates the convergence rate.

Despite the sensitivity issues, the quadratic fitting has one unique advantage that it can capture the lower bounds of the admissible CA50, COV of IMEP and knock integral. For instance, the minimum achievable COV of IMEP at 1000 RPM and 0.7 bar MAP (green dashed line in Figure 3.14) is 2%. The fitted quadratic function can capture this point and terminate the optimization immediately if the COV limit is set as 1%.

3.2.6 Simulation and Experimental Results

The three proposed SPKT online optimization approaches were tested together in simulation. The RLS polynomial approach uses quadratic fitting without a specifically tailored initial guess. Figure 3.20 shows a section of the results where the optimizers must

handle active COV limits (160 ~ 170 s and 180 ~ 190 s) and KI limits (200 ~ 210 s). During these situations, the optimizers find the SPKT that generates CA50 closest to the target without violating COV and KI constraints. It can be seen that these three optimizers calculate a similar SPKT proving that all of the approaches achieved their objective. However, it is also observed that the RLS polynomial approach has a significant advantage in terms of the number of iterations. This comparison could not be carried out online since the ETAS ES910 system can only compute the high-fidelity combustion model around 10 times per engine cycle (depending upon engine RPM).

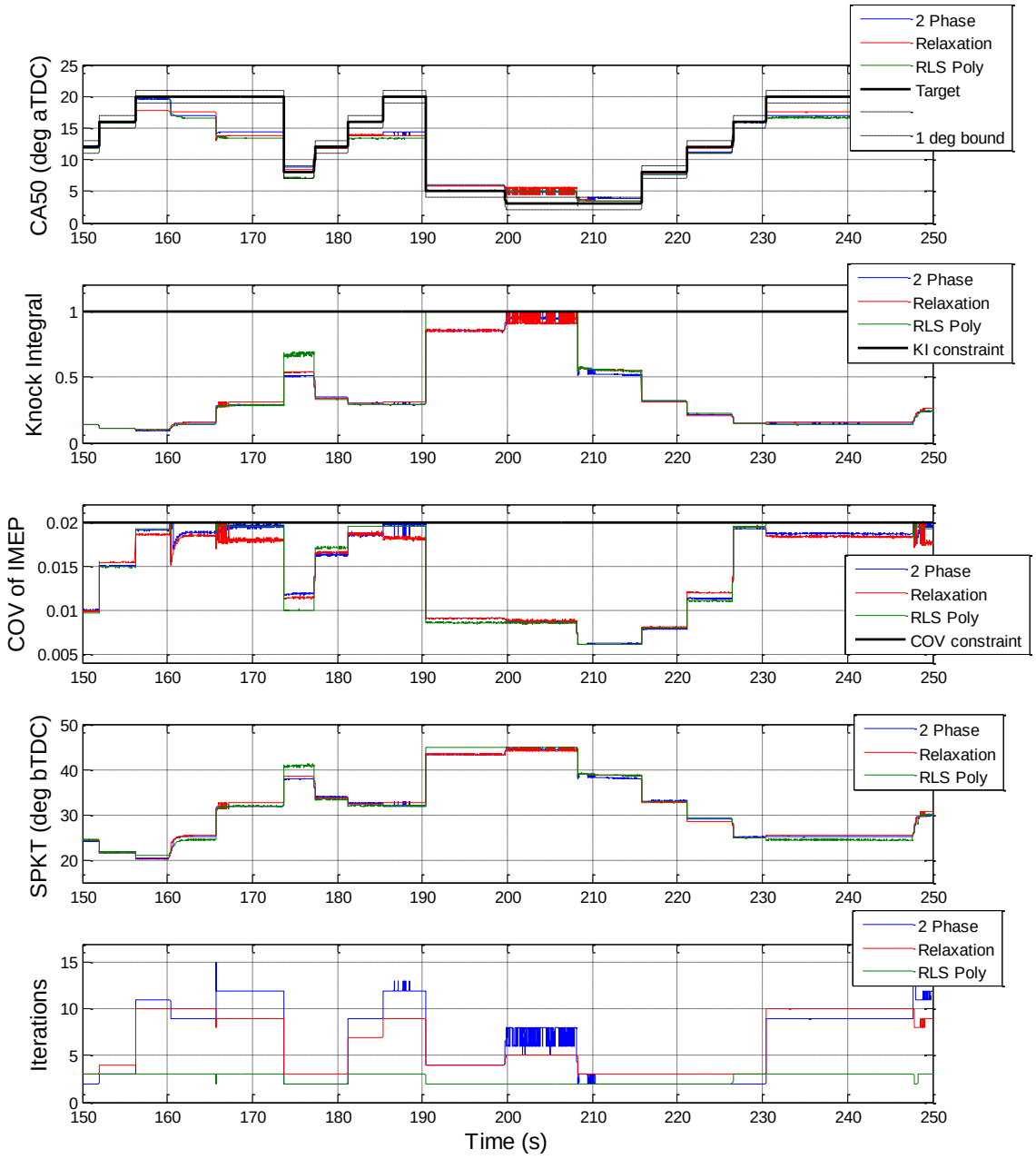

Figure 3.20: Comparison between the three proposed SPKT online optimization methods. The results are generated by simulation with model input data from dyno testing.

Figure 3.21 shows the dyno test results of the 2-Phase SPKT optimizer. The section from 7000 ~ 8000 engine cycles shows the optimizer handling the COV of IMEP limit while the KI limit compromises the original CA50 target during the section from

10000 ~ 12000 engine cycles. The black dashed line in the number of iterations plot shows the iterations for phase 1. The difference between the total number of iterations and that of phase 1 is the iterations required to run phase 2. It can be inferred that the 2-Phase algorithm can be very computationally efficient if provided with a feasible start point eliminating phase 1 optimization.

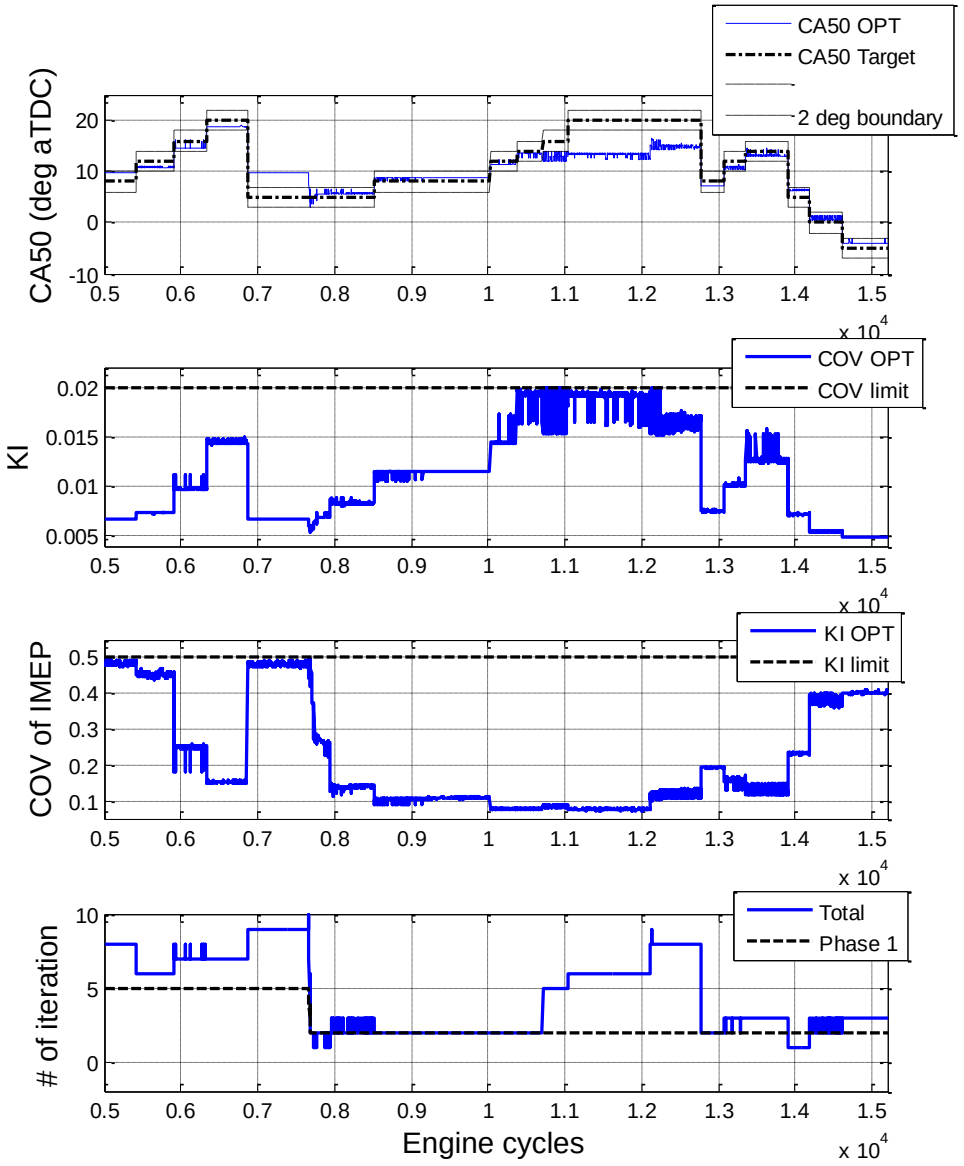

Figure 3.21: Dyno test results of the 2-Phase SPKT optimizer.

3.2.7 Conclusions

This research work proposes three online optimization methods for generating a SPKT to achieve a target combustion phasing without violation of knock and COV of IMEP constraints. These approaches can be integrated with complex and accurate combustion models. Online model based SPKT determination can significantly reduce calibration effort relative to traditional map-based SPKT control. Both simulation and real-time experimental results indicate that these three algorithms can find the optimal SPKT with relatively few iterations, making them candidates for implementation in future engine ECUs.

Table 3.2 compares the three proposed online SPKT methods. The unique advantages of each algorithm makes each preferable for certain types of combustion models. The RLS polynomial fitting method can find the optimal SPKT in the least number of iterations compared with the other two methods by solving three low order polynomial equations. The convergence rate of this method depends on how fast the RLS algorithm can identify the parameters of these polynomial equations to match the original complex combustion models. This process can be finished within a minimal number of iterations if the combustion models have a continuous and smooth correlation with SPKT.

There are two advantages of the 2-Phase approach although generally it requires more iterations. The first advantage is that the optimal solution does not violate any constraints if the program is terminated normally, whereas the other two algorithm permit slight violation of constraints. The interior point algorithm guarantees a feasible search

region and strictly decreasing objective function values. Although it may be possible to manipulate the termination rules to keep the algorithm running until finding a feasible solution, many more iterations will be added since the algorithm has already converged and the current step size is very small. The second advantage of the 2-Phase algorithm is that it does not require strict convexity and continuity of the objective and constraint functions. The constraint relaxation method integrates the original constraints into the objective functions with high penalties, demanding absolute convexity of the knock and COV of IMEP models. The most important advantage of the constraint relaxation method is that it does not need to handle constraints explicitly. Thus the program is more compact. The RLS algorithm has a slow convergence rate to fit the combustion models with coarse model resolution and inaccurate initial guesses. This advantage of the 2-Phase algorithm makes it favorable if one wants to reduce computational burden by decreasing the numeric integration step size of the combustion model.

Table 3.2: Comparison between the three proposed SPKT optimization algorithms

	2 phase	**Constraint Relaxation**	**RLS Polynomial Fitting**
Mean number of iterations	7	6	3
Algorithm Complexity	Medium	Low	High
Slight violation of constraints	No	Yes	Yes
Requirement of obj. and const. function continuity	No	Yes	Suggested

3.3 Model Based Combustion Phasing Estimation

The highly transient operational nature of passenger car engines makes cylinder pressure based feedback control of combustion phasing difficult. The problem is further complicated by cycle-to-cycle combustion variation. A method for fast and accurate differentiation of normal combustion variations and true changes in combustion phasing is addressed in this research. The proposed method combines the results of a feed forward combustion phasing prediction model and "noisy" measurements from cylinder pressure using an iterative estimation technique. A modified version of an Extended Kalman Filter (EKF) is applied to calculate optimal estimation gain according to the stochastic properties of the combustion phasing measurement at the corresponding engine operating condition. Methods to improve steady state CA50 estimation performance and adaptation to errors are further discussed in this research. Finally, the proposed CA50 observer was applied to a SI engine and validated with simulation and dynamometer tests using a prototype engine controller. The new method provides more responsive and accurate CA50 estimation performance than discrete low pass filter techniques.

3.3.1 Introduction

Control of combustion phasing with cylinder pressure feedback is difficult due to cycle-by-cycle variations and the highly transient operational nature of passenger car engines. The phasing of combustion, generally defined by crank angle location at which certain portion of the fuel energy is released (e.g. CA10, CA50 and CA90), has a significant impact on the engine performance (*Caton 2014* and *Zhu et al. 2003*). Real-

time calculation of these combustion phasing variables is possible using the Rassweiler and Withrow method (*Caton 2014* and *Rassweiler 1938*) on measured cylinder pressure. However, cycle-by-cycle combustion variations make it difficult to determine if a shift in mean combustion phasing occurs in a very small sample set of engine cycles. To demonstrate the effectiveness of the proposed methodology, this research uses the example of CA50 estimation. Although the proposed approach can be used with different types of IC engines with a corresponding combustion phasing model, its application with SI engines is primarily discussed in this document.

Applying a moving average, or discrete low pass filter (treating each engine cycle as an event k), is the most intuitive and common solution to the CA50 estimation problem. With this approach, filter design inevitably involves a tradeoff between accuracy and responsiveness. For most applications, the moving average filter order n is from 10 to 20 engine cycles to generate a reasonably accurate estimation of CA50. This response time is considered very slow for most real world driving situations, where there are not many steady-state events that last more than a few engine cycles.

$$CA50_{est}(k) = \frac{1}{n}\sum_{i=0}^{n} CA50(k-i)\,, k = 1,2\ldots \tag{3.29}$$

Although most simplified models developed for feed-forward CA50 control suffer from accuracy issues, these models can be implemented as a "virtual CA50 sensor". This additional prediction can be combined with the cylinder pressure based CA50 feedback, generating a fast and accurate estimation of the combustion phasing. Previous researchers

(*Song et al. 2001, Shrestha et al. 1999, Lafossas et al. 2005, Richard et al. 2009, Le Berr et al. 2006, Lee et al. 2010, Bougrine et al. 2009* and *Hall et al. 2012*) presented models that can be used to predict CA50 for a SI engine. Most of these models are physics based and control oriented, so they can be run online within each engine cycle. These models ignore cycle-by cycle dynamics since they are difficult to predict for most operating conditions.

A Kalman Filter (KF) method was developed to estimate linear system states under the influence of measurement noise and actuation disturbance (*The Analytic Sciences Corporation 1974*). If the noise\disturbance is Gaussian distributed and the system dynamics are Linear Time Invariant (LTI), the KF has proven to provide the optimal estimation of system states (*Kalman 1960).* The KF based estimation approach is especially favorable for systems whose states are affected by their time history. These dynamics help to converge steady state estimation error. *Ghazimirsaied et al. (2009)* and *Ravi et al. (2006)* identified that the CA50 of Homogeneous Charge Compression Ignition (HCCI) engines is strongly affected by the engine states of previous engine cycles. These dynamics were exploited by (*Ravi et al. 2007, Chiang et al. 2005, Shaver et al. 2005* and *Bengtson et al. 2006*), who applied EKF based techniques on nonlinear CA50 dynamics models for HCCI engine control. Most of these methods calculate their estimation gain using the stationary solution of the algebraic Riccati equation. The proposed method considers the dynamics of estimation variance. This approach improves the steady state estimation accuracy and transient state responsiveness. Previous combustion research has shown that the variation of combustion phasing can be very

different according to IC engine operating conditions (*Lee et al. 2009*). Therefore, the estimation gain should be calculated according to the combustion stochastic characteristics of current engine operation conditions. To achieve this goal with stationary KF, one can either solve the Riccati equation online or store pre-calibrated values in a look up table. Both approaches cost either additional computation power or memory demand and calibration time. As for the proposed approach, the variance of combustion can be conveniently included with recursive calculation of estimation gain. Applying a KF to the CA50 estimation of SI engines is rarely discussed due to the lack of cyclic dynamics that helps converge the estimation error. This document demonstrates that applying a KF to SI engine CA50 estimation can also significantly reduce the impact of measurement noise and modeling errors. The proposed approach utilizes steady and transient state switching operation modes to reduce steady state error without sacrificing transient response. The KF based combustion phasing estimator was augmented with a forgetting factor to guarantee observability for situations with significant modeling errors.

This chapter of the dissertation presents a generalized KF based CA50 estimation method which can be used for applications with and without consideration of cyclic dynamics. Methods to improve steady state estimation performance and response to un-modeled dynamics are also discussed. It is shown by this research work that the optimal estimation gain of a KF should be calculated considering the stochastic properties of combustion variation. Basic model assist filter algorithm is described in the next section. This section is followed by a discussion of methods to improve KF performance with an

adaptive switching mode structure, forgetting-factor, and determination of weighting based on combustion variation analysis. Finally, simulation and test results are presented and conclusions are drawn.

3.3.2 Model Assist Filtering

Most explicit models of CA50 consist of exogenous terms relating combustion phasing to current engine operation conditions and n^{th} order homogeneous or auto-regression terms reflecting the cyclic dynamics of CA50 (*Ravi et al. 2007, Chiang et al. 2005, Shaver et al. 2005* and *Bengtson et al. 2006*). The generalized canonical form of the CA50 model presented in this research is expressed as the following:

$$\begin{aligned} CA50_{est}^{(n)}(k) &= f\left[CA50_{est}^{(n)}(k-1)\right] \\ &\quad + \begin{bmatrix}1\\0\\\vdots\end{bmatrix}\left[g(RPM, MAP, SPKT \ldots) + w(k)\right] \\ CA50_{est}(k) &= [1 \quad 0 \quad \ldots]CA50_{est}^{(n)}(k) \\ w(k) &\sim N[0, Q(k)] \end{aligned} \tag{3.30}$$

The existence of $w(k)$ is due to the modeling error and measurement noise of engine operating conditions. While the homogeneous term f is often constructed linearly or it can be approximated with a 1st order Taylor series expansion and linearized at any specific operating point. Therefore, equation (3.30) can be transformed into:

$$CA50_{est}^{(n)}(k) = A(k)\, CA50_{est}^{(n)}(k-1) + H^T[g(RPM, MAP, SPKT \ldots) + w(k)]$$

$$CA50_{est}(k) = H\, CA50_{est}^{(n)}(k) \quad (3.31)$$

$$\text{with} \quad H = [1, 0, \ldots 0]$$

The CA50 measurement at the k^{th} cycle can be considered as the "true" CA50 corrupted with white noise v:

$$CA50_m(k) = HCA50_t^{(n)}(k) + v(k) \quad (3.32)$$

$$\text{with} \quad v(k) \sim N[0, R(k)]$$

The recursive estimation of CA50 can be formulized as the following:

$$CA50_{est}^{(n)}(k)^+ = CA50_{est}^{(n)}(k)^- + L(k)\left[CA50_m(k) - H\, CA50_{est}^{(n)}(k)^-\right]$$

With $CA50_{est}^{(n)}(k)^-$ Prior state estimate at step k (3.33)

Where $L(k)$ is estimation gain

The determination of estimation gain $L(k)$ is to minimize the covariance of estimation error $P(k)$. With the information of disturbance and noise variance [$Q(k)$ and $R(k)$, will be discussed in a later section], the estimation gain can be optimally obtained by the KF method. Prior and post estimate errors and corresponding covariance are defined as:

$$CA50_e^{(n)}(k)^+ = CA50_{est}^{(n)}(k)^+ - CA50_t^{(n)}(k) \tag{3.34}$$

$$CA50_e^{(n)}(k)^- = CA50_{est}^{(n)}(k)^- - CA50_t^{(n)}(k)$$

$$P(k)^{\pm} = E\left[\left(CA50_e^{(n)}(k)^{\pm}\right)\left(CA50_e^{(n)}(k)^{\pm}\right)^T\right]$$

Then, substitute equations (3.32) and (3.34) into (3.33) and rearrange:

$$CA50_e^{(n)}(k)^+ = [I - L(k)H]CA50_e^{(n)}(k)^- + L(k)v(k) \tag{3.35}$$

The post estimation error covariance can be updated from prior error covariance by substituting equation (3.35) into (3.34):

$$P(k)^+ = [I - L(k)H]P(k)^-[I - L(k)H]^T + L(k)R(k)L^T(k) \tag{3.36}$$

The prior error covariance is calculated from the post covariance of the previous engine cycle according to the linear system errors propagation theorem:

$$P(k)^- = A(k-1)P(k-1)^+A^T(k-1) + Q(k-1) \tag{3.37}$$

The optimal estimation gain $L^*(k)$ is used to minimize the post estimation error covariance $P(k)^+$ in equation (3.36). This can be achieved by finding the $L(k)$ that minimizes $J(k) = \text{trace}[P(k)^+]$:

$$\frac{\partial J(k)}{\partial L(k)} = 0 \tag{3.38}$$

The solution of equation (3.38) is:

$$L(k) = P(k)^-H^T[HP(k)^-H^T + R(k)]^{-1} \tag{3.39}$$

The update between prior and post error covariance can be simplified by substituting equation (3.39) into (3.36):

$$P(k)^{+} = [I - L(k)H]P(k)^{-} \tag{3.40}$$

In the cases that cycle-by-cycle dynamics are neglected (e.g. SI engines), the KF can be greatly simplified as $A(k) = 0$ and $H = 1$. Equation (3.31) is transformed into a stationary model:

$$CA50(k) = g(RPM, MAP, SPKT \ldots) + w(k) \tag{3.41}$$

It can be inferred from equation (3.37) that the prior estimation error covariance is constant:

$$P(k)^{-} = Q(k-1) \tag{3.42}$$

From equation (3.39), the optimal estimation gain can be calculated from the variance of noise $R(k)$ and disturbance $Q(k)$, which is the same as the least square estimation gain for a stationary system.

$$L(k) = \frac{Q(k-1)}{Q(k-1) + R(k)} \tag{3.43}$$

3.3.3 Adaptive Filtering

As a general concept, adaptive filtering represents a class of estimation techniques whose algorithm or involved models evolve with real time measurement. The application of adaptive filtering can reduce accuracy demands of modeling, improve robustness of

the control algorithm and generate better steady state results. The exogenous function $g(RPM, MAP, SPKT \ldots)$ can be extremely complex and highly nonlinear due to the dynamics of charge motion and flame propagation. Since adaptive filtering can update the system model through identification techniques, it is possible to use a fast yet less accurate model in the observer without sacrificing too much performance. A single layer Artificial Neural Network (ANN) with 10 neurons is used in this research to relate CA50 to RPM, intake manifold absolute pressure (MAP), intake camshaft centerline (ICL), exhaust camshaft centerline (ECL) and spark timing (SPKT). Test results indicate that the computational time for the proposed EKF approach with an ANN model is negligible for the prototype controller. Figure 3.22 shows the steady state performance of the ANN model. Though the model captures most of the tendencies, non-trivial steady state errors are present in some cases, which could be corrected by online ANN identification.

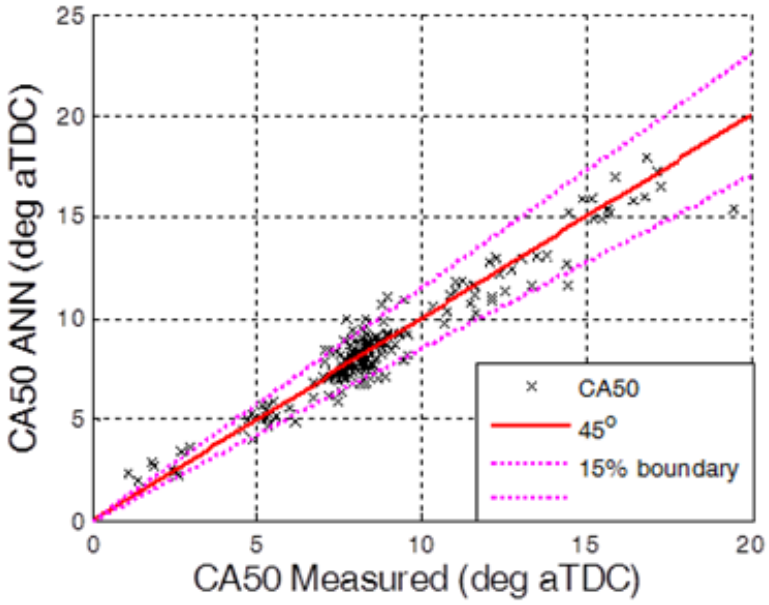

Figure 3.22: Steady state performance of the CA50 ANN model. The ANN has a single layer and 10 neurons. Significant error can be observed in this plot which is intentional to illustrate the benefits of the correction approach.

The online identification of $g(RPM, MAP, SPKT \ldots)$ can be a large computational burden on the engine ECU. Rather than identifying the entire model, this research proposes using a switching mode observer to adapt the system while in steady state conditions. Figure 3.23 shows a block diagram of the switching mode estimator.

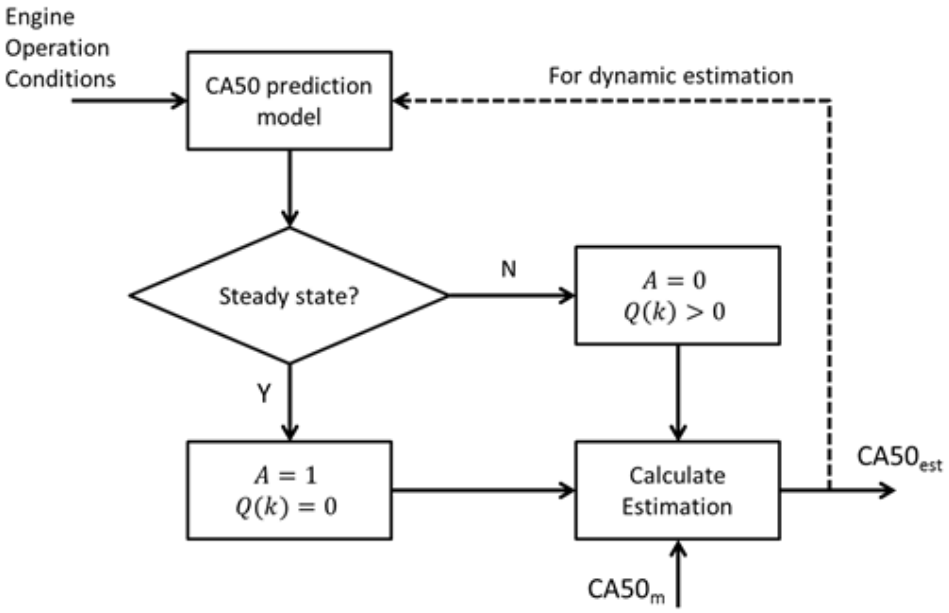

Figure 3.23: Flow chart of switching mode CA50 estimation. The dashed line is for estimation with cycle-by-cycle dynamics.

For steady state mode, by definition, the CA50 of this engine cycle should be the same as the previous engine cycle. Based on this assumption, $A(k) = 1, H = 1, Q = 0$ and the exogenous term is eliminated . Equation (3.31) is transformed into:

$$CA50(k) = CA50_{est}(k-1) \tag{3.44}$$

The estimation gain and covariance can be calculated as:

$$P(k)^- = P(k-1)^+ \tag{3.45}$$

$$L(k) = \frac{P(k)^-}{P(k)^- + R(k)} \tag{3.46}$$

$$P(k)^+ = [I - L(k)]P(k)^- \tag{3.47}$$

After the system switches to steady state mode ($k \geq 1$), the optimal observer gain can be solved analytically in this case:

$$L(k) = \frac{\frac{P(0)}{R(k)}}{1 + \frac{P(0)}{R(k)}k} \tag{3.48}$$

The system is still at transient state at $k = 0$. Therefore, the estimation error covariance is $P(0) = Q(0)$. Upon the system switching to steady state mode ($k = 1$) equation (3.48) returns to equation (15), which is the optimal estimation gain for transient operation. As k increases, the estimation gain $L(k)$ will be close to zero. Therefore, the new measurement will affect estimation results less, yielding to constant steady state results with negligible error from the mean value. The steady state estimation result is equivalent to a moving average method with infinite order. However, it does not require large memory space to store previous measurements due to the recursive nature of this algorithm.

3.3.4 Kalman Filter with Forgetting Factor

One risk of a switching mode observer is that it can fail to identify that the system is in a transient state under some rare occasions, including very slow state transitions, sensor failure, and in the case of significant modeling error. In order to enable the observer to adapt to these situations, it is necessary for the iterative estimation algorithm to "forget" some previous measurement information. This can be achieved by adding a "forgetting factor" α to equation (3.47). A similar concept has been discussed by *Zhu (1999)* and *Bicer et al. (2012).*

$$P(k)^{+} = \frac{1}{\alpha}[I - L(k)]P(k)^{-}, \quad 0 < \alpha < 1 \tag{3.49}$$

Figure 3.24 shows that in the case of steady state, single variable estimation, the estimation gain with forgetting factor decays to a nonzero number $(1 - \alpha)$, instead of zero resulting in loss of observability. This indicates that the new measurement can still affect the estimation results even if the observer is in steady state mode.

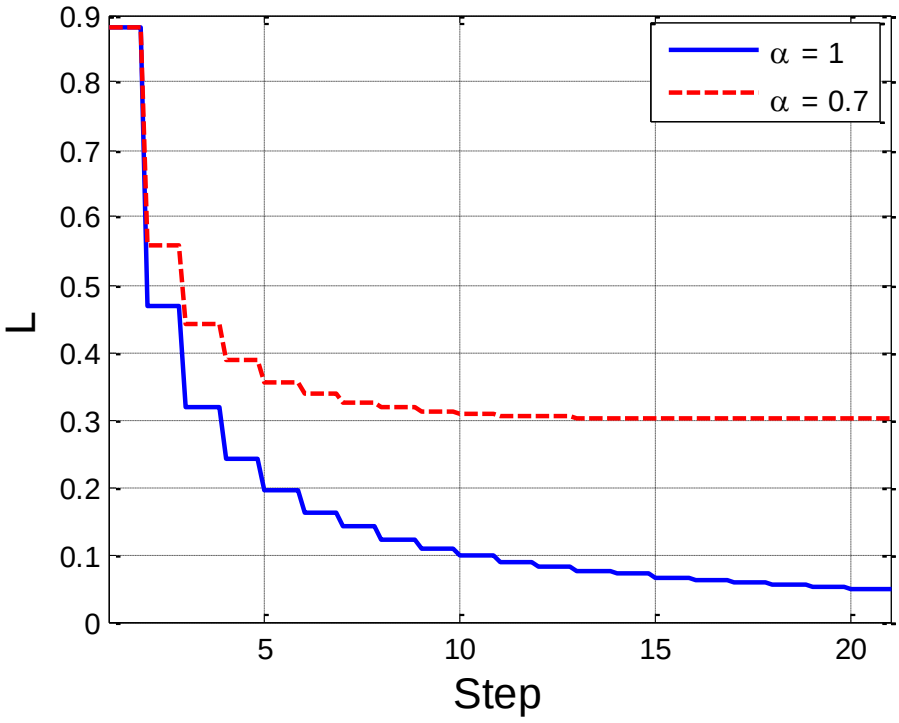

Figure 3.24: Comparison between estimation gains with and without a forgetting factor.

3.3.5 Determination of Weighting Parameters

Variance of the CA50 model (Q) is caused by variation in model inputs. Assuming reasonable sensor quality, the variance of model output is usually very small. On the other hand, the variance of CA50 measurement error (R) is significantly affected by combustion variability. *Lee et al.(2009)* focused on modeling stochastic combustion

characteristics providing a possible solution to predict CA50 variance using measurable engine operation conditions. In this research work, the variance of CA50 measurement is mapped to combustion phasing (CA50) and manifold pressure (Figure 3.25), which could be replaced with an advanced model with better accuracy as desired (Refer to Section 3.1). The accurate estimation of CA50 variance will help the EKF weigh the confidence between measurement and model prediction, resulting in a more reasonable estimation gain.

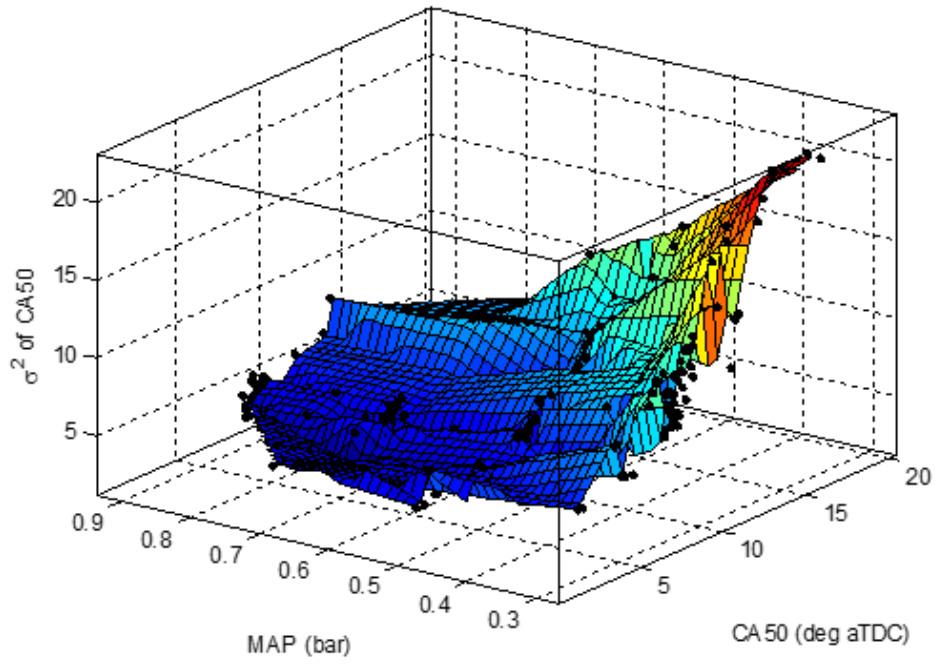

Figure 3.25: Surface plot of CA50 measurement variance corresponding to CA50 and intake MAP.

3.3.6 Results and Discussion

Figure 3.5 shows simulation results of the KF approach with and without the switching mode function. The spark timing is changed at 22s and 27s. The ANN, discussed previously, is used as a CA50 prediction model, and does not utilize an adaptive training function. The 'true' value is the average of the measured CA50 that

would occur over 500 consecutive cycles, which is the reference of a perfect estimation. From this plot, the KF method successfully filtered measurement noise (mostly from cycle-by-cycle combustion variation) and tracks the change of the true value. With the switching mode function, the steady state performance is further improved and demonstrates less oscillation and steady state error. It can also be observed from Figure 3.26 that for specific engine operation conditions the optimal estimation gain L of the stationary KF is constant, which is calculated according to the variance of CA50 measurement and the ANN CA50 prediction model. In comparison, the estimation gain of the KF with switching mode decays to zero (for a sufficiently long time) when the system stays in steady state.

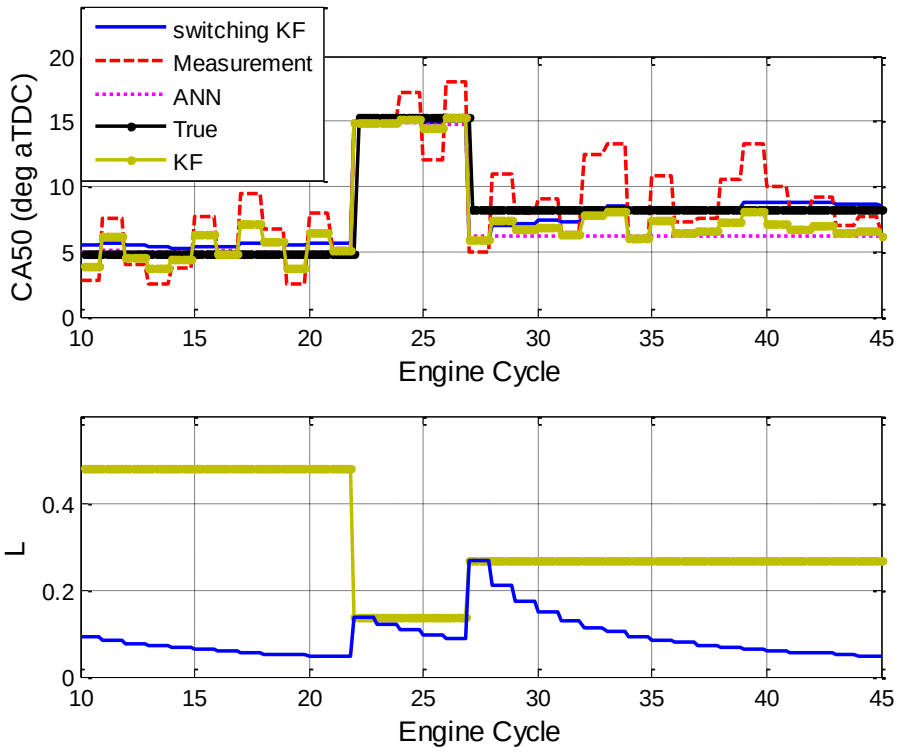

Figure 3.26: Comparison between the KF with and without the switching mode function.

Figure 3.27 shows a comparison between the switching mode KF with and without a forgetting factor. An un-modeled change of engine operating condition is intentionally added at 35s. Neither KF observes the change and both remain in steady state mode. However, since the KF with a forgetting factor has a higher estimation gain, it is still responsive to the new measurement and converges to the new true CA50 within 4 engine cycles.

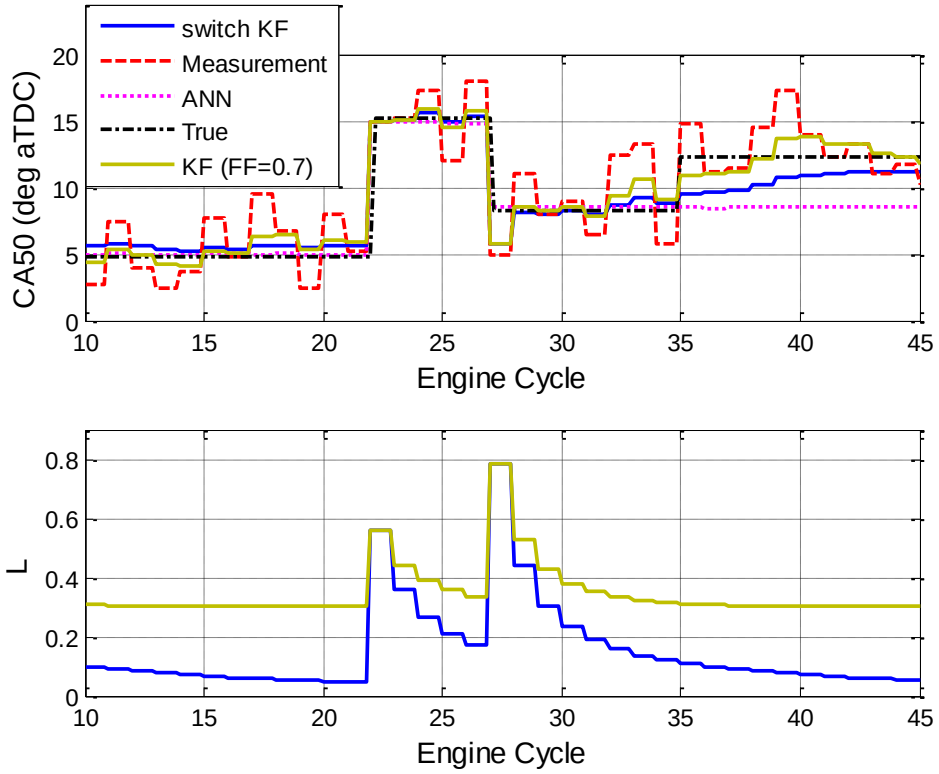

Figure 3.27: comparison between the switching mode KF with and without a forgetting factor (FF).

The switching mode KF with a forgetting factor of 0.7 was validated in real-time on the engine dynamometer (Figure 3.28 to 3.30). The proposed CA50 observer can accurately estimate the true value with acceptable response time even under the influence of significant modeling error. It is also observed from experiment that the proposed

method requires reasonable computational and memory resources, which enables it to be integrated within a production-intent engine ECU. The data demonstrates the proposed KF based approach can generally produce an accurate CA50 estimate within two engine cycles of a mean combustion phasing change, which is significantly faster than mean CA50 estimation with a 10-cycle moving average. This advantage is further demonstrated with actual driving cycle test data in Figure 3.30. The KF based method can quickly determine the mean CA50 change among measurements with poor signal to noise power ratios. Negligible steady state error is observed during real-time experiments. Compared to a moving average (10 engine cycles), the RMS of steady state estimation error for the KF estimation is one order of magnitude lower under both transient and steady state engine operating conditions.

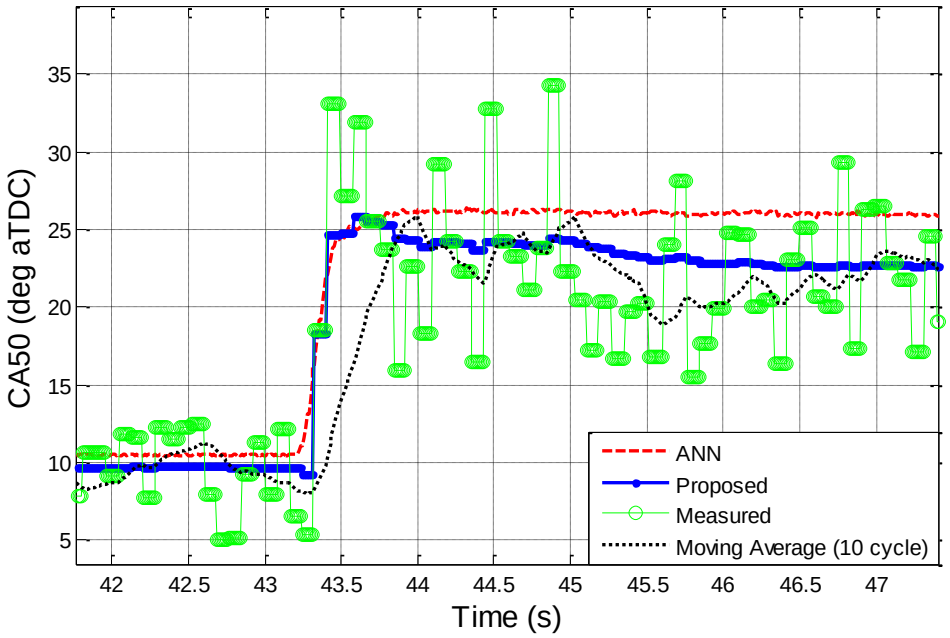

Figure 3.28: Real-time model validation with an intake manifold pressure change at 1500 rpm. The proposed KF method responds faster than a 10 cycle moving average, and creates similar steady-state errors.

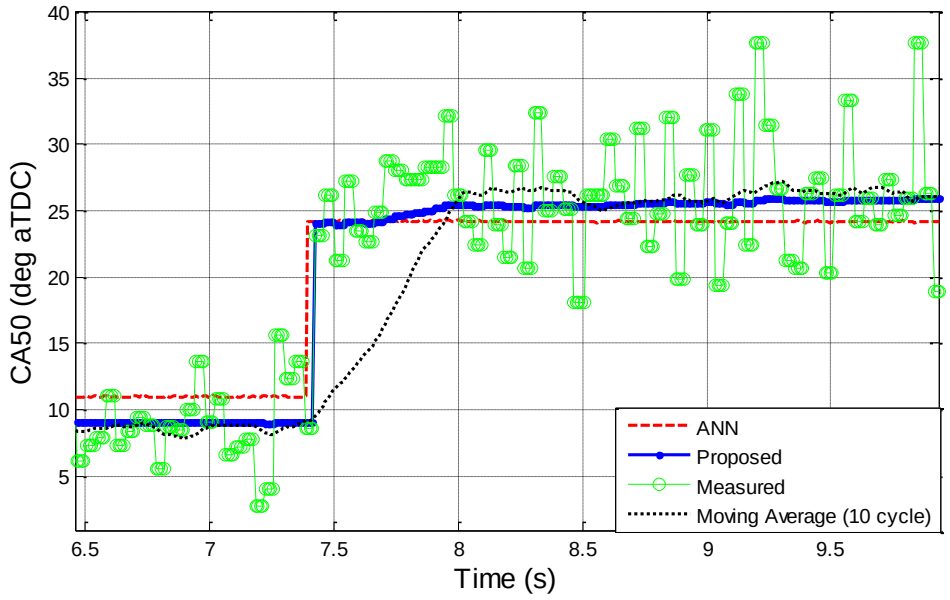

Figure 3.29: A spark timing step change at 3000 rpm shows that that proposed Kalman Filter based CA50 estimation strategy responds significantly faster than a 10-cycle moving average.

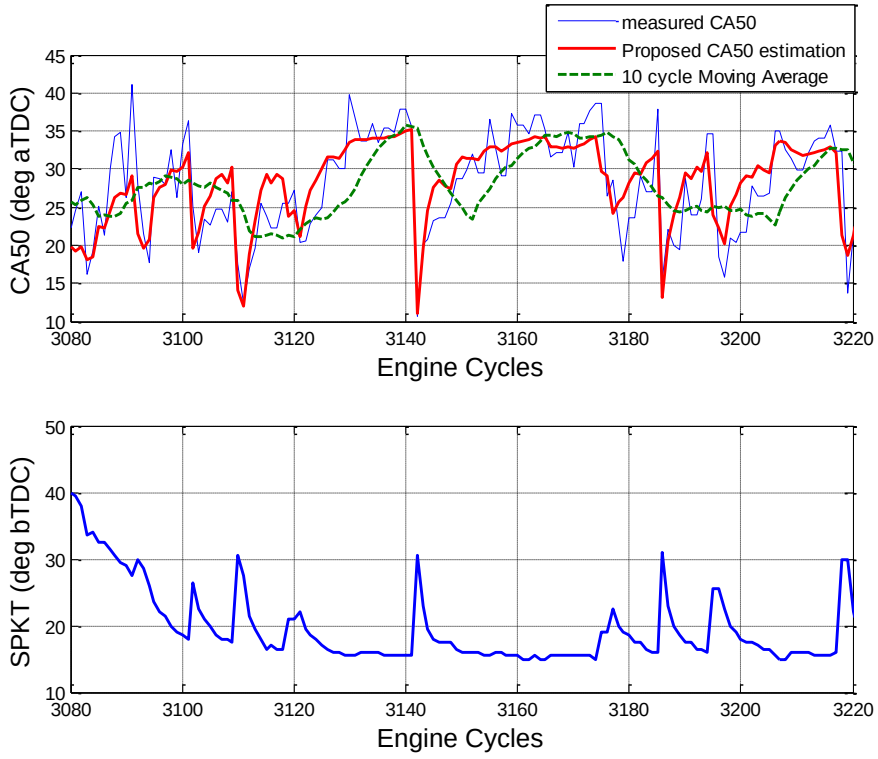

Figure 3.30: Comparison between proposed KF approach and 10 cycle moving average during driving cycle test.

Figure 3.31 compares the discrete low pass filter (Moving Average) technique and switching mode KF with forgetting factor approach in terms of steady state variance versus transient response time. As the filter order increases the moving average approach generates better steady state estimation of the true CA50 while losing responsiveness during transient scenarios. The KF based approach "breaks off" the moving average curve since it is able to achieve less "noisy" steady state estimation without sacrificing transient response time. The forgetting factor ranged from 0.5 to 1. A lower forgetting factor will increase the RMS of steady state estimation and lead to instability (the EKF is not stable when $\alpha < 0.5$). However, lower forgetting factors grant the switching mode KF the ability to recognize un-modeled changes of CA50.

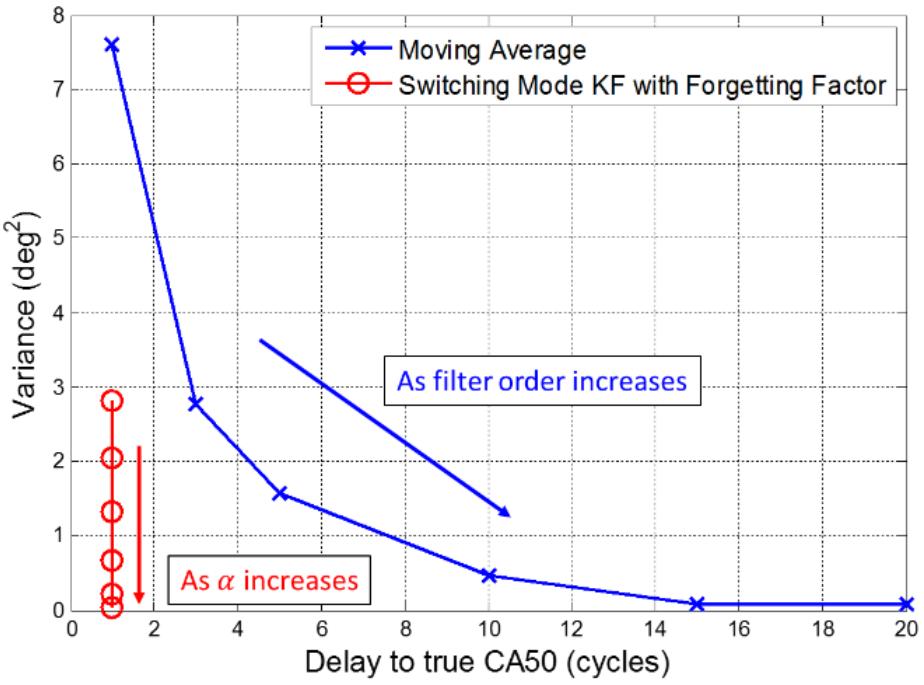

Figure 3.31: Plot of steady state variance versus delay to true CA50.

3.3.7 Conclusions

This research demonstrates an extended Kalman filter based approach to conditioning the CA50 measurement from cylinder pressure sensor feedback. By employing a CA50 prediction model as a "virtual sensor", the Kalman Filter effectively solves the conflict of signal processing between responsiveness and accuracy. The proposed CA50 estimation method was applied to a SI engine and validated with both simulation and real-time transient dynamometer tests. The contributions of this research include:

- The KF based approach can respond to CA50 changes within one engine cycle. Because of this unique property, the approach can be applied to different engine types where strong cycle-by-cycle dynamics are present.
- For applications in SI engines where cycle-to-cycle dynamics can be neglected, steady state error is inevitable since the CA50 model is not perfectly accurate. Instead of adapting the model, it is proposed to use a switching mode estimation adapting to whether the engine is in steady-state or transient operation. Negligible steady state error is observed during real-time experiments. Compared to a moving average (10 engine cycles), estimation error RMS of the KF approach is one order of magnitude lower under both transient and steady state situations.
- The application of a forgetting factor in the switching mode KF significantly improves estimation performance when the CA50 prediction model is very inaccurate or fails to capture certain engine dynamics.

A responsive and reasonably accurate estimation of CA50 makes it possible to employ feedback controllers to regulate combustion phasing. This could potentially reduce amount of calibration work during the development of an IC engine significantly. The estimation results can also be integrated with model based feed forward algorithms to adapt models online.

CHAPTER FOUR

MULTIPLE INPUT MULTIPLE OUTPUT SI ENGINE IMEP OPTIMAL CONTROL

4.1 Introduction

One of the most fundamental control objective of modern IC engine management systems is to provide engine torque output as demanded. At the same time, the control system should minimize fuel consumption while prevents abnormal combustion phenomena that could damage the mechanical components and interrupt the normal operation of the engine. This control objective favors the application of model based optimal control strategy with its clearly stated cost function and constraints. While many articles discussed the possibility of applying MPC to control engine air path (e.g. *Colin et al. 2007* and *Santillo et al. 2013*) and speed (*Di Cairano et al 2012* and *Hrovat et al.* 1996), using MPC to directly regulate torque while reducing fuel consumption and respecting combustion constraints is neither adopted by the industry nor extensively discussed by academic research. *Ali et al.* (2006) demonstrated potential of using LTI MPC to track torque reference. *Lee et al.* (2011) applied Nonlinear MPC (NMPC) on SI engine with VVT to track torque reference and reduce NO_x emission. Both papers were supported by simulation results. There are three reasons contributing to this dilemma:

- It is difficult to directly measure engine torque output and some combustion related engine states on production vehicles. Without these

feedback information, the prediction models in the feed forward loops are required to be very accurate to guarantee engine performance.

- Calibrating these accurate models costs significant amount of time and resources, especially with increasing number of engine actuators. Most of these models cannot be integrated with the modern optimal control theories because of their complex structure and heavy computational burden.
- The optimization program that computes the optimal control actions based on these complex models can be very challenging to solve in real time operation. Each evaluation of the high-fidelity engine models takes significant amount of time for current engine ECUs. This requires the optimizer to find the optimal solution with few number of iterations. Furthermore, the non-convexity of these complex models makes the optimization problem to have multiple local optimums. Some optimization algorithms can find the global optimal solution among these local optimal points like dynamic programming, genetic algorithm and particle swarm. However, the price of these algorithms is that they need to evaluate the objective and constraint functions for thousands of times.

The development of low cost cylinder pressure sensors makes it possible to directly measure IMEP and combustion phasing (*Bertola et al 2015* and *Schten et al 2007*). This provides the opportunity to apply model based estimation techniques to improve the calculation of both measurable and unmeasurable engine states (*Zhu et al.*

2015 and *Arsie et al. 2015*). Therefore, the first challenging factor preventing optimal engine torque control can be solved. Numerous control oriented engine combustion models were developed recently (*Ghojel 2010, Bonatesia et al. 2010, Hall et al. 2012, Lee et al. 2010* and *Bougrine et al. 2009*). Although their physics based nature makes them more adaptive to different engine designs and easier to calibrate, these models are generally more complex and difficult to compute than the traditional look up tables. This chapter of the dissertation focuses on developing a model predictive IMEP control strategy that can utilize these control oriented engine models. Both optimization strategy and control structure are investigated to reduce the computational load during execution. The research focuses on SI engine IMEP control manipulating the air mass flow through throttle, external EGR and combustion phasing. Together with constraints from the system dynamics, the COV of IMEP and auto-ignition are also considered during the optimization of control actions.

Control oriented engine air path and torque generation models are well established (*Guzzella et al.* 2009). Most of these models are constructed in time domain making them favorable to be integrated with controllers of fixed sampling time. The most important drawback of this control strategy is that the IC engine is an inherently discrete event system with its cyclic operation characteristics. If the sampling time scale is finer than the engine cycle, delays caused by the four stroke operation pattern must be considered. For example, the period between induction and power stroke determines that there is a dead time delay of $2\pi/\omega_e$ between torque generation and any air path actuation. On the other hand, some important cyclic dynamics will be neglected if the sampling

time is coarser than the engine cycle. It can be concluded that modeling the engine systems in time domain conflicts with the natural rhythm of the engine and increase the model dependency on the engine speed. The SI engine system is modelled and controlled in the engine cycle domain in this research. While this approach solves the issues discussed previously, it also benefits from the fact that most control oriented combustion models were constructed in the engine cycle domain. This advantage makes it convenient to impose abnormal combustion constraints like auto-ignition and combustion stability during the calculation of optimal control actions. Previous researchers have proposed that engine knock can be accurately predicted by integrating the Arrhenius function output for the end gases (*Livengood et al 1955* and *Xiao et al 2013*). Most automotive OEMs adopted empirical and map based knock model in the engine controllers. The limit for SPKT retard is determined by the COV of IMEP, which is considered as an indicator of combustion stability. The extreme case of unstable combustion corresponds to misfire phenomenon. Researchers have illustrated that combustion variation is the main cause of COV of IMEP (*Ozdor et al. 1994* and *Lacour et al. 2011*). *Lee et al.(2009)* suggested that the COV of IMEP has strong correlation with combustion phasing. Finally, regression models of COV of IMEP have been proposed by *Young (1980), Dai et al. (2000)* and *Galloni (2009)*.

In the context of discrete model predictive control, the control objective and constraints of a certain horizon N into the future are correlated to the control action sequence as functions via the discretized system models. These objective and constraints

functions are employed to formulate an optimization problem (Equation 4.1), the solution of which contains the desired control sequence.

$$\min_{u} h\big(x(N)\big) + \sum_{k=0}^{N-1} g\big(x(k), u(k)\big)$$

$$s.t. \quad \begin{cases} x(0) = x_0 \\ x(k+1) = f\big(x(k), u(k)\big) \\ 0 \geq l_k\big(x(k), u(k)\big), \qquad k = 0,1,2 \ldots N-1 \end{cases} \tag{4.1}$$

where $x \in \mathbb{R}^n$, $u \in \mathbb{R}^m$.

Due to the complex nonlinear nature of turbulent combustion, this optimization problem described in (4.1) is nonlinear for the proposed optimal IMEP control. It is straight forward to apply nonlinear programming techniques to solve this optimization problem. Many research papers discuss the possibility of using nonlinear programming algorithms in the context of MPC (e.g. *Vermillion et al. 2010* and *Benson et al. 2006*). Most of these attempts were not supported by experiment results due to the heavy computational burden of numerous evaluations of system and constraints models. The most practical method to handle this nonlinear optimization problem is to linearize the system dynamics and constraint functions at a specific operating point (x_0, u_0). Often the control objective is correlated to the first and second order terms of the system states x and control action u. Therefore, the nonlinear optimization (Equation 4.1) renders to a Linear Time Variant (LTV) quadratic programming problem, which has more computationally efficient solvers than other nonlinear programming problems. Choosing an efficient linearization method for the originally nonlinear models are not a trivial

question. The plant and constraint models are evaluated many times during this process, which takes significant amount of time to complete. Most LTV MPC applications commonly select first order Taylor series expansion to generate the linear version of their plant models. If the models are complicated, Algorithmic Differentiation (AD) can be applied to efficiently evaluate derivatives (*Quirynen et al 2014* and *Griewank et al 2008*). Both methods rely on the original nonlinear model to be explicit and differentiable. Numeric differentiation methods like Euler methods are favorable if the nonlinear models cannot be linearized analytically. This situation is highly possible in the IC engine control applications where numerous look-up tables are used to model different dynamics.

The LTV MPC technique was successfully applied to many control systems (e.g. *Zhu et al 2015* and *Sharma et al. 2010*). There is a critical disadvantage of applying LTV MPC to control systems with nonlinear dynamics and constraints. The linear approximation of the original models diverges from the true nonlinear behavior as the search for the optimal solution progress further away from the operating point (x_0, u_0). The controller performance evaluated by the control objective decreases if the divergence occurs at the objective functions. It is more critical if the divergence happens at the constraint functions. This will make the calculated control action to be infeasible to be applied to the actual nonlinear system interrupting the operation of the system. For the proposed optimal IMEP control, violating the knock and combustion stability constraints can damage the engine and cause misfire. Furthermore, these constraints are highly nonlinear making the LTV MPC less desirable for this control application.

Sequential Quadratic Programming (SQP) is one of the most successful methods for the numerical solution of constrained nonlinear optimization problems like (4.1). The original SQP was developed by *Wilson* (1963). SQP is an iterative numerical solver of nonlinear constrained optimization. During each major iteration k, the search step Δu_k is calculated by solving a QP sub-optimization problem (with minor iterations).

$$\begin{aligned} &\min_p \frac{1}{2}\Delta u_k^T H_k \Delta u_k + \nabla J_k^T \Delta u_k \\ &s.t. \quad l_{eq}(u_k) + \nabla l_{eq}(u_k)^T \Delta u_k = 0 \\ &l_{ineq}(u_k) + \nabla l_{ineq}(u_k)^T \Delta u_k \le 0 \end{aligned} \tag{4.2}$$

where J is the objective function in (4.1). H_k is the Hessian of J at u_k. G_{eq} and G_{ineq} are functions that complies the equality and inequality constraints in (4.1).

The solution of (4.2) converges to a local optimal solution of (4.1) near the start point u_0 as $k \to \infty$ (*Bertsekas* 1982, *Fletcher* 1981 and *Goodman* 1985) if H_k is the exact Hessian at u_k. In practice, H_k is often approximated with first order derivatives to reduce computational burden. Quasi-Newton methods are well discussed by *Dennis et al* (1983) and *Fletcher* (1987). The *Broyden-Fletcher-Goldfarb-Shanno* (BFGS) rank-two update method is widely used in SQP applications (*Broyden* 1970 and *Nocedal* 2000). The Hessian was estimated iteratively (major iterations) using the following equation:

$$\widehat{H}_{k+1} = \widehat{H}_k - \frac{\widehat{H}_k \delta \delta^T \widehat{H}_k}{\delta^T \widehat{H}_k \delta} + \frac{\varepsilon\, \varepsilon^T}{\varepsilon^T \delta} \tag{4.3}$$

$$\delta = u_{k+1} - u_k$$

$$\varepsilon = \nabla_u J(u_{k+1}) - \nabla_u J(u_k)$$

There are other approaches to compute or approximate the Hessian matrix. *Goldsmith* (1999) proposed disaggregated Hessian approximation approach, which is more computational effective than the BFGS method. *Quirynen et al.* (2014) proposed to use algorithmic differentiation approach to calculate the exact Hessian. It was claimed that this computation can be fast enough to be considered for real time MPC applications.

Another challenge for SQP approach is that currently efficient QP solvers can only handle convex problems. However, the exact Hessian for the nonlinear programming problem may not be positive definite, making the sub-QP problem non-convex. *Goldsmith* (1999) developed a non-convex QP solver to work with the disaggregated Hessian approximation method. Although the solver was proved to converge within finite iterations, finding the solution of the sub-QP problem is still not efficient enough to make it a viable option for MPC application. The BFGS methods artificially guarantees the estimated Hessian to be positive definite. However, conflicts arises when the exact Hessian is not positive definite, making the BFGS SQP to have slow convergence rate. *Quirynen et al.* (2014) proposed to use mirrored version of Hessian from eigenvalue decomposition to replace the original indefinite Hessian. Although this method guarantees the Hessian to be positive definite and the sub-QP to be convex, its impact on SQP convergence rate is not well discussed in the literature.

The SQP was developed to solve general continuous nonlinear programming problems. The most important advantage of SQP is that it transformed complex nonlinear programming problems in a sequence of quadratic programming (hence the name), which has computationally efficient solvers. Thus the original nonlinear models are only evaluated during each major iterations, saving significant amount of computation time compared to other nonlinear programming solvers that completely rely on the evaluation of the nonlinear models. The calculation of Hessian is the most critical process of the SQP, which still cost precious time to complete for fast MPC applications. For MPCs designed to track designated references, the objective function takes a specific least square format. Knowledge of this format can be utilized to simplify the SQP formulation and solution. The control objectives of the proposed IMEP optimal control makes it an obvious "tracking" MPC strategy. While SQP is the approach to solve the nonlinear programming in real time, concept of LTV MPC is borrowed to accelerate the conventional SQP algorithm. Methods to improve convergence rate are also discussed in this document.

The reset of this chapter is organized as follows: Section 4.1 introduces the cascaded control structure of the proposed optimal SI engine IMEP management system. The SQP MPC is place at a control tier that can greatly simplify the prediction model without losing control authority completely. The next section discusses the cycle-by-cycle model predictive IMEP control. This section includes sub-sections of modeling and analysis, optimization problem formulation and modified SQP algorithm for tracking MPC applications. Section 4.3 presents some simulation results of the proposed control

system. Finally Section 4.4 concludes the contribution of this chapter and possible future extension.

4.2 Cascaded Control Structure

There are two reasons to place the SQP MPC at the higher control level with slower update frequency. The first reason is to simplify the modeling process by transferring nonlinear and fast dynamics to lower level controllers. Although the SQP is able to solve nonlinear programming problems, the formulation of the sub-QP problem during each major iteration takes a significant portion of the computation time since it often requires numerous evaluations of the system and constraint models. Simple models can significantly reduce the computational load of entire control system. It is almost impossible to construct perfectly accurate models for IC engine systems, especially considering the turbulence combustion characteristics. Therefore, it is not reasonable to believe that the control action calculated using these models are perfect. Automotive OEMs need simple and effective ways to correct for modelling errors. Therefore, it is desirable for the MPC controller to relinquish some control authority to the simpler fast controllers downstream the control hierarchy. These map or simple feedback controllers provide the abilities to fine tune the controller performance. They are also fast enough to fully exploit the actuators' bandwidth.

Figure 4.1 shows the block diagram of the SI engine system with external EGR. This document focuses on the optimal IMEP controller manipulating throttle air mass flow per cycle, EGR mass flow per cycle and CA50 (Figure 4.1labelled in green). These variables are sent to lower level controllers as references to track. The manipulated variables of the lower level controllers are represented by yellow in Figure 4.1.

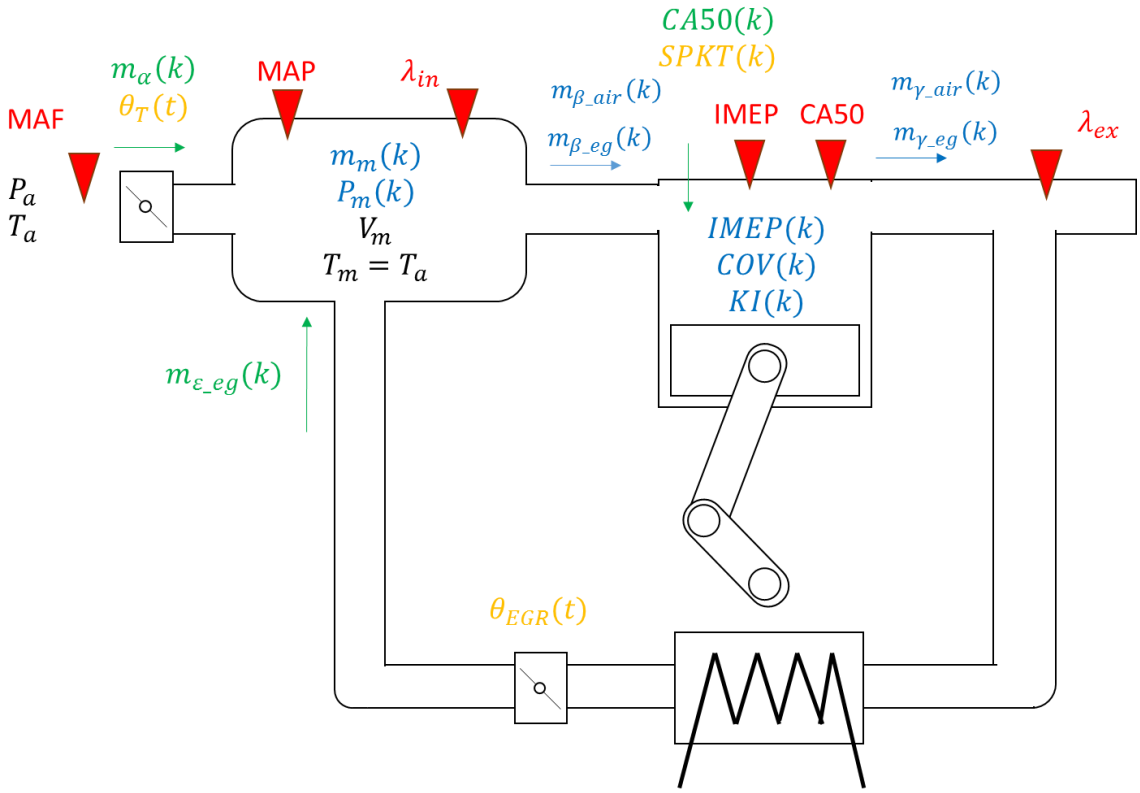

Figure 4.1: Block diagram of the SI engine system with external EGR. Variables in red are measured by sensors. Blue represent system states that need to be modelled. Green variables are manipulated by the proposed optimal IMEP controller. Variables in yellow are controlled by lower level controllers.

The throttle and EGR valve opening are controlled in time domain with sampling rate much faster than one engine cycle. The correlation between the flow rate and valve opening can be accurately modelled with orifice flow equations:

$$\dot{m} = C_D A \frac{P_i}{\sqrt{RT_i}} \begin{cases} \sqrt{\gamma \left(\frac{2}{\gamma+1}\right)^{\frac{\gamma+1}{\gamma-1}}}, & P_o < P_{cr} \\ \left(\frac{P_o}{P_i}\right)^{\frac{1}{\gamma}} \sqrt{\frac{2\gamma}{\gamma-1}\left[1-\left(\frac{P_o}{P_i}\right)^{\frac{\gamma-1}{\gamma}}\right]}, & P_o \geq P_{cr} \end{cases} \tag{4.4}$$

$$\text{with } P_{cr} = P_i \left(\frac{2}{\gamma + 1}\right)^{\frac{\gamma}{\gamma - 1}}$$

where C_D is discharge coefficient. A is effective valve opening area. P_i and P_o are the pressure of the inlet and outlet of the valve. R is gas constant. γ is heat capacity ratio. T_i is the inlet air temperature. Although the orifice model is highly nonlinear, the relationship between flow rate and valve opening is primarily static without dependence on time history. Therefore, tracking the accumulated air mass flow for one engine cycle can be easily achieved by a look-up table and PI controller.

The CA50 is widely used as an indicator of combustion phasing, which has important influence on the engine efficiency, combustion stability and emission. The combustion phasing physically describes the synchronization between the combustion process and piston movement regardless of the engine operation conditions, making it to have a more definitive correlation with engine performance related variables than using SPKT directly. However, the demanded combustion phasing must be translated into SPKT. A lower level controller is used to track the CA50 output from the SQP MPC IMEP controller, avoiding the necessity to incorporate combustion phasing model with optimization process. This lower level controller can be a simple version of one dimensional combustion phasing optimal control described in Chapter 2. Since the CA50 target generated by the MPC controller has already consider the knock and combustion stability constraints, the number of iterations to find the desired SPKT can be greatly reduced. Furthermore, the MPC control loop includes a model based estimator for most engine states including the CA50, it is convenient for the lower level combustion phasing

controller to maintain its adaptive and feedback functions. Figure 4.2 illustrates the control hierarchy of the proposed MPC oriented IMEP management system for SI engine with external EGR.

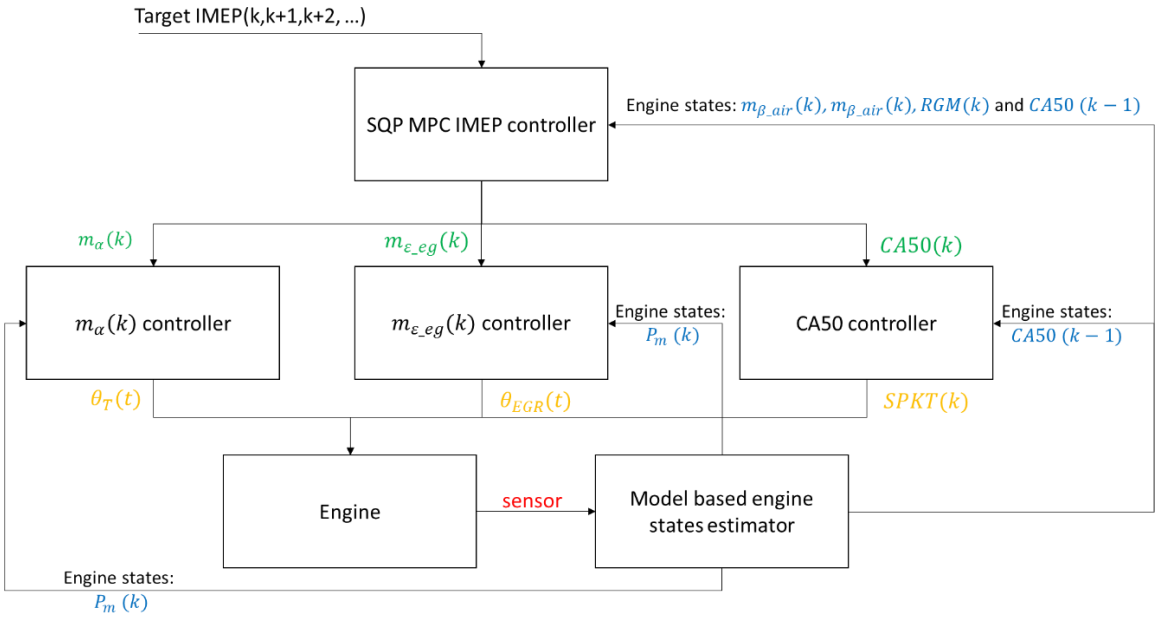

Figure 4.2: Block diagram of the control hierarchy of the proposed optimal IMEP control. Variables in red are measured by sensors. Blue represent system states that need to be modelled. Green variables are manipulated by the proposed optimal IMEP controller. Variables in yellow are controlled by lower level controllers.

4.3 Cycle-by-cycle model predictive IMEP control

4.3.1 Control Oriented Cycle-by-cycle SI Engine System Modelling and Analysis

The air path dynamics contributes most of time history dependency of the IC engine systems. The air path dynamics were modelled in time domain to work with controllers of fixed sampling time. In order to generate engine cycle based air path dynamics model, one can discretize the time domain model (*Guzzella*, 2009 page 161-163). Similar result can generated by considering the cyclic mass balance. The proposed IMEP controller focuses on one cylinder and applies the same control action to the other cylinders. Thus, the sampling time is 4π of crank angle, one cycle of a single cylinder. Assuming the air mass inside the intake manifold is constant during one engine cycle, the combined air and exhaust gas mass flow into the engine m_β can be calculated as:

$$m_\beta(k) = \frac{\eta_V(k) V_d m_m(k)}{V_m} \tag{4.5}$$

where η_V is volumetric efficiency. V_d is engine displacement. V_m is manifold volume. m_m is the air mass inside the manifold.

From the mass balance of the manifold, we have:

$$m_m(k+1) = m_m(k) + m_\alpha(k) + m_\varepsilon(k) - m_\beta(k) \tag{4.6}$$

where $m_\varepsilon(k)$ is the external EGR mass flow into the manifold. For SI engine that often operate at close to stoichiometric AFR, the air and fuel content in the exhaust gas are minimal. They can be treated as external disturbance sources that are neglected under the

discussion of the prediction model for the optimal IMEP controller. From equation (4.5) and (4.6), the air mass flow into the engine during next cycle is:

$$m_\beta(k+1) = \frac{1}{K+1} m_\beta(k) + \frac{K}{K+1} m_\alpha(k) + \frac{K}{K+1} m_\varepsilon(k)$$
$$\text{with } K = \frac{\eta_V(k) V_d}{V_m} \tag{4.7}$$

Equation (4.7) can be separated according to air and exhaust gas species:

$$m_{\beta_{air}}(k+1) = \frac{1}{K+1} m_{\beta_{air}}(k) + \frac{K}{K+1} m_\alpha(k)$$
$$m_{\beta_{eg}}(k+1) = \frac{1}{K+1} m_{\beta_{eg}}(k) + \frac{K}{K+1} m_\varepsilon(k) \tag{4.8}$$

Both equations in (4.8) describes zero order hold discrete equivalent of a continuous first order lag dynamics of air and exhaust gas flow into the engine. Comparing to air-path models in time domain that is strongly depended on engine speed, it is remarkable that the air-path dynamics are invariant in engine cycle domain considering the slow change of volumetric efficiency η_V. Since the air-path dynamics is the slowest in the focused SI engine system, the prediction horizon of the MPC should be determined by the time constant of the first order lag τ described in engine cycle domain with (4.8), which is:

$$\tau \approx \frac{V_m}{V_d} = 2.29$$
$$\text{with } \eta_V \approx 1 \tag{4.9}$$

Therefore, the prediction horizon for the MPC is selected as 2 engine cycles ahead. In time domain, this corresponds to 0.2 ~ 0.02 s (600 RPM to 6000 RPM) preview of the IMEP reference. For modern vehicles with drive-by-wire system and integrated powertrain control, this preview time is not an unreasonable demand.

The manifold pressure can be calculated as:

$$P_m(k) = \frac{m_\beta(k) R T_m}{\eta_V(k) V_d} \tag{4.10}$$

The manifold pressure cannot be higher than the ambient pressure since the engine is naturally aspirated. This is a potential constraint during the formulation of the optimization problem.

The gas composition inside cylinder includes air, exhaust gas, fuel and other minor species that are neglected in this research. The amount of air and fuel can be determined by $m_{\beta_{air}}$ assuming stoichiometric AFR. The amount of exhaust gas inside cylinder is the summation of $m_{\beta_{eg}}$ and RGM. This research adopts the semi-empirical methods proposed by *Fox and et al.* 1993. The Fox model separates the RGM into two parts: 1) exhaust gas backflow into the cylinder and intake runner during the valve overlap period and 2) from trapped residual at exhaust valve closing (EVC) due to un-swept cylinder volume.

$$RGM = m_{trapped} + m_{backflow} \tag{4.11}$$

The trapped mass $m_{trapped}$ can be calculated from the engine clearance volume V_c and burned gas density ρ_b:

$$m_{trapped} = C_1 \rho_b V_c \tag{4.12}$$

where C_1 is a fitting constant.

The burned gas density ρ_b can be estimated with exhaust gas temperature T_{exh} and pressure P_{exh} according to ideal gas law:

$$\rho_b = \frac{P_{exh}}{RT_{exh}} \tag{4.13}$$

The backflow happens during the valve overlap period. The air mass flow for the backflow process is determined by the pressure difference between intake and exhaust manifold, effective flow area, piston motion and engine speed. The original Fox model proposed to use the following equation to compute the backflow mass $m_{backflow}$:

$$m_{backflow} = C_2 \sqrt{\rho_b (P_{exh} - P_m)} A_{flow} \frac{OLV}{\omega_e} \tag{4.14}$$

Where C_2 is a fitting constant.

A_{flow} in equation (4.14) is the effective flow area during the valve overlap period, which can be calculated as:

$$A_{flow} = \int_{IVO}^{OLC} D_i L_i d\theta + \int_{OLC}^{EVC} D_e L_e d\theta \tag{4.15}$$

where IVO is the crank angle of intake valve open. OLC is the crank angle location where the intake and exhaust valves have the same lift. EVC is the crank angle of exhaust valve close. D_i and D_e are the intake and exhaust valve diameter. L_i and L_e are the lift of intake and exhaust valve. θ is crank angle.

OLV in equation (4.14) stands for overlap volume, which is employed to capture the impact of piston motion on the backflow mass. The OLV is calculated according to:

$$OLV = V_{EVC} - V_{IVO} \tag{4.16}$$

The future extension of this research work will discuss the optimal IMEP control with VVT actuation. This document assumes fixed camshaft position, resulting in constant A_{flow} and OLV.

Wang et al. (2014) proposed to add correction factors ΔP_{exh} and ΔP_m to the pressure of intake and exhaust manifold to account for pressure wave dynamics. The same technique is also adopted by this research work to model RGM. The complete RGM model is:

$$RGM(k) = C_1 \frac{P_{exh}}{RT_{exh}(k)} V_c + C_2 \sqrt{\frac{P_{exh}}{RT_{exh}(k)} \left((P_{exh} + \Delta P_{exh}(k)) - (P_m(k) + \Delta P_m(k)) \right)} A_{flow} \frac{OLV}{\omega_e(k)} \tag{4.17}$$

The rest of the engine dynamics are combustion related and cannot be modelled as compact as the air-path system. Although complicated and highly nonlinear physical models exist for some combustion related variables, most combustion related engine states are modelled with thousands of maps in reality. The physics based control oriented combustion models can significantly reduce the calibration effort compared to the traditional map based modelling approach. However, most of these models still have numerous tuning factors that are generated with “black box” methods like look-up tables

and ANNs. These factors are selected to account for neglected dynamics from the main physics, leading to improved model accuracy. In summary, most combustion related models with reasonable accuracy are complicated and contain “black box” factors because of the complex nature of turbulent combustion. The optimal IMEP controller must be able to utilize these accurate models so that the calculated solution is truly optimal. In this research the combustion related states are calculated with complex physics models, look-up tables and ANNs. Simulation results prove that the proposed optimal IMEP control frame work is able to handle the selected complex combustion models. It is suggested that other forms of combustion models should be compatible with this control frame work including the currently prevailing map based models.

For the many high-fidelity complex combustion models, the quasi-dimensional flame entrainment models are the most computationally efficient and potentially applied with control applications. A brief introduction of the quasi-dimensional flame entrainment model is presented in Section 3.2 of this dissertation, Cycle-by-cycle Model Predictive Spark Timing Control. With the accurate estimation of the mass fraction burnt, the heat release can be calculated, leading to precise modelling of cylinder pressure and exhaust gas temperature. Although the one dimensional combustion phasing optimal control discussed in Chapter III utilizes the quasi-dimensional combustion model and demonstrates that the model is fast enough for several iterations with the prototype ECU, there are some drawbacks to apply it with the Multiple Input Multiple Output (MIMO) optimal IMEP control. The first issue is that it is required to compute the combustion model for the entire combustion process in order to generate IMEP and exhaust gas

temperature. The computational time is almost doubled comparing to the computation of CA50 which only requires to run the combustion model until MFB reaches 50%. The quasi-dimensional combustion model is a nonlinear ODE system, which requires numeric integration methods (often in crank angle resolution) to generate its results. Like all other numeric integration applications, the error accumulates as the integration progresses. Therefore, the prediction of heat release for the second half of the combustion process is not as accurate as the first half, leading to worse estimation of the IMEP and exhaust gas temperature. Finally, the optimization problem formulated for the MIMO IMEP control is much more complicated than the one dimensional combustion phasing control. Not only does the MIMO problem have higher dimensions with more control actuators and further prediction horizon, the constraint system is also more complicated considering the air-path dynamics. Therefore the MIMO IMEP control needs much more number of iterations than the 1D combustion phasing control, making the quasi-dimensional combustion model less favorable with its heavy computation burden. Instead of switching to completely empirical models, the combustion related engine states are modelled considering the engine energy balance in this research. During one engine cycle, the chemical energy stored in the injected fuel are transformed into three types of energy: mechanical work, exhaust enthalpy and heat transfer to coolant. The heat radiation and incomplete combustion also takes away small portion of the energy. Their effects are neglected in this research.

Firstly, the mechanical work is estimated among the three aspects of the energy balance. The relationship between mechanical work and IMEP is:

$$W = IMEP \cdot V_d \tag{4.18}$$

Willians approximation were applied to estimate engine IMEP output in many articles (*Greene*, 1969 and *Guzzella*, 2009 page 64 – 76). The advantages of this approach includes simple model structure, separating the impact of different engine dynamics on IMEP output and decent accuracy. For this research, the IMEP can be estimated with the following affine function:

$$IMEP = e\left(\omega_e, CA50, x_{egr}\right)P_f - P_0 \tag{4.19}$$

Where x_{egr} is the portion EGR of the total in-cylinder mass. P_f is fuel effective pressure that can be calculated as (assuming stoich AFR σ_0):

$$P_f = LHV \cdot \frac{m_f}{V_d} = LHV \cdot \frac{m_{\beta_{air}}}{\sigma_0 V_d} \tag{4.20}$$

P_0 is the PMEP without FMEP in this research since the control objective is to track IMEP reference instead of BMEP. The reason to exclude friction effects is that both PMEP and IMEP can be measured directly with cylinder pressure sensor. This approach allows the IMEP and PMEP models to serve for model based engine state estimation. The PMEP can be simply calculated as the pressure difference between intake and exhaust manifolds:

$$P_0 = P_{exh} - P_m \approx 1.1\ bar - P_m \tag{4.21}$$

The slope factor e in equation (4.19) determines the portion of the fuel chemical energy transferred into mechanical work. For SI engines with stoich AFR, this slop factor

e is affected primarily by engine speed ω_e, combustion phasing CA50 and fraction of EGR x_{egr}. The Willians approximation separate these effects as individual slope factors:

$$e(\omega_e, CA50, x_{egr}) = e_\omega(\omega_e) e_\zeta(CA50) e_{egr}(x_{egr}, \omega_e) \tag{4.22}$$

Figure 4.3 ~ 4.5 depicts these individual slope terms for the engine in this research. Figure 4.6 shows the IMEP model has decent accuracy with $R^2 = 99.23\%$.

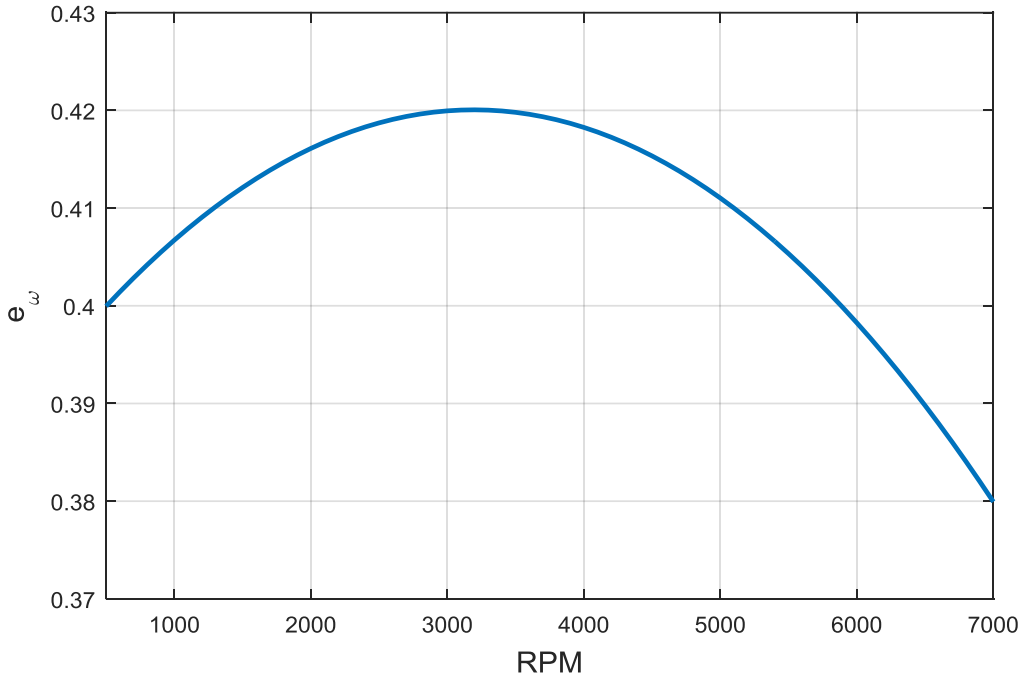

Figure 4.3: Engine speed effect on slope term e.

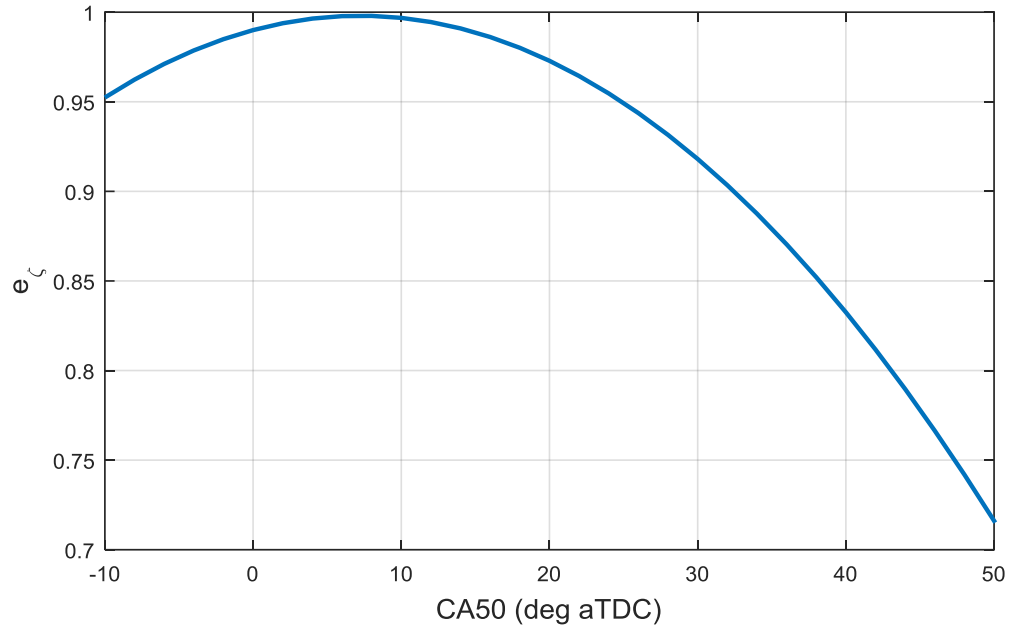

Figure 4.4: Combustion phasing effect on slope term e.

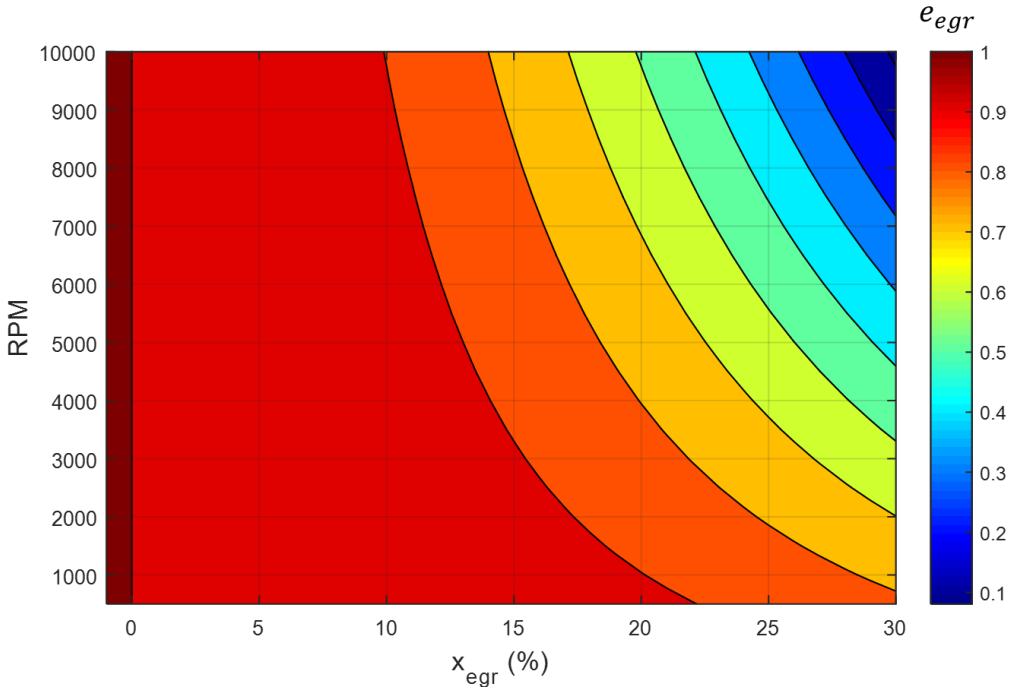

Figure 4.5: EGR fraction effect on slope term e. It is noticed that this effect varies with engine speed. The EGR faction greatly reduces engine efficiency when the engine speed is high.

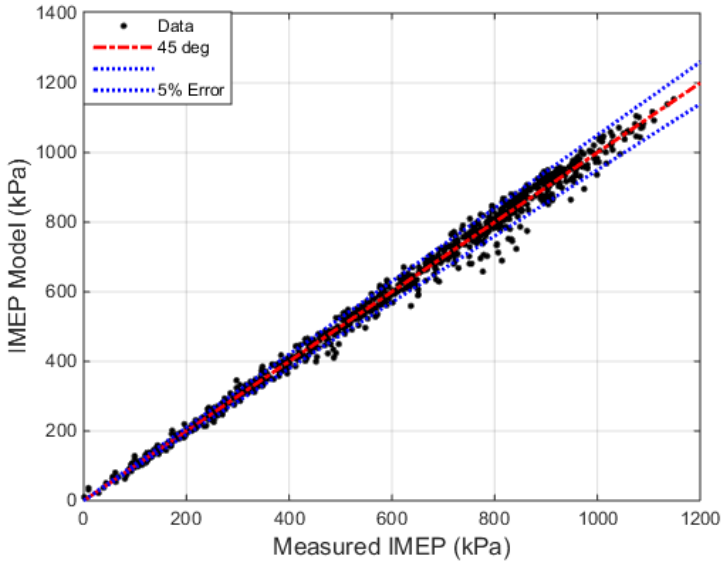

Figure 4.6: Validation of the IMEP model.

After subtracting the mechanical work from the chemical energy stored in the injected fuel, the rest of the chemical energy transformed into rejected heat. This portion of the energy dissipates through exhaust enthalpy and coolant heat transfer, both of which are not usually measured in production vehicles. In order to calculate exhaust gas temperature for the RGM model, at least one of the heat sink source needs to be modelled. Since most engine test laboratory are equipped to monitor both exhaust gas enthalpy and coolant heat transfer, selecting which one to model is not a critical issue. This research chose to model the portion of the rejected heat transferred to coolant considering the future integration with advanced engine thermal management system. While the engine heat transfer to coolant is determined by coolant temperature, engine load and speed for production vehicles (*Arici et al.* 1999, *Cortona et al*, 2002 and *Shibata et al.* 1993), the coolant temperature is controlled by dynamometer management system

in our engine test environment. Thus, the ratio of transferred heat $\vartheta(k)$ (in terms of the total rejected heat) is modelled as map of engine speed and load:

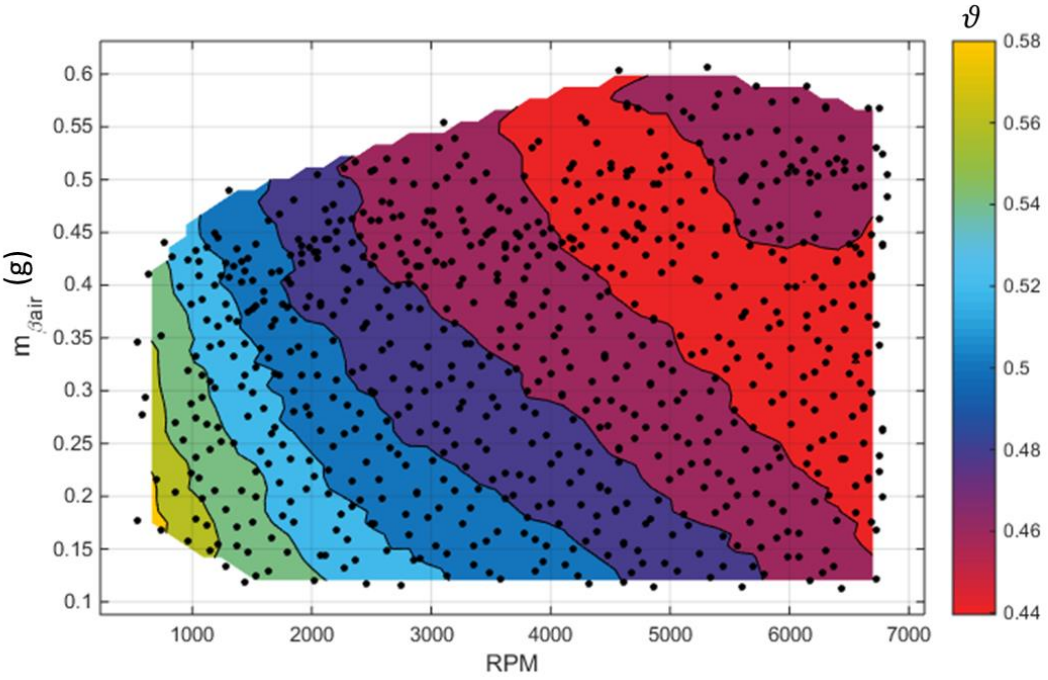

Figure 4.7: Map of coolant heat transfer ratio ϑ versus cylinder air mass flow and engine speed. The black dots are the calibration data points.

After subtracting the coolant heat transfer from the total rejected heat, the exhaust temperature is calculated using the following equation:

$$T_{exh}(k) = \frac{V_d \left(P_f(k) - IMEP(k)\right)\left(1 - \vartheta(k)\right)}{c_p m_{\beta_{air}}(1 + 1/\sigma_0)} \tag{4.22}$$

where c_p is constant pressure heat capacity of air.

Figure 4.8 shows that the exhaust temperature model has decent accuracy with $R^2 = 97.82\%$.

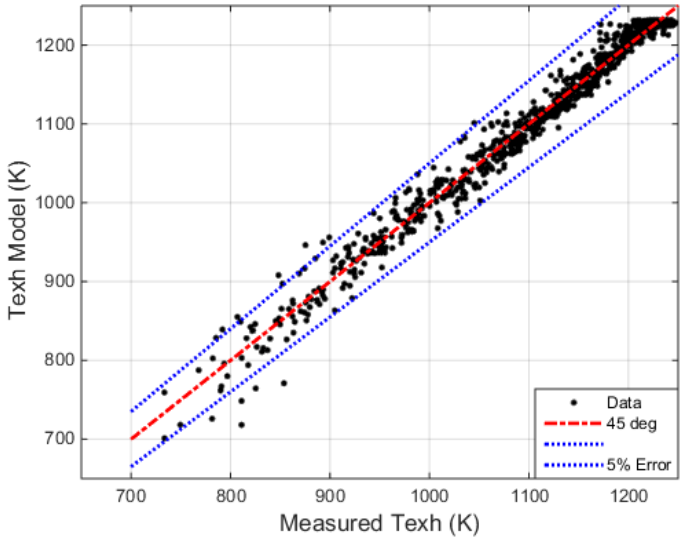

Figure 4.8: Validation of the exhaust temperature model.

The combustion stability is indicated with COV of IMEP in this research. Section 3.1 of this dissertation detailed describes an approach that can accurately predict the COV of IMEP. However, this approach requires SPKT, u' and S_L at TDC information, which are not available without quasi-dimensional combustion model. A simplified version of the COV of IMEP models discussed in Section 3.1 is applied for the optimal IMEP control. Section 3.1 analyzes the critical impact of combustion phasing on COV of IMEP. It can be observed from Figure 4.9 that the COV of IMEP can be estimated using only CA90 and cylinder air mass flow $m_{\beta_{air}}$.

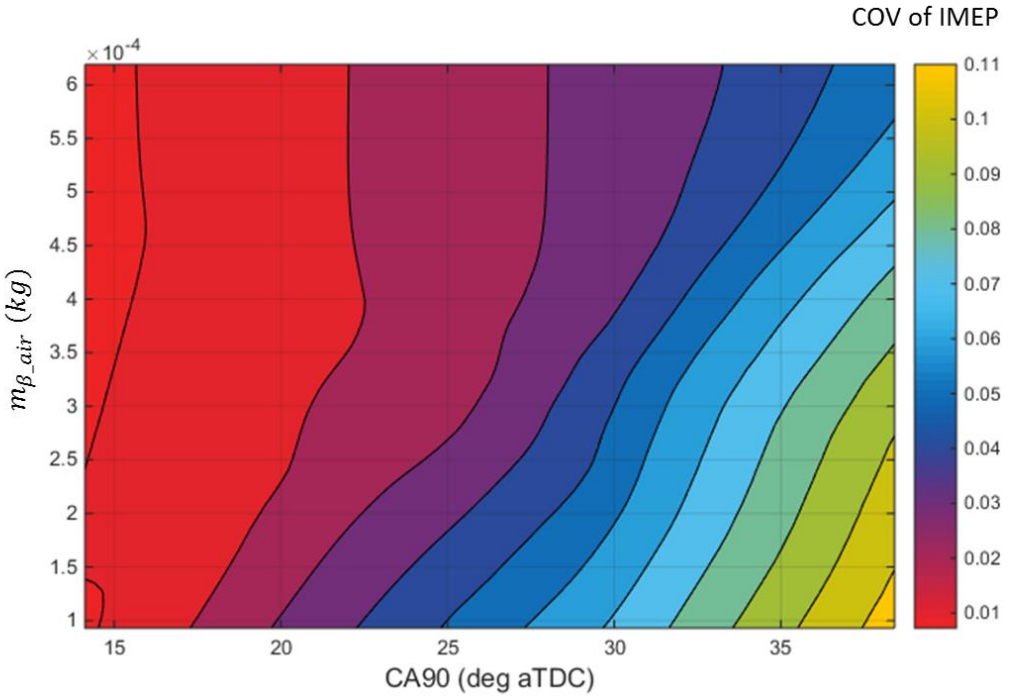

Figure 4.9: Contour plot of COV of IMEP vs. $m_{\beta_{air}}$.and CA90

The CA90 is estimated with an artificial neural network of 1 hidden layer and 10 neurons. The inputs to the ANN are CA50, RPM and m_{β_air}. The performance of the simplified COV model is demonstrated in Figure 4.10. Although not as accurate as the original COV model discussed in Section 3.1, the simplified model has a reasonable accuracy with $R^2 = 88.34\%$

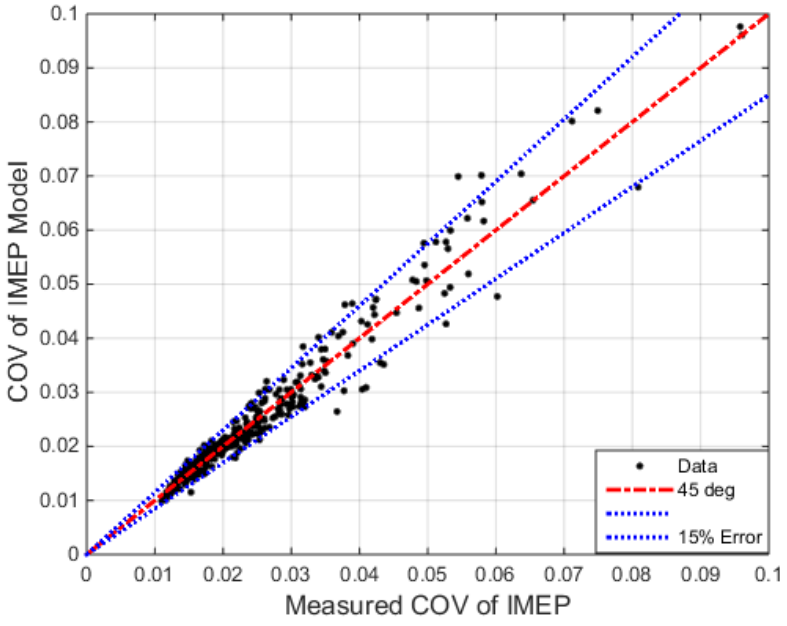

Figure 4.10: Validation of simplified COV of IMEP model.

Knock modelling is not the focus of this research work. Since the optimal IMEP control does not utilize the quasi-dimensional combustion model, crank angle resolution cylinder pressure and temperature are not available. Therefore, the Arrhenius function based knock model discussed in Section 3.2 cannot be applied with the optimal IMEP control. A simple 3D map is used to correlates the knock intensity KI with engine speed, CA50, $m_{\beta_{air}}$ and $m_{\beta_{eg}}$. The KI is normalized so that $KI \geq 1$ indicates a likely knocking engine cycle.

4.3.2 Formulation of model predictive IMEP control

The previous section introduces the control oriented SI engine modelling. Although the modelling process and structure can be very complex, the entire engine model can be summarized as a nonlinear state space model with four states:

$$x(k+1) = f_x\big(x(k), u(k)\big)$$

$$y(k) = f_y(x(k))$$

$$\text{with } x \in \mathbb{R}^n, x(k) = \left[m_{\beta_{air}}(k), m_{\beta_{eg}}(k), RGM(k), x_{CA50}(k)\right]^T \tag{4.23}$$

$$u(k) \in \mathbb{R}^m, u(k) = [m_\alpha(k), m_\varepsilon(k), CA50(k)]$$

$$y(k) \in \mathbb{R}^p, y(k) = IMEP(k)$$

The state $x_{CA50}(k)$ is the MPC demanded CA50 from previous engine cycle ($CA50(k-1)$). The reason for this additional delay is because the control action computed by MPC optimizes the performance for future prediction horizon. This fact implicitly determines the computed control action cannot affect the system output within the same step.

The objective of the optimal IMEP control is to track the IMEP target while minimize fuel consumption for the prediction horizon. The fuel consumption is determined by engine air mass flow since the stoich AFR operation is discussed in this research work. According to the intake manifold mass balance, air mass come through the throttle will eventually end up entering the cylinders with certain lag. It is reasonable to penalize the throttle air mass flow m_α to account for fuel consumption. Thus for each step into the horizon, a weighted summation of the IMEP least square error and m_α are penalized. The prediction horizon is selected as 2 engine cycles according to the time constant of the air-path dynamics. The complete cost function combines the cost of each prediction step into the future:

$$J\big(x(k),U(k)\big)=\sum_{k_i=k+1}^{k+N} r\left(y(k_i)-y_{ref}(k_i)\right)^2+\tilde{s}u(k_i-1)$$

$$\text{with } U(k)=[u(k),u(k+1),\dots u(k+N-1)]^T$$

$$\tilde{s}=s\begin{bmatrix}1&0&0\\0&0&0\\0&0&0\end{bmatrix} \tag{4.24}$$

$$N=2$$

where r and s are weighting factors.

Equation (4.24) can be written in a more compact form:

$$J\big(x(k),U(k)\big)=\left(Y(k)-Y_{ref}(k)\right)^T R\left(Y(k)-Y_{ref}(k)\right)+SU(k)$$

$$\text{with } Y(k)=[y(k),y(k+1),\dots y(k+N-1)]^T$$

$$R^{(p\times N)\times(p\times N)}=\begin{bmatrix}r&\cdots&0\\\vdots&\ddots&\vdots\\0&\cdots&r\end{bmatrix}, S^{(m\times N)\times(m\times N)}=\begin{bmatrix}s&\cdots&0\\\vdots&\ddots&\vdots\\0&\cdots&s\end{bmatrix} \tag{4.25}$$

The constraints that needs to be considered for the optimization problem can be categorized into states and actuation constraints. The MPC control actuation is bounded by the dynamics of the lower level control loop. In this case, the throttle and EGR valve air mass flow is limited between zero and maximum allowable mass flow per engine cycle at current speed and pressure difference. Fortunately, the size of the throttle and EGR valve on a production engine are normally so large that the maximum air mass flow

is rarely restricted by them. As for the CA50 demanded by the MPC, the physical limitation is much more relaxed than the combustion limitations. Therefore, the constraints on control actuation are only the non-negativity constraints on throttle and EGR air mass flow per engine cycle $m_\alpha(k)$ and $m_\varepsilon(k)$. The constraints on engine states are more complex than that of control actuations. The first constraint is that the manifold pressure cannot exceed ambient pressure for naturally aspirated engines. Since the discrete air-path dynamics described in (4.8) do not include the orifice flow model, the throttle air mass flow is not determined by pressure difference between manifold and ambient. Thus the model by itself cannot maintain manifold pressure to be less than the atmosphere. According to the relationship between engine air mass flow m_β and manifold pressure P_m from (4.10), the summation between engine states $m_{\beta_{air}}$ and $m_{\beta_{eg}}$ must be restrict with an additional constraint to guarantee the reasonable manifold pressure. Finally, COV of IMEP and knock intensity are modelled with engine states x as inputs in the previous section. The complete optimization problem is:

$$\min_{U(k)} J\big(x(k), U(k)\big)$$

$$\text{s.t.} \quad \begin{cases} P_m(k_i) \le P_{ambient} \\ m_\alpha(k_i) \ge 0 \\ m_\varepsilon(k_i) \ge 0 \quad , \quad k_i = k+1, k+2, \dots k+N \\ COV(k_i) \le COV_{ub} \\ KI(k_i) \le KI_{ub} \end{cases} \tag{4.26}$$

The equation (4.25) can be written in a more compact form:

$$\min_{U(k)} J\big(x(k), U(k)\big) \tag{4.27}$$

$$\text{s.t.} \quad l\big(x(k), U(k)\big) \leq \mathbf{0}$$

The convexity of this optimization problem is difficult to prove analytically with the complex structures of the models. However, it is easy to find an example to show that the objective function is not convex. The relationship between IMEP and CA50 is concave from Figure 4.4 (so is the relationship between IMEP and x_{egr}.). Assuming the x_{egr} and engine speed is constant, Figure 4.11 shows the surface of the cost function with $m_{\beta_{air}}$ and CA50 as input. It can be observed that the surface is neither convex nor concave. Thus it cannot be proved that the optimization problem (4.26) has a unique local minimum.

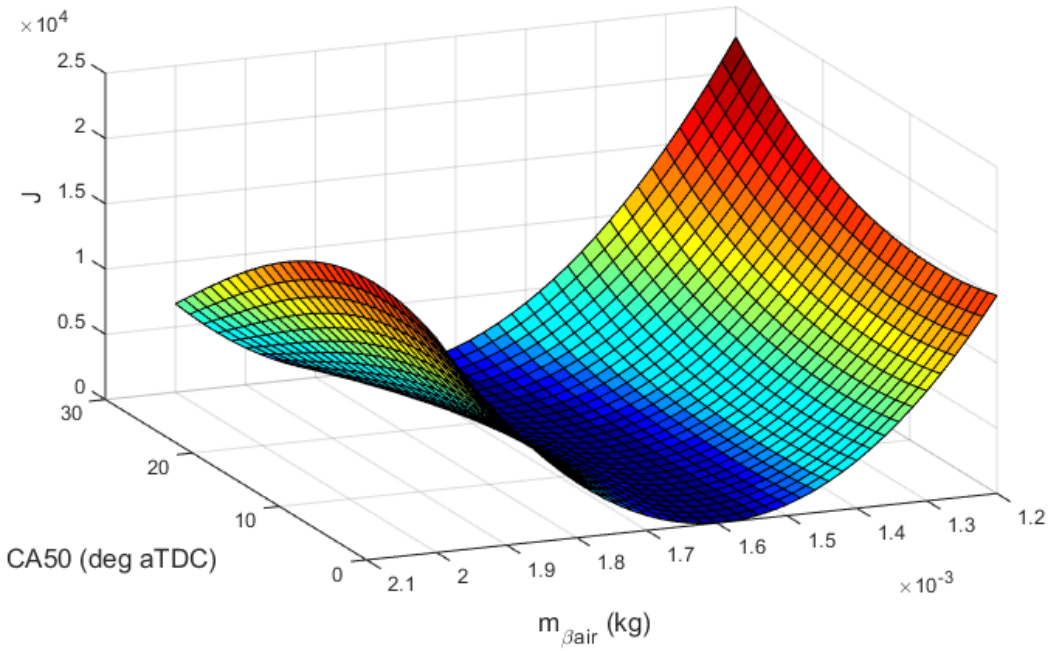

Figure 4.11: Surface of the optimization cost function vs. engine air mass flow and CA50.

4.3.3 Modified SQP algorithm for tracking MPC applications

It is discussed in the introduction of this chapter that the nonlinear programming algorithms capable of handling multiple local minimum problems are not realistic to be implemented with MPC application due to their astronomical number of function evaluations. Sequential quadratic programming has a great potential with MPC applications for each of its iterations is relatively faster to compute compared with other NLP algorithms. However, the SQP algorithm can only find a local minimum near the start point. For proposed optimal IMEP control application, this disadvantage is not critical. Although the local minimum point has worse fuel economy and IMEP tracking performance than the global optimal solution, the performance is still better than the starting point which can be generated with benchmark calibration. Furthermore, the performance difference from global optimal solution can be negligible if the calibration of the starting point has good quality, i.e. it is close to the global optimal solution.

In order to further improve the computational efficiency of the MPC IMEP control, the original SQP algorithm is modified considering the specific structure of tracking MPC applications with least square cost functions. Some concepts from the LTV MPC are applied to the SQP MPC algorithm. Firstly, let us consider solving the optimization problem (4.27) in the context of LTV MPC. The state space model described in (4.23) and constraints in (4.26) needs to be linearized with the initial guess of control actions $U_0(k)$. Applying first order Taylor series expansion to (4.23):

$$\delta x(k+1) = \left[\frac{\partial f_x}{\partial x}\right]\Big|_{x(k),u_0(k)} \delta x(k) + \left[\frac{\partial f_x}{\partial u}\right]\Big|_{x(k),u_0(k)} \delta u(k) + H.O.T. \tag{4.28}$$

$$\delta y(k) = \left[\frac{\partial f_y}{\partial x}\right]\Big|_{x(k)} \delta x(k)$$

Or

$$\begin{aligned} \delta x(k+1) &= A(k)\delta x(k) + B(k)\delta u(k) \\ \delta y(k) &= C_y(k)\delta x(k) \end{aligned} \tag{4.29}$$

In order to linearize the models for the next step, the updated system states needs to be calculated, which is the summation of linearized state variation and the nominal value of the original nonlinear state equation:

$$\begin{aligned} x(k+1) &= \delta x(k+1) + f_x\big(x(k), u_0(k)\big) \\ y(k) &= \delta y(k) + f_y\big(x(k)\big) \end{aligned} \tag{4.30}$$

The first order partial differential of f_x and f_y can be approximated with Euler approach with an intentional perturbation of the inputs Δx. The following is an example of one element in $\left[\frac{\partial f_x}{\partial x}\right]\Big|_{x(k),u_0(k)}$

$$\begin{aligned} &\frac{\partial f_x}{\partial x_i}\Big|_{x(k),u_0(k)} \\ &= \frac{f_x\big([x_1(k), x_2(k), \dots x_i(k) + \Delta x_i, \dots x_n(k)], u_0(k)\big) - f_x\big(x(k), u_0(k)\big)}{\Delta x_i} \end{aligned} \tag{4.31}$$

The MAP, COV of IMEP and knock intensity can be considered as the outputs of the state-space engine model. Thus the original state-space model becomes:

$$x(k+1) = f_x\big(x(k), u(k)\big)$$

$$z(k) = f_z(x(k)) \tag{4.32}$$

$$\text{with } z(k) \in \mathbb{R}^q, z(k) = [\, P_m(k), COV(k), KI(k)]$$

The unknown parameters in the linear state-space equation are in the $C_z(k)$ and the third row of $A(k)$. These parameters can be calculated with the Euler technique by running the original nonlinear engine model (together with COV and KI models) five times for each prediction step.

Since the original nonlinear dynamics are evaluated during the numeric linearization process, this document proposed to compute the nominal points with the original nonlinear state-space model instead of integrated from initial states x_0 through the entire prediction horizon, which was adopted by conventional LTI and LTV MPC formulation. Let us consider the state update first. From (4.30)

$$\begin{aligned} x(k+1|k) &= \delta x(k+1) + f_x\big(x(k), u_0(k)\big) \\ &= A(k)\delta x(k) + B(k)\delta u(k) + f_x\big(x(k), u_0(k)\big) \\ x(k+2|k) &= \delta x(k+2) + f_x\big(x(k+1), u_0(k+1)\big) \\ &= A(k+1)A(k)\delta x(k) + A(k+1)B(k)\delta u(k) + B(k+1)\delta u(k+1) + \\ & f_x\big(x(k+1), u_0(k+1)\big) \end{aligned} \tag{4.33}$$

$$\vdots$$

$$x(k+N|k) = A(k+N-1)\dots A(k)\delta x(k) + A(k+N-1)\dots A(k+1)B(k)\delta u(k) + \cdots +$$
$$B(k+N-1)\delta u(k+N-1) + f_x\big(x(k+N-1), u_0(k+N-1)\big)$$

Since $x(k)$ is the feedback of the current system states whose variation $\delta x(k)$ is 0, the system states of the future prediction horizon is determined by nominal states computed by the initial guess of control action sequence $U_0(k)$ and its variation $\delta U(k)$. Equation (4.33) is transformed into:

$$\begin{aligned}
x(k+1|k) &= \delta x(k+1) + f_x\big(x(k), u_0(k)\big) \\
&= B(k)\delta u(k) + f_x(x(k), u_0(k)) \\
x(k+2|k) &= \delta x(k+2) + f_x\big(x(k+1), u_0(k+1)\big) \\
&= A(k+1)B(k)\delta u(k) + B(k+1)\delta u(k+1) + f_x(x(k+1), u_0(k+1)) \\
&\vdots \\
x(k+N|k) &= A(k+N-1)\dots A(k+1)B(k)\delta u(k) + \cdots \\
&+B(k+N-1)\delta u(k+N-1) + f_x(x(k+N-1), u_0(k+N-1))
\end{aligned} \tag{4.34}$$

The computation of the nominal conditions $f_x(x, u_0)$ has already been completed during the linearization process. Similarly, the linearized engine IMEP output of the prediction horizon can be computed as:

$$\begin{aligned}
y(k+1|k) &= C_y(k+1)B(k)\delta u(k) + f_y\big(x(k+1)\big) \\
y(k+2|k) &= C_y(k+2)A(k+1)B(k)\delta u(k) + C_y(k+2)B(k+1)\delta u(k+ \\
&1) + f_y\big(x(k+2)\big)
\end{aligned} \tag{4.35}$$

$$\vdots$$

$$y(k+N|k) = C_y(k+N)A(k+N-1)\dots A(k+1)B(k)\delta u(k) + \cdots$$

$$+C_y(k+N)B(k+N-1)\delta u(k+N-1) + f_y\big(x(k+N)\big)$$

Equation (4.35) can be written in a more compact form:

$$Y(k) = \phi_y(k)\delta U(k) + Y_0(k)$$

$$\text{with } Z_0(k) = \big[f_y\big(x(k+1)\big), f_y\big(x(k+2)\big), \dots f_y\big(x(k+N)\big)\big]^T \tag{4.36}$$

If we consider the manifold pressure, COV of IMEP and KI as outputs, then equation (4.36) becomes:

$$Z(k) = \phi_z(k)\delta U(k) + Z_0(k)$$

$$\text{with } Z_0(k) = \big[f_z\big(x(k+1)\big), f_z\big(x(k+2)\big), \dots f_z\big(x(k+N)\big)\big]^T \tag{4.37}$$

ϕ_z is formulated similar to ϕ_y, by replacing C_y with C_z in (4.34).

After substituting these linearized results into the original nonlinear programming problem (4.27), the optimization becomes a quadratic programming problem with linear constraints:

$$\min_{\delta U(k)} \frac{1}{2}\delta U^T(k)H(k)\delta U(k) + \delta U^T(k)F(k)$$

$$\text{s.t.} \quad M(k)\delta U(k) - b(k) \leq \mathbf{0} \tag{4.38}$$

with $$H(k) = 2\phi_y^T(k)R\phi_y(k)$$

$$F(k) = -2\phi_y^T(k)R\big(Y_{ref}(k) - Y_0(k)\big) + S$$

$$M(k) = [\phi_z(k), -\phi_z(k), I^{m\times N}, -I^{m\times N}]^T$$

$$b(k) = [Z_{ub} - Z_0(k), -Z_{lb} + Z_0(k), U_{ub} - U_0(k), -U_{lb} + U_0(k)]^T$$

The optimal control action sequence for the prediction horizon is summation of the solution to (4.38) and the initial guess of control sequence:

$$U^*(k) = \delta U(k) + U_0(k) \tag{4.39}$$

At this point one may apply the first step of the optimal control sequence to the system, which concludes the proposed LTV MPC formulation. The most critical drawback of LTV MPCs is that the linearized system model becomes invalid if the optimal solution $U^*(k)$ is very different from $U_0(k)$. This factor influences the optimality and even feasibility of the calculated control action. Let us solve the original NLP (4.27) in the context of SQP. The SQP is an iterative numeric algorithm to solve general nonlinear optimization problem. During each major iteration i (compared to minor iterations in the sub-QP algorithm), the original nonlinear cost function is approximated as a quadratic surface around the start of search point $U_0(i)$. Furthermore, the nonlinear constraints are linearized at the start point. Then a quadratic programming problem is formulated as :

$$\min_{\delta U(i)} \frac{1}{2}\delta U^T(i)\hat{H}(i)\delta U(i) + \delta U^T(i)\hat{F}(i) \tag{4.40}$$

$$\text{s.t.} \quad \widehat{M}(i)\delta U(i) - \hat{b}(i) \leq \mathbf{0}$$

$$\text{with} \qquad \widehat{H}(i) = \left.\frac{\partial^2 J}{\partial U^2}\right|_{x(k),U_0(i)}$$

$$\hat{F}(i) = \left.\frac{\partial J}{\partial U}\right|_{x(k),U_0(i)}$$

$$\widehat{M}(i) = \left[\left.\frac{\partial Z}{\partial U}\right|_{x(k),U_0(i)}, -\left.\frac{\partial Z}{\partial U}\right|_{x(k),U_0(i)}, I^{m\times N}, -I^{m\times N}\right]^T$$

$$\hat{b}(i) = [Z_{ub} - Z_0(i), -Z_{lb} + Z_0(i), U_{ub} - U_0(i), -U_{lb} + U_0(i)]^T$$

The solution of (4.40) is the of the optimal solution variation, which can also be considered as the search step of the major iterations. The start point of the next major iteration is:

$$U_0(i+1) = \delta U(i) + U_0(i) \tag{4.41}$$

For the next major iteration, the QP described in (4.40) is reformulated around the latest start point $U_0(i+1)$ and so forth. The iteration stops under certain termination conditions. The most common one is to compare the norm of solution variation $\delta U(i)$ with certain threshold.

It can be observed that the QP in (4.40) is very similar to the QP formulated for the LTV MPC. In fact, it can be shown that the $\hat{F}(i)$, $\widehat{M}(i)$ and $\hat{b}(i)$ are exactly the same as the $F(k)$, $M(k)$ and $b(k)$ if $U_0(i) = U_0(k)$. It is straight forward to see that equation

(4.36) and (4.37) is actually the first order Taylor series expansion of the system outputs $Y(k)$ and $Z(k)$. Therefore, we have:

$$\phi_z(i) = \left.\frac{\partial Z}{\partial U}\right|_{x(k),U_0(i)}$$

$$\phi_y(i) = \left.\frac{\partial Y}{\partial U}\right|_{x(k),U_0(i)} \tag{4.42}$$

Thus:

$$\widehat{M}(i) = M(k)$$

$$\hat{b}(i) = b(k) \tag{4.43}$$

$$\text{with } i = k$$

Differentiate equation (4.25) with respect of $U(k)$:

$$\hat{F}(i) = \left.\frac{\partial J}{\partial U}\right|_{x(k),U_0(i)} = 2\left.\frac{\partial Y}{\partial U}\right|_{x(k),U_0(i)} RY(k) - 2\left.\frac{\partial Y}{\partial U}\right|_{x(k),U_0(i)} RY_{ref}(k) + S \tag{4.44}$$

Substitute (4.42) into (4.44):

$$\hat{F}(i) = -2\phi_y^T(i)R\big(Y_{ref}(i) - Y_0(i)\big) + S \tag{4.45}$$

Thus:

$$\hat{F}(i) = F(k)$$

$$\text{with } i = k \tag{4.46}$$

The quadratic coefficient matrix H is different between SQP MPC and LTV MPC. For the SQP algorithm, the H is the Hessian of the original nonlinear objective function, which can be calculated as:

$$\begin{aligned}\widehat{H}(i) &= \left.\frac{\partial^2 J}{\partial U^2}\right|_{x(k),U_0(i)} \\ &= 2\left(\left.\frac{\partial Y}{\partial U}\right|_{x(k),U_0(i)}\right)^T R \left.\frac{\partial Y}{\partial U}\right|_{x(k),U_0(i)} + 2\left.\frac{\partial^2 Y}{\partial U^2}\right|_{x(k),U_0(i)} R\left(Y_0(i) - Y_{ref}(i)\right)\end{aligned} \tag{4.47}$$

Substitute (4.42) into (4.47):

$$\widehat{H}(i) = 2\phi_y^T(i) R \phi_y(i) + 2\left.\frac{\partial^2 Y}{\partial U^2}\right|_{x(k),U_0(i)} R\left(Y_0(i) - Y_{ref}(i)\right) \tag{4.48}$$

It can be observed that the first term in the system's Hessian (4.48) is the same as the $H(k)$ with $k = i$. There are two reasons strongly suggesting to neglecting the second term of the Hessian calculation for tracking SQP MPC applications. The first reason is that the second term is usually very small if the MPC has a decent initial guess and a reasonable tracking reference, i.e. $Y_0(i) \approx Y_{ref}(i)$. In this case, the approximated Hessian is very close to the exact value, resulting excellent global convergence performance of the SQP algorithm. The second reason is that the first term of the Hessian calculation (or H from LTV MPC) is guaranteed to be positive definite. Thus the sub-quadratic programming has a unique global minimum making it possible to apply many existing efficient QP solvers. Geometrically, the sub-quadratic programming with the approximated Hessian simplifies the objective function surface into the summation of a

plane and a quadratic surface. The plane is the supporting plane of the original nonlinear surface at $U_0(i)$, described with $\delta U^T(i)\hat{F}(i)$. The quadratic surface is described by $\delta U^T(i)\phi_y^T(i)R\phi_y(i)\delta U(i)$, which penalizes any excessive solution variation from the initial guess $U_0(i)$. Figure 4.12 shows the tendency of the normalized optimal solution variation $\|\delta U(i)\|$ as number of iterations increases for a 100 consecutive engine cycles simulation. In order to improve the visualization of the tendency, the SQP is forced to run 150 iterations regardless of the termination conditions. It can be observed from Figure 4.12 that the proposed SQP algorithm has global convergence tendency.

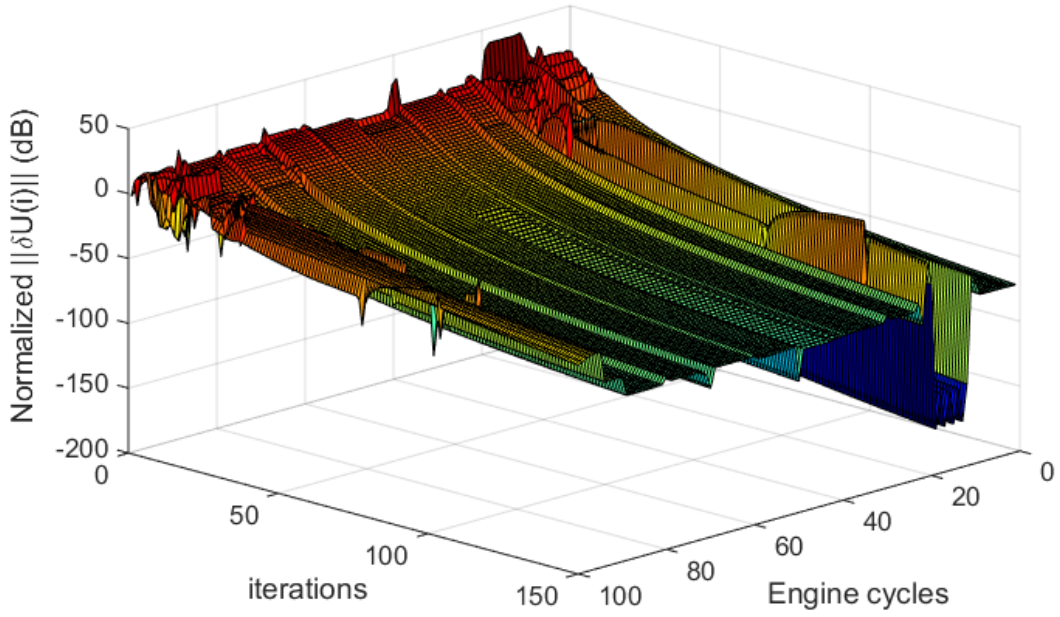

Figure 4.12: Tendency of normalized optimal solution variation.

There are some local period that $\|\delta U(i)\|$ increases with SQP progression from Figure 4.12. The reason for this phenomenon is caused by SQP search skipping a local minimum point without proper termination conditions. This situation means that the SQP

could terminate at different local minimum points for similar engine states $x(k)$ and initial guess $U_0(k)$. Therefore it could lead to control action chattering, which is not desirable for it could excite the un-modeled dynamics. Figure 4.13 shows the results of the section from 0 to 30 cycles from the 100 consecutive engine cycles simulation discussed before. The chattering happens at CA50 output between 10 to 20 engine cycles.

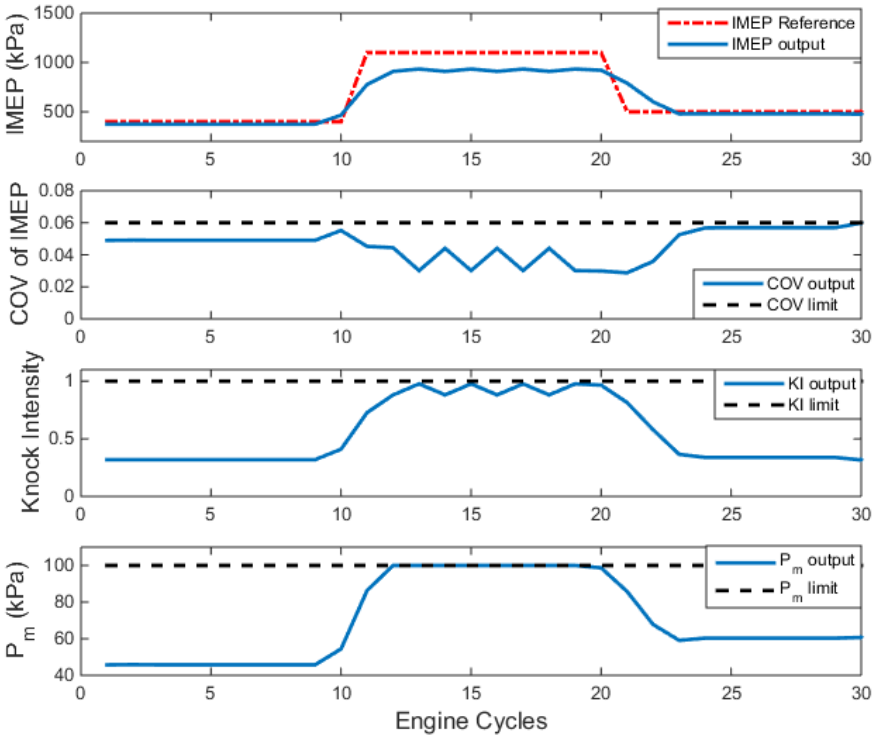

Figure 4.13 a: Engine performance of the SQP MPC with simplified Hessian approximation.

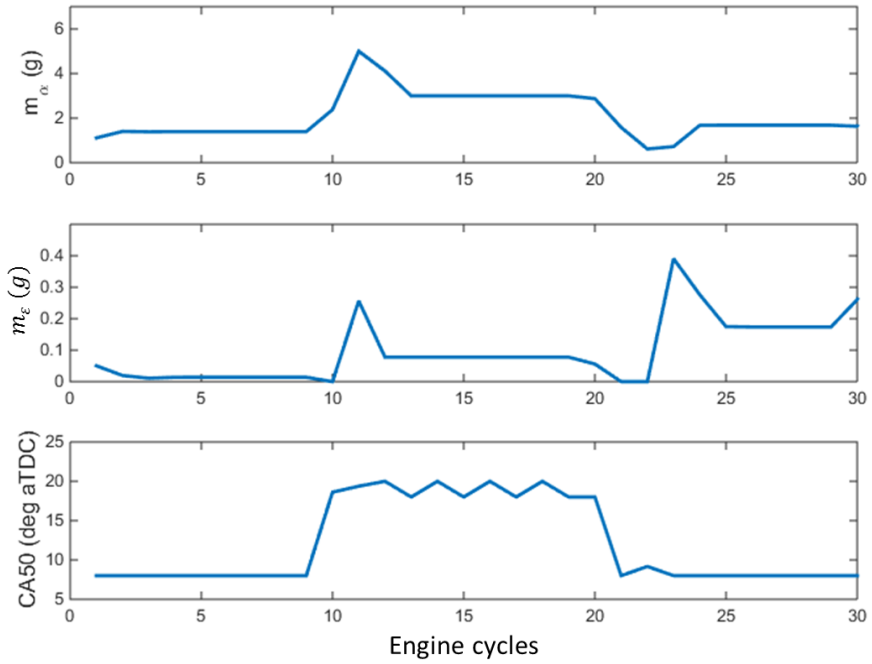

Figure 4.13b: Control actuations of the SQP MPC with simplified Hessian approximation.

Two modifications are applied to the SQP discussed previously to ensure the SQP terminates at the local minimum that is the nearest to the starting point. The first modification is to penalize the control variation with a cost that is increasing as the SQP progresses. This artificial cost can have exponential correlation with the number of iterations i so that it does not interfere with the original QP during the beginning phase of the SQP. As the number of iteration increases, the solution variation $\delta U(i)$ shrinks quickly to accelerate the convergence rate. The original sub-QP is transformed into:

$$\min_{\delta U(i)} \frac{1}{2}\delta U^T(i)\left(\widehat{H}(i)+Q(i)\right)\delta U(i)+\delta U^T(i)\hat{F}(i) \tag{4.49}$$

$$\text{s.t.} \quad \widehat{M}(i)\delta U(i)-\hat{b}(i)\leq \mathbf{0}$$

with $Q(i) \propto i$

The termination condition is also improved to prevent the SQP from skipping local minimum points. In addition to the ordinary termination conditions that stops the iteration when the search step is smaller than certain threshold, it is proposed to monitor the objective function value after each major iteration (i.e. sub-QP) to determine if the SQP should be terminated. The increase of objective function is often accompanied with skipping local minimums. The SQP should be terminated prematurely when the objective function value increased by certain amount. However, this termination condition should be neglected if the calculated solution is infeasible, which could also increase the objective function value. Figure 4.14 shows the effects of these two proposed techniques on the convergence performance of the SQP model predictive IMEP controller. The result is generated from a 10,000 consecutive engine cycle simulation with random IMEP reference. Compared to Figure 4.12, the new SQP MPC has a much faster convergence rate. Although there are still some local increase of the step size, they are mostly caused by compromising constraints and significantly less dominant. The simulation results demonstrated next section will show that the control chattering phenomenon does not present with the proposed SQP model predictive IMEP control.

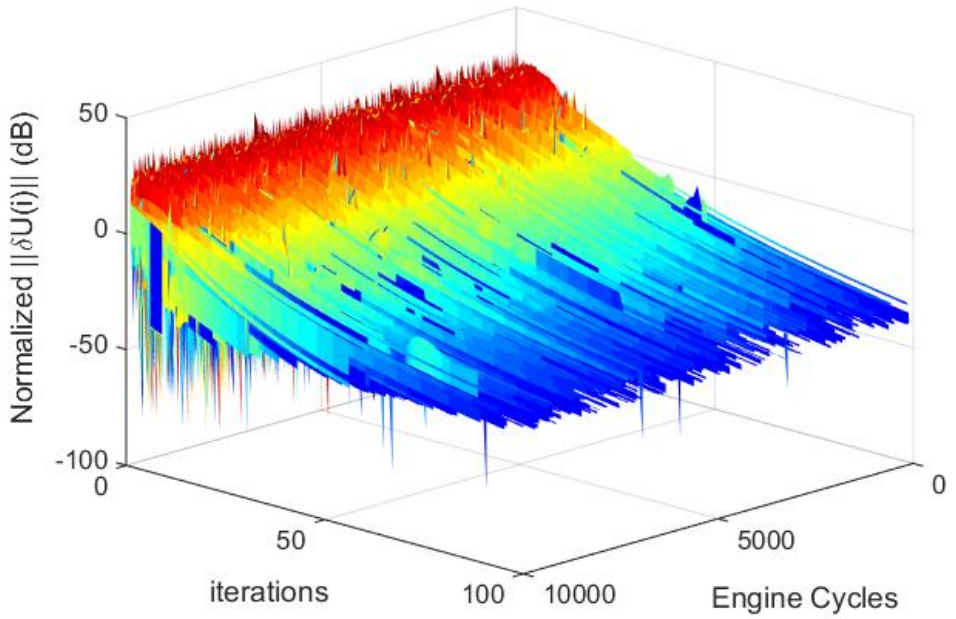

Figure 4.14: Tendency of normalized optimal solution variation with modified SQP MPC to improve convergence performance.

4.4 Simulation Results

Figure 4.15 shows the engine performance and control actuation of the proposed SQP model predictive IMEP controller. In general, the engine IMEP output follows the IMEP reference for most of the time. The COV, KI and manifold pressure do not violate the constraints for the entire simulation. Furthermore, the control action is free of chattering phenomenon during the simulation. It can be concluded that the proposed IMEP control is generating reasonable control actions.

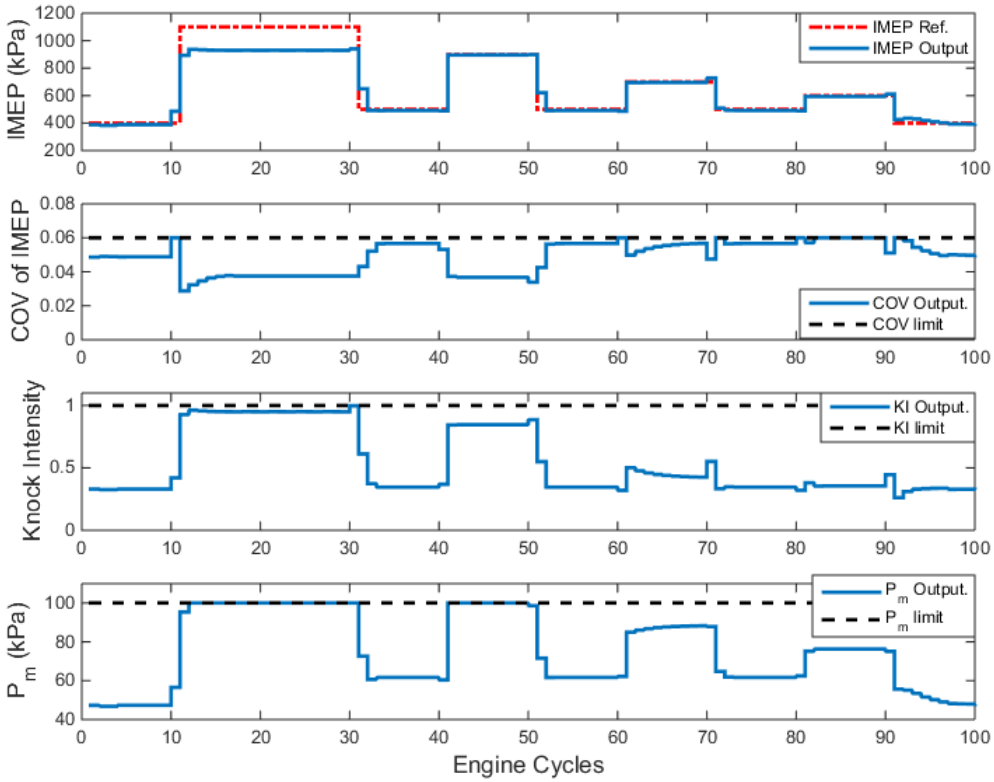

Figure 4.15 a: Engine performance of the proposed SQP model predictive IMEP control.

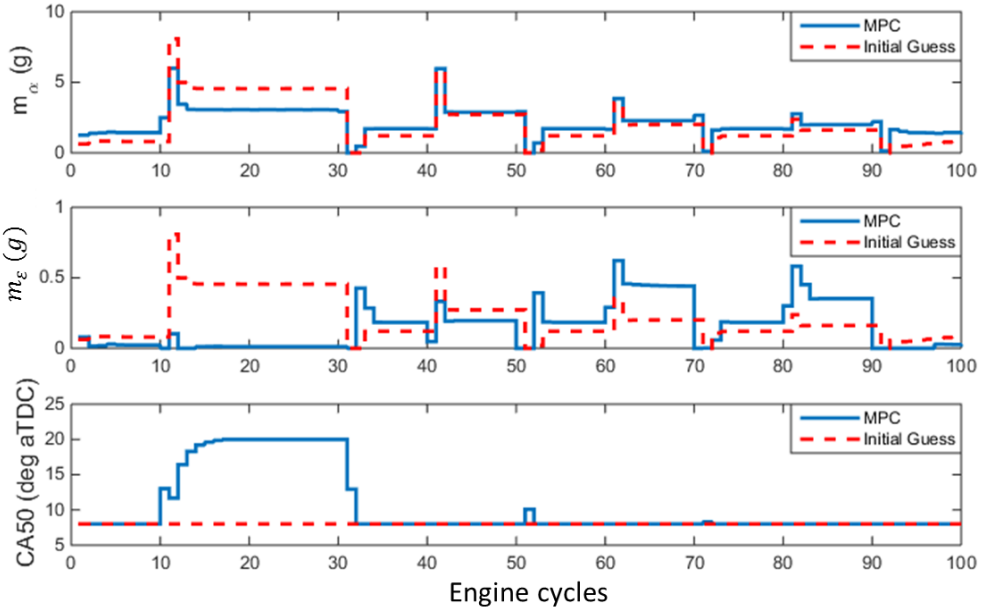

Figure 4.15b: Control actuations of the proposed SQP model predictive IMEP control.

For the situation of "tipping in" (around 10s, 40s and 60s), the throttle air mass flow output m_α spikes at the instance of IMEP reference steps. This maneuver is to compensate for the manifold delay and quickly increase the IMEP output. When magnitude of the spike is limited (around 10s), the MPC will open the throttle earlier while retard the combustion phasing to maintain torque output. At the instance of reference step, the combustion phasing will be advanced to quickly increase torque output. However, the combustion phasing is not fully advanced to MBT due the knock limit at 10s. During "tipping out" situation (around 30s, 50s, 70s and 90s), the throttle air mass is reduced to zero initially to compensate for manifold delay. Then it converges to steady state value with no oscillation. It can be observed that the EGR flow is shut down before the throttle in order to prevent excessive RGF and meet with the COV of IMEP constraint. When the IMEP demand is not high (30~40s and 50~100s), the MPC asks for

MBT combustion phasing and maximum amount of EGR without violating COV constraints. If the IMEP demand is very high (10~30s and 40~50s), the MPC reduces EGR to maximize engine air mass flow. All these observations agrees with calibration rules for traditional map based IMEP controls. Therefore, the proposed IMEP management system successfully achieved its control objectives.

Figure 4.16 compares the engine performance and control actuation between the SQP MPC with the proposed LTV MPC IMEP control with real time linearization. This LTV MPC can considered as a special case of the SQP MPC with 1 major iteration. It can be observed from Figure 4.16 that the LTV MPC has a worse IMEP tracking performance. Furthermore, COV of IMEP violates the constraints during some transient situation, when the optimal solution is very different from the initial guess.

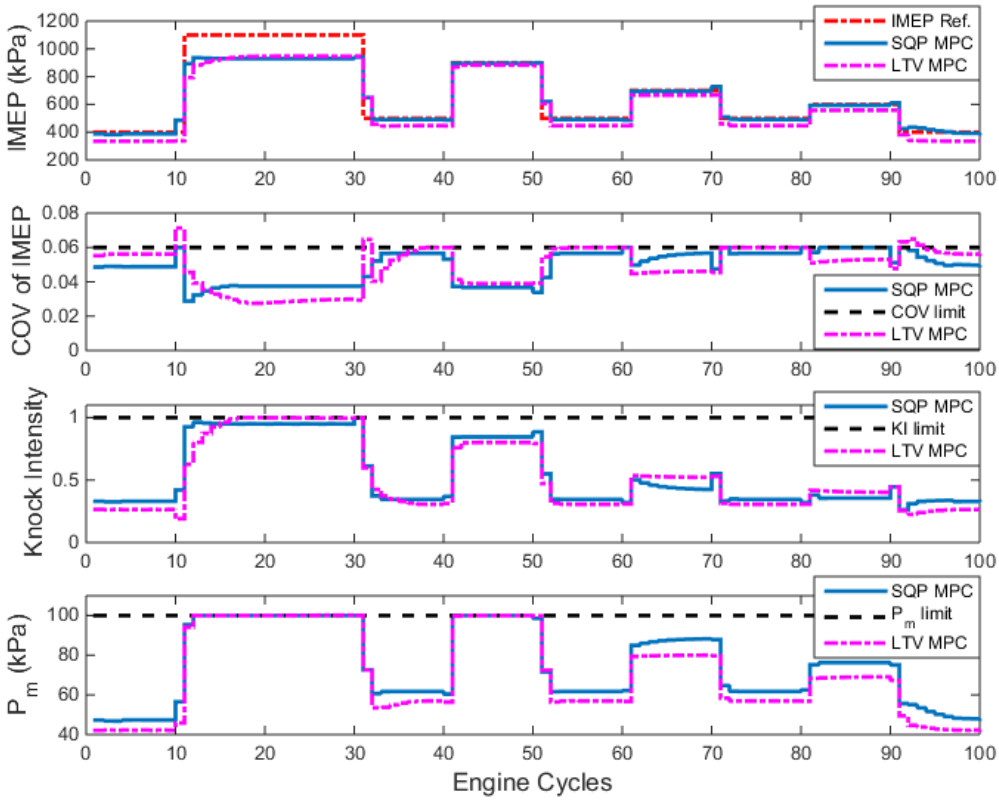

Figure 4.16 a: Engine performance comparison between LTV MPC and SQP MPC IMEP control.

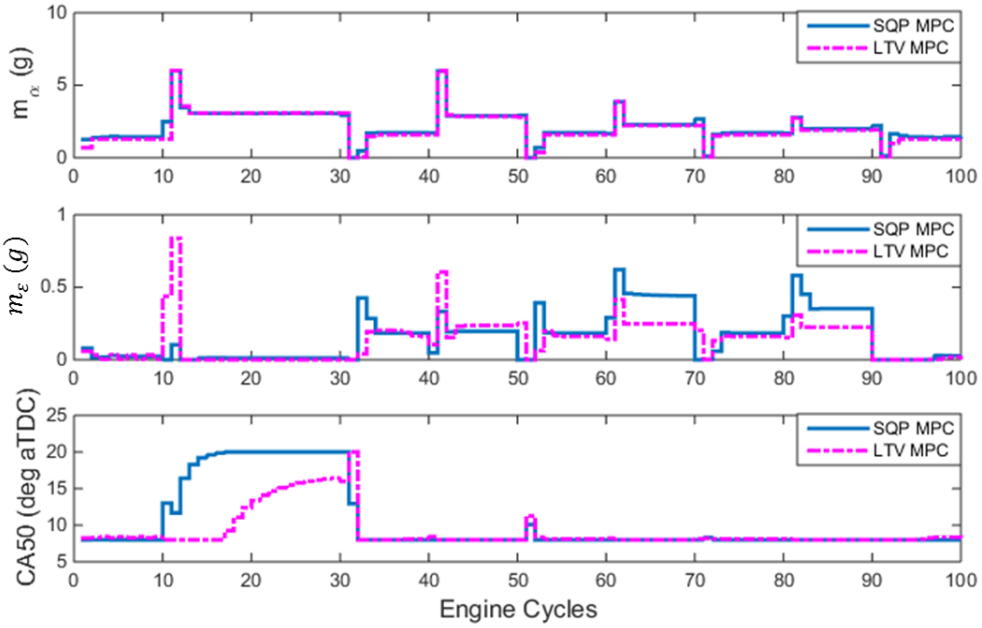

Figure 4.16b: Control actuation comparison between LTV MPC and SQP MPC IMEP control.

The proposed SQP model predictive IMEP controller is also evaluated for 10,000 consecutive engine cycles with random IMEP tracking reference. Table 4.1 summarizes the execution time statistics of the proposed IMEP controller. The simulation is carried out on a desktop computer with 4.2 GHz 64 bit CPU and 16 GB of RAM.

Table 4.1: Statistics of the proposed SQP model predictive IMEP controller.

	Mean	Max	Min
Number of major iterations	42	108	2
Execution time per engine cycle	26.00 ms	53.50 ms	1.70 ms
Execution time per major iteration	0.63 ms	0.76 ms	0.41 ms
Execution time for model evaluation per iteration	0.39 ms	0.42 ms	0.38 ms

Execution time for QP per iteration	0.23 ms	0.32 ms	0.02 ms

It can be observed from Table 4.1 that the evaluation of the nonlinear engine models and solving the sub-QP problems takes 62% and 36% of the total execution time respectively. Improving the computational efficiency of either one can greatly reduce the execution time of the SQP. While the engine model can be simplified by replacing physics with maps, the next chapter of this dissertation introduces methods to accelerate the solving of QP and reduce the number of major iterations.

4.5 Conclusions

This chapter of the dissertation introduces a model predictive IMEP control frame work and algorithm. Compared to traditional feed forward based IMEP control, the optimal IMEP control has great potential of improving IMEP reference tracking performance and reduce calibration effort.

The proposed IMEP control frame work is designed to maximize the feasibility and potential of MPC strategies. The cascaded control structure fully exploit the frequency separation of different engine dynamics to simplify the optimization of MPC and maximize the actuators bandwidth potential. The main MPC controller is chose to operate in engine cycle domain instead of in time domain with constant sampling time. By doing this, the air path dynamics are greatly simplified and many combustion models developed in engine cycle domain can be directly integrated into this IMEP control structure. The lower level controllers can use simple feedback or look-up tables, providing easy tuning of the control performance.

In this research, the SI engine system is modelled with physics based methods and empirical approaches, representing a very typical ad hoc modeling process of a production engine. The two MPC algorithms, LTV and SQP MPC, discussed in this dissertation are able to utilize this complex engine model to compute optimal control actions for the future horizon. Both LTV and SQP algorithms utilizes real time linearization technique to approximate the original highly nonlinear engine model. The proposed SQP algorithm exploit the characteristics of tracking MPCs, leading to much

easier computation of the system's Hessian at the nominal point. This advantage reduces the number of evaluating the nonlinear engine model saving significant amount of execution time. Although the proposed SQP has global convergence behavior, exponential step size penalty and additional termination conditions are applied to improve the convergence rate and avoid control chattering. Simulation results proves that the SQP model predictive IMEP controller successfully meets with its design objectives. The engine is able to track the IMEP reference without violating combustion and other constraints.

The LTV MPC can be considered as a special case of the proposed SQP MPC with one major iteration. Without more iterations to converge the quadratic surface to the nonlinear objective function and constraints, the LTV MPC could have bad tracking performance and constraints violation, as the simulation results have demonstrated. However, the execution time of the LTV MPC is almost one magnitude lower than that of the SQP MPC. With good initial guess of the optimal control sequence, the LTV model predictive IMEP control may be a viable option.

CHAPTER FIVE

EFFICIENT QP BASED MPC ALGORITHMS

5.1 Pattern recognition technique based QP strategy

Application of constrained Model Predictive Control (MPC) to systems with fast dynamics is limited by the time consuming iterative optimization solvers. This chapter of the dissertation proposes a fast and reliable Quadratic Programming (QP) strategy to solve MPC problems. While the optimal control action is calculated with a fast online dual QP algorithm, a "warm start" technique is adopted to reduce iterations of the online search process. The warm start solution is calculated from a predicted active constraint set generated by a pattern recognition function (Artificial Neural Network, ANN, is discussed). This function is calibrated with data from Monte Carlo simulation of the MPC controller over finite sampling points of the state-space. The proposed MPC strategy can adapt to applications with long prediction/control horizons, Linear Parameter Varying (LPV) dynamics and time varying constraints with balance between computation time, memory requirement and calibration effort. This concept is expanded to SQP and LTV applications where the system Hessian and Jacobean is identified in real time. Simulation results show that the ANN assisted SQP can achieve close to optimal control action with much less number of iterations, making the SQP algorithm fast enough to be implemented with systems of fast dynamics such as cycle-by-cycle engine IMEP control.

5.1.1 Introduction

Applications of MPC in the automotive industry are being discussed intensively for its ability to improve system transient performance, manage constraints and reduce control effort (e.g. *Hrovat et al. 2012, Junmin et al. 2012* and *Zhu et al. 2014*). However, for systems with fast dynamics, the heavy computation burden of constrained MPC is a big challenge for hardware implementation. Although microprocessors are getting faster, most MPC methods for mechanical system control are difficult to implement into prototype controllers and validate with hardware. The automotive industry has very restrictive control of product cost due to its production volume. Therefore, choosing more expensive processors are not favored over improving MPC algorithm efficiency.

Receding horizon constrained linear MPC controllers are the most common and fundamental design applied to systems with fast dynamics. These controllers optimize their control sequence for the future horizon using Quadratic Programming (QP). Since the development of active set QP algorithms in the 1980s, this solver has been the fastest option for online operation (*Gill et al. 1984, Goldfarb et al. 1983,* and *Schmid et al. 1994*). This active set algorithm is based on the fact that QP problems have closed form solutions if the active constraint set of the optimal solution is known. In the research work of *Gill et al. (1984),* active set algorithm based on the primal QP problem is proposed. The advantage of this method versus dual active set methods is that it keeps the solution feasible during the search for the optimal solution. However, because of the formulation of MPC, the primal QP problem usually contains large number of constraints. It requires a time consuming Phase I optimization to find a feasible initial

solution. The dual of the original QP problem with Lagrange multipliers as independent variables, on the other hand, has a much more uniformed constraint set ($\lambda>0$). The search for the dual feasible initial solution can be done by calculating the optimal solution of the primal problem without any constraints. Dual active set QP methods (e.g. *Goldfarb et al. 1983,* and *Schmid et al. 1994*) exploit this speed advantage, making them favorable for online operation with fast update frequency. *Bartlett et al. (2006)* employed the Schur-complement dual active set QP method to the MPC application. Most dual QP methods can be applied to MPC and tested with fast prototype controllers. However, they are still not fast enough to be implemented into the ECUs of a production vehicle or other common industry level microprocessors. In addition to these two types of active set methods, the primal-dual (or interior point) method is another option to solve QP for MPCs (*Goncalves 1972*). It is not widely considered for fast MPCs since it requires more computational effort to complete each iteration. Furthermore, the difficulty of finding a "warm" start point is another reason that makes it not suitable for fast online operation.

Computational effort of QP can be greatly reduced with a reasonable guess of the initial search point (*Bartlett et al. 2006* and *Ferreau et al. 2008*). All active set QP methods can benefit from a reasonable guess of which constraints may be active. *Ferreau et al. 2008* proposed the online active set QP based MPC strategy. Based on the assumption that the active set of constraints does not vary a lot between consecutive control steps for most MPC applications, this approach utilized the active set information of previous the control step to formulate the warm start point for the QP problem of current control cycle. Then the QP is solved using a parametric programming method,

which generates a suboptimal solution if terminated prematurely. This MPC approach was tested experimentally with the application of diesel engine EGR and VGT control (*Ferreau et al. 2007*). The disadvantage of this approach is the assumption on which it is based. For some MPC applications, especially with nonlinear system models, time varying dynamics and constraints, the active constraint set can change dramatically between each control update, leading to an increased number of iterations to find the optimal solutions.

It has been discussed in literature that the QP searching for optimal solution of MPC could be completed offline, while the online execution of MPC was transformed into a fast state and reference based control law (Piece-Wise Affine, PWA, function) (*Bemporad et al. 2002*). This approach was applied to multiple automotive related MPC research applications (*Cairano et al. 2012, Alberer et al. 2008, Ortner et al. 2006, Langthaler et al. 2007, Corona et al. 2008 and Caruntu et al. 2011*). The fast and straight forward execution process made it possible to validate these results with hardware tests. The calibration and execution process of this MPC approach shares some similarities with that of dynamic programming, including its disadvantages. In the cases with long prediction horizon and a large number of constraints, the calibration time and memory required to store the PWA function gain matrices become less acceptable. On the other hand, the stability of MPC controllers often relies on long prediction / control horizons (*Lee et al. 2011*) and a high number of constraints (*Herceg et al. 2006*). For Linear Time Invariant (LTI) MPC applications, it is possible to examine the Karush – Kuhn – Tucker (KKT) conditions for all constraint combinations to guarantee the validity of the control

action calculated with the PWA function. However, for MPC with time varying dynamics and constraints this process may be difficult even impossible to complete. Although the PWA gain matrices can be interpolated or extrapolated from stored values in these cases, the control action may not be optimal or feasible for the control horizon.

In this chapter of the dissertation, the proposed MPC strategy can be considered as a combination between online active set methods and a similar concept of the PWA approach. For the execution process, a fast dual active set QP solver is selected to search for the optimal solution from the warm start point that is calculated according to current system states and future reference. Since the start point is not used directly to compute the control action, a pattern recognition function is used to estimate the initial guess of the active constraint set with reasonable accuracy. For the offline calibration process, instead of checking the KKT condition of all possible constraint combinations, a pattern function is trained with data from objective oriented Monte Carlo simulation. In addition to reducing calibration time, this pattern recognition method can improve active set identification accuracy for time varying dynamics and constraints. The memory requirement of this approach is also greatly reduced since it only needs to store a function instead of numerous PWA gain matrices. Compared to using the active constraint set of the previous control step as a warm start, the pattern function can generate a better "guess" of the start point and reduce the number of iterations to find the optimal solution.

5.1.2 Pattern Recognition Technique Based Active Set QP Strategy

The previous chapter introduces the formulation of a special case of LTV MPC and SQP MPC. This chapter discusses an efficient QP strategy designed for general MPC

application. The most common MPCs focus on systems whose dynamics can be linearized and discretized into state-space formation. Without loss of generality, the state-space matrices can be different for each step, describing a LPV system whose states $x \in R^n$, control inputs $u \in R^m$ and outputs $y \in R^p$.

$$x(k+1) = A(k)x(k) + B(k)u(k)$$
$$y(k) = C(k)x(k) \tag{5.1}$$

with $A(k) \in \mathbb{R}^{n\times n}, B(k) \in \mathbb{R}^{n\times m}, C(k) \in \mathbb{R}^{p\times n}$

With the information of current system states X_0, the sequence of future system outputs Y_N of the prediction horizon N_p can be considered as an affine function of the future control action sequence U_N of control horizon N_c. The gain matrices F_N and G_N are formulated with the LPV state space function (5.1) (refer to Appendix A).

$$Y_N = F_N X_0 + G_N U_N \tag{5.2}$$

with $Y_N = \left[y(k+1), \cdots y\left(k+N_p\right)\right]^T$

$$X_0 = x(k)$$

$$U_N = [u(k), u(k+1), \cdots u(k+N_c)]^T$$

For the convenience of discussion, we dropped the step index k of the most variables that is stacked for the future horizon. If the control objective is to minimize tracking error and control effort, the optimal control action sequence can be calculated by solving the optimization problem whose cost function penalizes the sum of weighted

quadratic norm of both tracking errors and control action. The constraints that are commonly encountered in MPC include control magnitude, control changing rate and state magnitude. These constraints can be integrated and transformed into one linear inequality constraint system that is imposed on the future control action sequence U_N.

$$\min_{U_N} \left[\left(Y_N - Y_{ref}\right)^T R_y \left(Y_N - Y_{ref}\right) + U_N^T S_u U_N \right] \tag{5.3}$$

$$s.t.\ M_{cons} U_N - b_{cons} \leq \mathbf{0}$$

$$\text{with} \quad M_{cons} \in R^{j \times p}, b_{cons} \in R^j$$

$$Y_{ref} = \left[y_{ref}(k+1), \cdots y_{ref}(k+N_p) \right]^T$$

R_y and S_u are symmetrical positive definite weighting matrices of reference tracking error and control effort.

The above process transfers the equality constraints of system dynamics into the objective function, accelerating the search for an optimal solution. After substituting (5.2) into (5.3), the original optimization problem can be transformed into a QP form.

$$\min_{U} \left(\frac{1}{2} U_N^T H U + U_N^T F \right) \tag{5.4}$$

$$s.t.\ M_{cons} U_N - b_{cons} \leq \mathbf{0}$$

$$\text{with} \quad H = 2\left(G_N^T R_y G_N + S_u\right)$$

$$F = -2 G_N^T R_y \left(Y_{ref} - F_N X_0\right)$$

Equation (5.4) is referred to as the primal QP problem of the MPC. The primal QP algorithms can be applied at this point to solve (5.4) and obtain the optimal control action sequence. However, the primal QP has multiple linear inequality constraints, which make it difficult to find a feasible initial solution. A phase one optimization is usually required to identify a feasible start point. Instead of conducting a two phase optimum search for the primal optimization problem, this work employs dual QP algorithms to find the optimal solution. The conversion of the primal QP into a dual QP with Lagrange multipliers λ as independent variables is demonstrated by:

$$\min_{\lambda} \left(\frac{1}{2} \lambda^T \widehat{H} \lambda + \lambda^T \widehat{F} \right)$$
$$s.t.\ \lambda \geq 0 \tag{5.5}$$

Where:

$$\widehat{H} = M_{cons} H^{-1} M_{cons}^T$$

$$\widehat{F} = b_{cons} + M_{cons} H^{-1} F$$

Since the weighting matrices R_y and S_u are positive definite and constraints are linearly independent for most MPC applications, $\widehat{H}$ is strictly positive definite for most cases. Therefore, the QP represented by (5.5) is convex. The initial solution U_0 of this QP can be easily obtained by solving the primal QP without any constraints (equivalent to letting $\lambda = 0$).

$$U_0 = -H^{-1} F \tag{5.6}$$

Once the optimal solution (λ^*) of the dual problem is found, the optimal control action U^*can be calculated according to:

$$U^* = U_0 - H^{-1}M_{cons}^T\lambda^* \tag{5.7}$$

5.1.2.1 *Pattern Recognition Based Active Set Identification*

The warm start of the dual QP is a semi-positive vector λ_0 that is close to the optimal solution λ^*. If it is known which constraints are active for the optimal solution, the constraint system of the primal and dual QP can be separated as the following:

Primal	Dual	
$M_{act}U_N = b_{act}$	$\lambda_{act} > 0$	(5.8)
$M_{ina}U_N < b_{act}$	$\lambda_{ina} = 0$	(5.9)

Equation (5.8) shows active partition of the constraint system while (5.9) shows the inactive partition. After dropping the inactive constraints and substituting the primal active constraints partition into the objective function (5.4), the primal-dual problems have the closed form solutions as:

$$\lambda_{act}^* = -(M_{act}H^{-1}M_{act}^T)^{-1}(b_{act} + M_{act}H^{-1}F)$$
$$\lambda_{ina}^* = 0 \tag{5.10}$$

$$U^* = U_0 - H^{-1}M_{act}^T\lambda_{act}^* \tag{5.11}$$

Substituting F from (5.4) into (5.10), λ_{act}^{*} can be transformed into a PWA function corresponding to X_0 and Y_{ref} with three gain matrices. For LTI MPC, these gain matrices are constant.

$$\lambda_{act}^{*} = K_X X_0 + K_R Y_{ref} + K_0 \tag{5.12}$$

with $K_R = 2(M_{act}H^{-1}M_{act}^{T})^{-1}M_{act}H^{-1}G_N^{T}R_y$

$$K_X = -K_R F_N \tag{5.13}$$

$$K_0 = -(M_{act}H^{-1}M_{act}^{T})^{-1}b_{act}$$

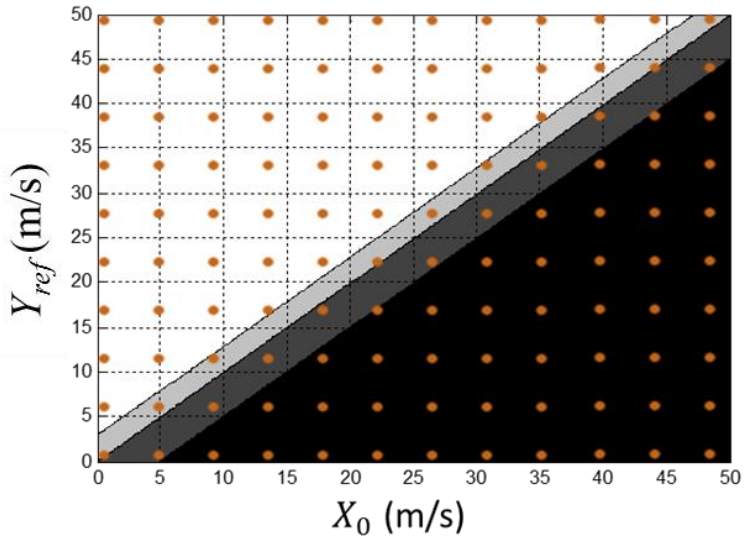

Figure 5.1: Visualization of active constraint set for MPC applied to driving cycle tests with 1 step prediction horizon. Orange dots represent sampling points for Monte Carlo simulation.

Similar to the primal PWA methods, it is possible to check the KKT conditions for all possible scenarios and store the corresponding gain matrices into the memory. The initial guess λ_0 can be exactly the same as the optimal solution λ^{*} . For LTI MPCs with single state ($n = 1$) and one step prediction horizon ($N_p = 1$), the active constraint sets

can be visualized as 2D polyhedra in the state space (Figure 5.1). This plot is generated using the MPC controller designed for the driving cycle application (discussed in next chapter) with 1 step prediction horizon and constant dynamics and constraint assumptions. In this case, Y_{ref} is the speed reference for the next step while X_0 is the current vehicle speed. One drawback of the PWA calibration is that the calibration time grows exponentially for control applications with long horizons and a large number of constraints. Furthermore, almost all matrices in (5.13) can be varying for Nonlinear MPC (NMPC) and non-constant constraint applications. For instance, if the limitation of engine power and quadratic aerodynamic drag are considered, the edge of active constraint set polyhedra are curved making the calibration of PWA gain matrices by checking KKT conditions difficult (Figure 5.2).

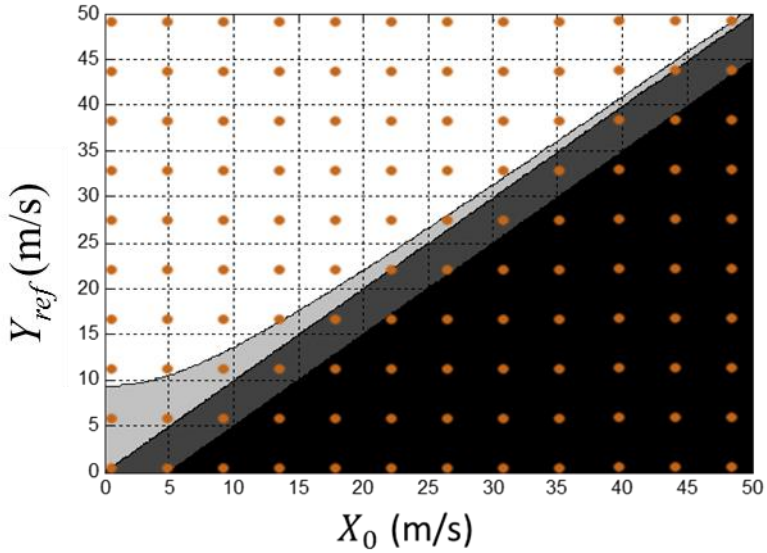

Figure 5.2: Visualization of active constraint set for MPC applied to driving cycle test with varying dynamics and constraints.

The identification of active constraint sets in the state-space can be considered as a pattern recognition process. Let ξ be a binary vector that has the same length p as λ.

Elements of ξ represent that the corresponding constraint is active with 1 and inactive with 0:

$$\begin{cases} \xi(i) = 0, & if\ \lambda(i) = 0 \\ \xi(i) = 1, & else \end{cases}, \text{for i} = 1,2, \dots\ j \tag{5.14}$$

Therefore, different ξ vectors can uniquely represent active constraint sets. Then the identification problem can be reduced to the fitting of the pattern function:

$$\xi = h(X_0, R_N) \tag{5.15}$$

The training data to fit the pattern function can be generated using Monte Carlo simulation with a sufficient finite number of state-space samplings (Figure 5.1 and 5.2). The selection of sampling resolution and range can be practical operation oriented to reduce calibration time. Many pattern recognition techniques can be applied to this application, including ANN (*Bishop 1995*), fuzzy logic (*Bezdek 1999*) and optimal margin classification *(Boser 1992*). For this research work, an ANN with scaled conjugate gradient training algorithm is selected because of its fast execution and calibration with MATLAB® Neural Network Toolbox™.

Table 5.1: ANN pattern function with different hidden layer size.

Hidden layer size	Max ξ diff.	Mean ξ diff.	Memory (KB)
5, 0	10	1.79	7.2
5, 5	10	1.78	8.2
10, 0	8	1.14	11.3
10, 5	7	1.11	12.0
10, 10	5	1.08	13.4

20, 0	5	0.83	19.3
50, 0	5	0.80	33.8

The most obvious advantage for the proposed active set method is the reduction in memory requirements. Storage of the pattern function h is usually negligible compared to hundreds of gain matrices for the traditional PWA methods. In order to better evaluate the proposed approach, the MPC applied to the driving cycle test is evaluated under random step inputs for 10^6 consecutive control cycles with prediction and control horizon expanded to 50 and 20 steps, resulting in 80 control constraints ($p = 80$). The traditional PWA cannot be evaluated with this case since it requires checking of the KKT conditions of 10^{24} points. The resulting gain matrices take GBs of memory to store. It is arguable that many of the constraints combination is infeasible and can be removed with a pre-process program. The magnitude of memory requirement is still not acceptable for current microprocessors. Table 5.1 compares the performance and memory requirement of the ANN pattern function with different hidden layer sizes. It can be observed that a simple double-layer ANN can predict the active sets with reasonable accuracy and memory demand. The rest of the analysis focuses on the ANN with 10 neurons on the two hidden layers.

Table 5.2: Comparison between cold start and different warm start techniques.

		Cold start	**Warm start**	
			Previous cycle	**ANN**
Constant system	Max ξ diff.	80	13	5

	Mean ξ diff.	74	5	1
	Max iter. #.	59	11	8
	Mean iter #	41	7	3
Varying system	Max ξ diff.	80	27	8
	Mean ξ diff.	70	9	1
	Max iter. #.	59	23	9
	Mean iter #	3	14	3

The performance of active set prediction methods is measured with ξ difference, which is defined as the number of ξ elements that is different from the ξ^* of the optimal solution. Most optimization algorithms takes more iterations to find the optimal solution with larger ξ difference although this relationship may not be exactly linear. Table 5.2 shows that the two warm start techniques generate close to optimal initial guesses of active sets. Comparing to the warm start technique that uses active set information of previous control cycle (traditional online active set method), the proposed ANN pattern function can provide more accurate initial guesses of active sets. This significantly reduces the number of online iterations to find the optimal solution. Figure 5.3 shows that the ξ predicted ANN has two elements different from the optimal ξ^* for more than 90% of control updates. Another important characteristic of the new approach is that it does not rely on the active sets to be straight polyhedra (Figure 5.2) and accuracy of active sets prediction is not as sensitive to varying dynamics and constraints as the traditional online active set method (Figure 5.2 and 5.3). However, identifying active sets for varying

system applications can benefit from training data with higher resolution of the state-space.

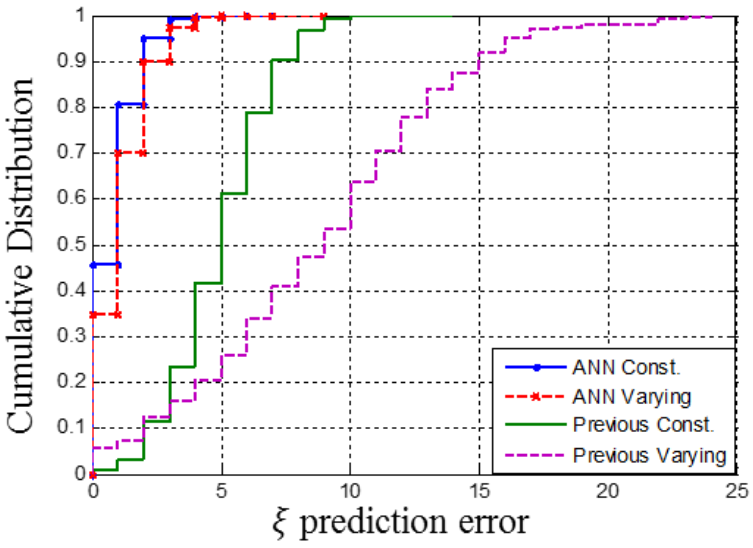

Figure 5.3: Cumulative distribution function of ξ prediction error between different warm start techniques. Both constant and varying system dynamics/constraints are evaluated.

Depending on the control objectives, the pattern function can include other inputs to capture non-state dependent variation of dynamics and constraints. For instance, the vehicle mass m can alter the vehicle longitudinal dynamics. The pattern function inputs are augmented by including the vehicle mass to predict the active sets with consideration of vehicle loading conditions:

$$\xi = h(X_0, Y_{ref}, m) \tag{5.16}$$

5.1.2.2 Hildreth Search Method for λ^*

Without using the predicted active sets to compute control actions directly, the online optimal search process increases tolerance to initial guess error. Therefore, it is possible to use training data with coarser resolution to calibrate the pattern function. For

applications with long prediction and control horizons, this trait of the proposed MPC strategy allows for faster calibration and more robustness against system variations than PWA methods.

The dual QP methods of Hildreth and D'Espo (*Luenberger 1969* and *Wismer et al. 1978*) are applied to search for optimal solution λ^* for computational efficiency. Without matrix inversions during each iteration, the algorithm is fast and reliable (*Wang 2009*). The following are the important steps of the Hildreth approach:

Step 1: The unconstrained optimal solution of dual QP (5.5) can be calculated by finding the point with zero gradients for all directions (stationary points):

$$\frac{\partial\left(\frac{1}{2}\lambda^T\widehat{H}\lambda+\lambda^T\widehat{F}\right)}{\partial\lambda}=0 \tag{5.17}$$

From (5.17), linear equations can be obtained for the dual QP with p non-negative constraints as shown in the following:

$$\widehat{F}_i+\sum_{k=1}^{j}\widehat{H}_{ik}\lambda_k=0, k=1,2,\dots j \tag{5.18}$$

Step 2: during each iteration, solve (5.18) for λ_i with λ_k $(k\neq i)$ from previous iteration. Then $\widetilde{\lambda_i}=\max(0,\lambda_i)$.

Step 3: go back to Step 2, if the new Lagrange multiplier $\widetilde{\lambda_i}$ is different from the previous iteration (by some tolerance). Otherwise, solution has converged to the optimal value λ^*.

5.2 Extension to SQP applications

The proposed pattern recognition based active set MPC strategy is based the assumption that the QP can be formulated explicitly with the linearized state space model of the system. For most MPC applications this is assumption is valid. However for the SQP MPC applications, the Hessian and Jacobean for the system depends on the nominal control action U_0, which is different for every major iteration. The proposed LTV MPC has the similar situation that the nonlinear state-space model has to be linearized according to the nominal control action. If the nominal control U_0 is very different from the optimal solution U^*, the linearized model is not a reasonable approximation of the original nonlinear system. This could impact the optimality and feasibility of the solution. Therefore for both of the SQP and LTV MPCs with real time system Hessian and Jacobean identifications, providing decent guess of Lagrange multiplier λ^* along is not sufficient to properly initialize the QP. A decent guess of the optimal control action U_0 that is close to the optimal solution is necessary to reduce the computation burden of these nonlinear MPC options.

The tracking MPC controllers can be considered as functions of optimal control actions $U^*(k)$. The inputs to this function are the current system states $x(k)$ and future reference for the prediction horizon $Y_{ref}(k)$. There are some literature proposed to use ANNs to imitate these "MPC functions" to approximate optimal control actions (*Gómez* 1994 and *Piche* 2000). Although the ANNs trained with offline Monte Carlo simulation were able to generate control actions that are very close to the optimal solution, they

often relied on real time adaptation and learning to account for fitting errors. Thus the stability and robustness could not be proved analytically. In this research, we employ the ANN approximated control action as the initial guess of optimal control action. This initial guess initializes the SQP and LTV algorithms with real time linearization techniques. The ANN used in this research has 50 neurons on two hidden layers. Figure 5.4 shows the validation result of the ANN approximated optimal control against the exact SQP MPC solution discussed in previous chapter. The training data of the ANN is from a 10^6 consecutive engine cycles Monte Carlo simulation with random IMEP reference. The R^2 is 99.84%, indicating that ANN prediction of the optimal control is reasonably accurate.

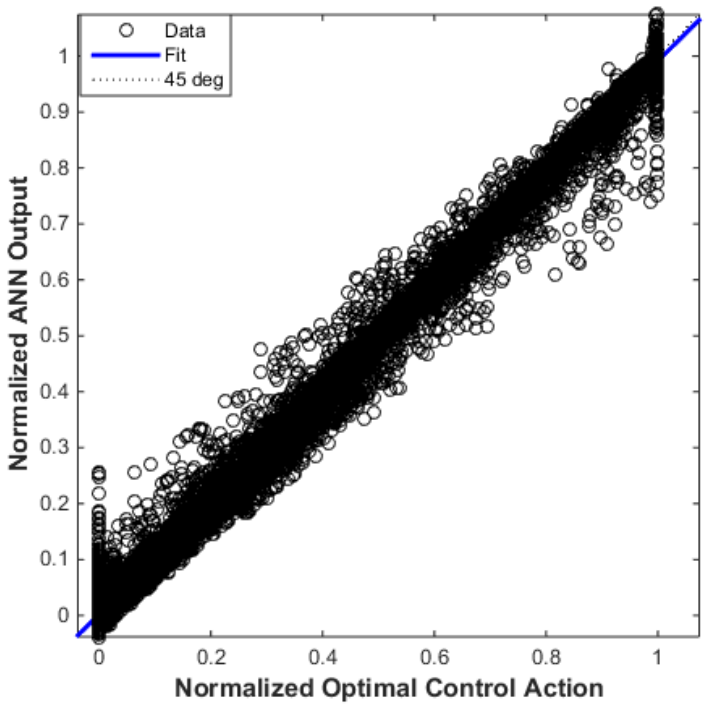

Figure 5.4: Validation of the optimal control action calculated by ANN.

However, it can be observed that the ANN is not perfectly accurate in some cases. Since the exact MPC solution is applied to the system instead of the ANN approximation, online training is no longer necessary to guarantee the stability and robustness of the controller. The sub-QP is solved by Hildreth algorithm, which is discussed in previous section. The Hildreth algorithm is a dual active set solver that requires an initial guess of Lagrange multiplier λ, which can also be calculated knowing the active constraint set index ξ (equation 5.10). ξ can be generated with another ANN like the approach discussed in previous section. It can also be easily calculated with the initial guess of U^* and the constraint matrices M_{cons} and b_{cons}, which are available after the real time linearization at U_0.

$$\xi_0 = M_{cons}U_0 - b_{cons} > 0 \tag{5.19}$$

Figure 5.5 shows the engine performance and control actuation of the ANN assisted SQP model predictive IMEP control. This IMEP controller generate equivalent results as the SQP MPC discussed in previous chapter.

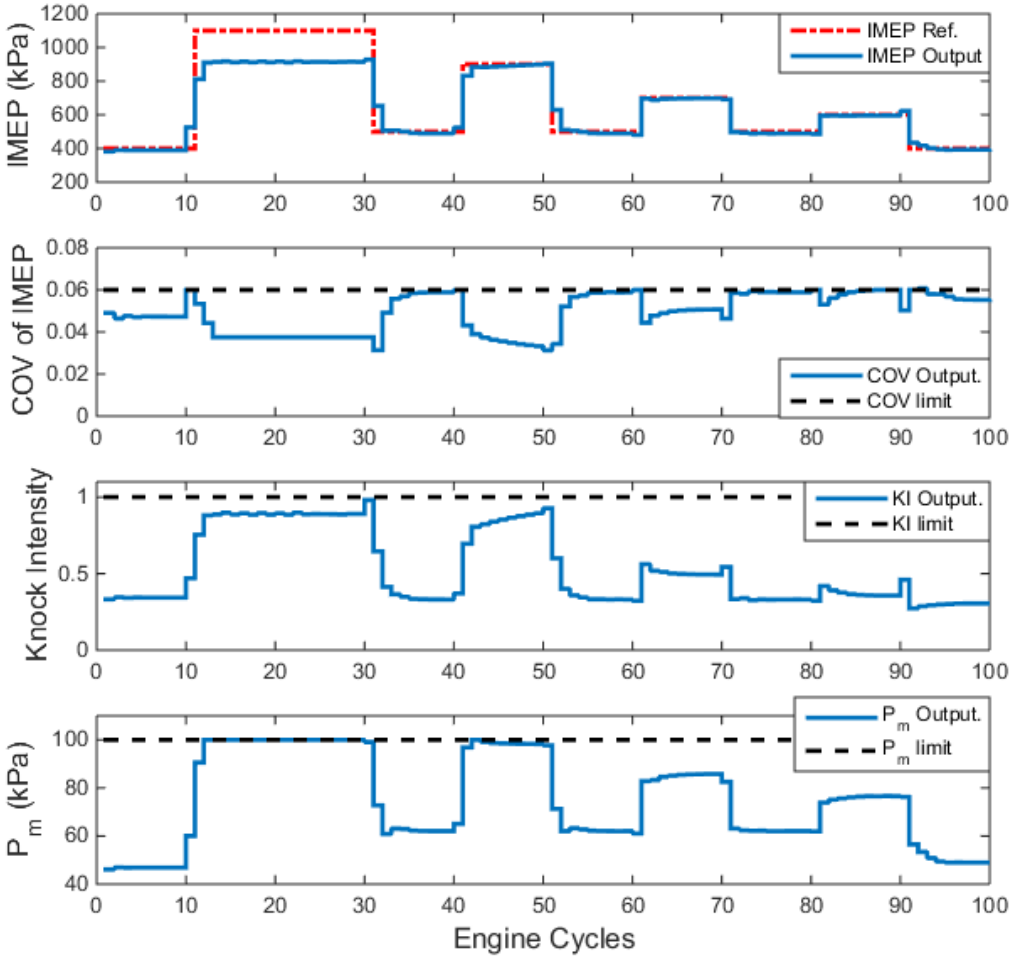

Figure 5.5 a: Engine performance of the ANN assisted SQP model predictive IMEP control

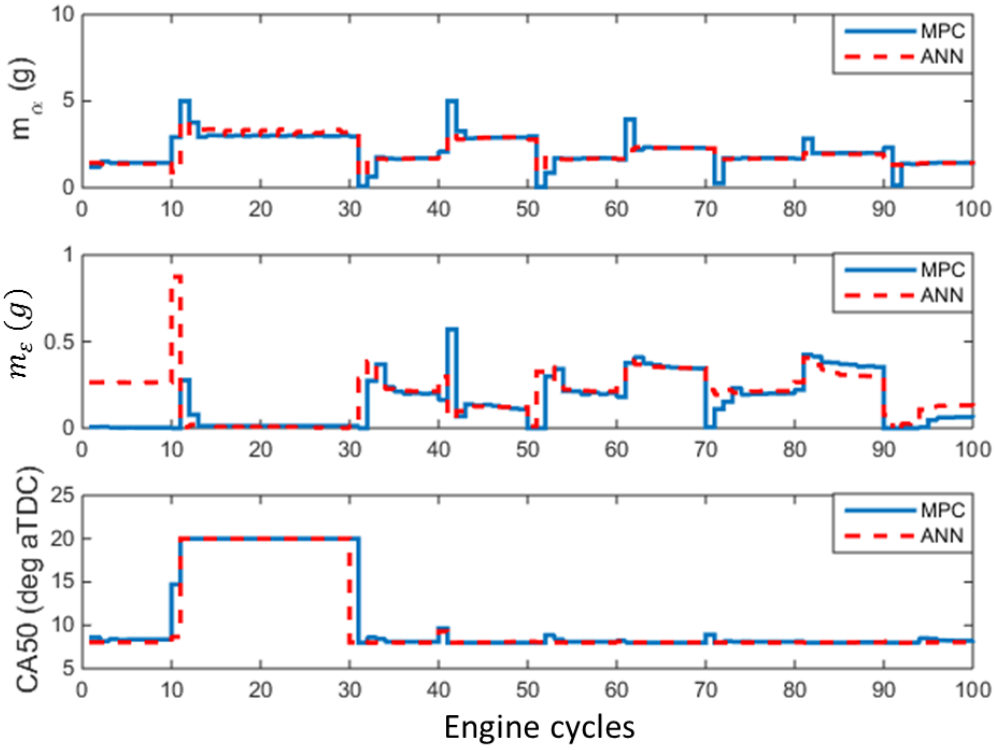

Figure 5.5b: Control actuation of the ANN assisted SQP model predictive IMEP control

However, Simulation results show that the initial guess generated by ANN can significantly reduce the number major iterations of the SQP. Furthermore, the number of minor iterations to solve the sub-QP is also reduced by around 50%. These advantages results in an execution time 1 magnitude less than that of the SQP without ANN assist, making it possible to implement the proposed ANN assist SQP model predictive IMEP control with prototype engine controllers.

Table 5.3: Computation time comparison between ANN assisted SQP and the SQP discussed in Chapter 4. The values are the mean of 10^6 engine cycles Monte Carlo simulation.

	SQP	ANN SQP
Number of major iterations	42	3.6

Execution time per engine cycle	26.00 ms	1.91 ms
Execution time per major iteration	0.63 ms	0.53 ms
Execution time for model evaluation per iteration	0.39 ms	0.40 ms
Execution time for QP per major iteration	0.23 ms	0.13 ms
Number of minor iteration per QP	43	21

5.3 Conclusions

In this chapter of the dissertation, efficient strategies to solve QP in the MPC context is discussed. Firstly, a pattern recognition based active set QP strategy is proposed to solve general MPC problems. These MPCs are solved by means of an online QP based on the Hildreth algorithm, a dual search method. Without matrix inversions each iteration, this algorithm is fast and reliable. The initial point of the online search is calculated from current system states and future reference with a pattern function. The recognition of the pattern function is complete with data generated from Monte Carlo simulation. The pattern function can also include non-state dependent variables as input to further improve the adaptive-ness of nonlinearities. Compared to a traditional PWA approach, the pattern function requires less memory space, making it possible to handle problems with long prediction/control horizons and a large number of constraints. The online search process guarantees the robustness against pattern function fitting error. Simulation results indicate that it may be possible to employ a simple ANN to reasonably predict the active constraint sets for MPC with a long control horizon and varying dynamics and constraints. The prediction accuracy is better than using the previous active set directly. As a result, the warm start point generated by the pattern function can significantly reduce iterations when finding the optimal solution.

The similar concept is expanded to the SQP MPC applications. Instead of guessing the index of active constraint set, an ANN is used to directly estimate the optimal control action, which is then used to initialize the sub-QP formulation and

algorithm. Like the pattern recognition based general MPCs, the ANN results are only used to provide the warm start to the MPC instead of generating control actions directly. Thus the accuracy of the ANN is not critical to the stability and optimality of the solution to the optimization. Simulation results proves that the SQP can have much less major and minor iterations with the ANN predicted optimal solution. The execution time is one magnitude less than the SQP without ANN making it possible to be applied to prototype engine controllers.

CHAPTER SIX

ENGINE-IN-LOOP DRIVING CYCLE TEST WITH MPC DRIVER MODEL

Driving cycle tests are a comprehensive evaluation of vehicle powertrain performance. *Filipi et al. (2006), Shidore et al. (2005)* and *Nabi et al. (2004)* discussed Hardware-in-Loop (HIL) or Engine-in- Loop (EIL) setups to complete driving cycle tests on the engine dynamometer. While the actual engine and control system was installed in the dyno test environment, the rest of the powertrain and vehicle longitudinal dynamics were simulated with real time models. These test methods allow testing of powertrain component design and control before building the prototype vehicle. Since it is unlikely a human driver would be utilized for this type of testing, most previous work used classical controllers (e.g. PID) to track the designated speed profile. It is speculated that using MPC in this application could solve many potential tuning issues and provide better speed tracking performance. Furthermore, the MPC can "foresee" the incoming speed profile. This predictive behavior can mimic a real driver response to the incoming traffic conditions. Thus the MPC is able to generate smooth throttle and brake actuation, which is close to real driver actuation. The vehicle model embedded with the "MPC driver" considers the quadratic aerodynamic drag and engine torque reserve, making the MPC a LTV controller. The pattern recognition technique based QP strategy is applied to solve for the optimal control action.

6.1 HIL Driving Cycle Test Setup and Modeling

Figure 6.1 shows a block diagram of the HIL driving cycle test setup. Other than the engine and dynamometer (red dash circle), the rest of the components are simulated with real time models in dSPACE prototype control system. The engine dyno speed is determined by current vehicle speed and gear ratio. Through the software interface the throttle and engine speed are sent to the dyno, while the engine torque measured by the dyno is sent back to the software interface.

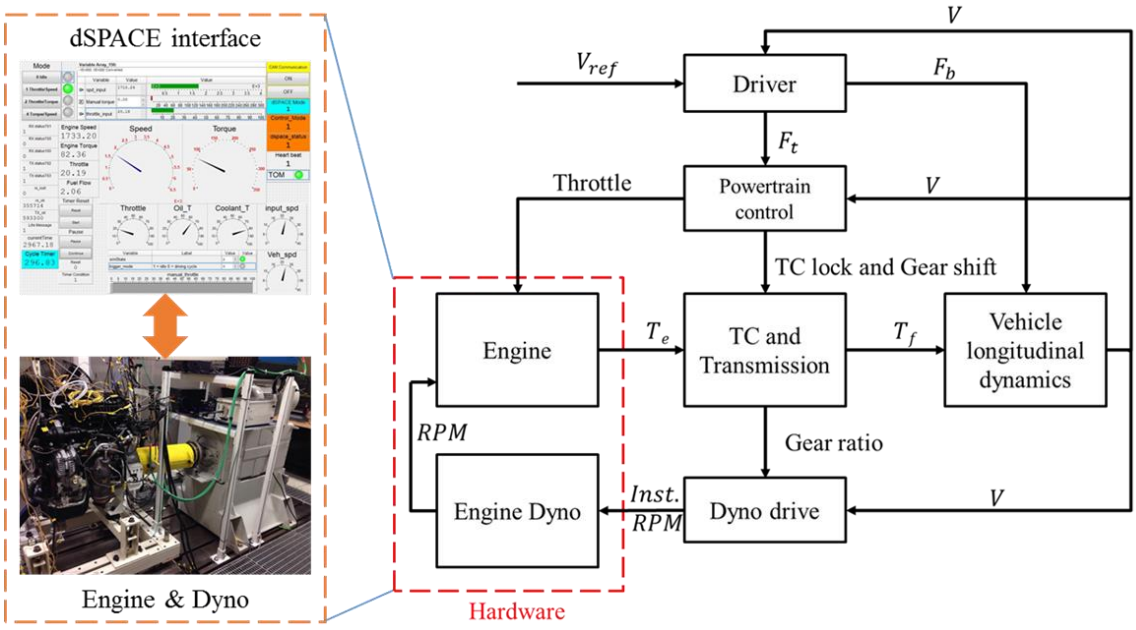

Figure 6.1: Schematic diagram of engine-in-loop driving cycle testing. V_{ref} is the reference speed. T_e and T_f are torque output from engine and final drive, respectively.

The entire system of Figure 6.1 is shown to work in simulation. Both engine and dyno are replaced with mathematical models currently. The engine model is the control oriented model described in Section 4.3.1. This engine model can generate reasonable torque response and steady state fuel consumption (assuming stoichiometric air-to-fuel

ratio), which were validated with experiment data. The dyno is assumed to be able to measure engine torque instantaneously. Its delay to RPM command is considered as a first order delay with time constant of 0.7s.

A MPC controller is implemented as the "driver". The MPC control objective is to mimic a real driver on actual roads, who foresees the desired vehicle speed several seconds ahead of time. The update frequency of the MPC is set to be 0.5s. Both prediction and control horizons are selected as 10 steps during the simulation. The optimization problem is formulated as described in Section I. Both speed tracking error and control effort are being minimized with respected weightings. The gas and braking pedal actuation are interpreted as demand of traction force and braking force ranging from 0 to the maximum value. While the maximum braking force is assumed to be constant, the maximum of traction force is limited by the maximum engine power at the specific vehicle speed. The following equation is used as the vehicle model implanted to the MPC "driver".

$$\mu mg + \frac{1}{2} C_D A_{front} \rho V_e^2 + m\dot{V}_e = F_t - F_b \tag{6.1}$$

where A_{front} is frontal area. C_D is aerodynamic drag coefficient. F_t and F_b are traction and braking force respectively. V_e is vehicle speed. μ is the coefficient of rolling resistance.

The longitudinal vehicle dynamics in equation (6.1) are linearized at each step according to reference velocity along the prediction horizon. Therefore, both control constraints and system dynamics are time varying within the horizon, making MPC a

LTV controller. The proposed pattern recognition QP strategy is applied to solve for the optimal control action in real time.

The powertrain control system coordinates the throttle voltage and gear shifting. Throttle voltage is mapped to the desired engine torque output, which is calculated according to the driver's traction force demand and current gear ratio. Target RPM is defined as the engine speed at which the power demand line intersects with the best BSFC curve (Figure 6.2). Finally, the gear is selected as the one that can match the target RPM closest for the current vehicle velocity.

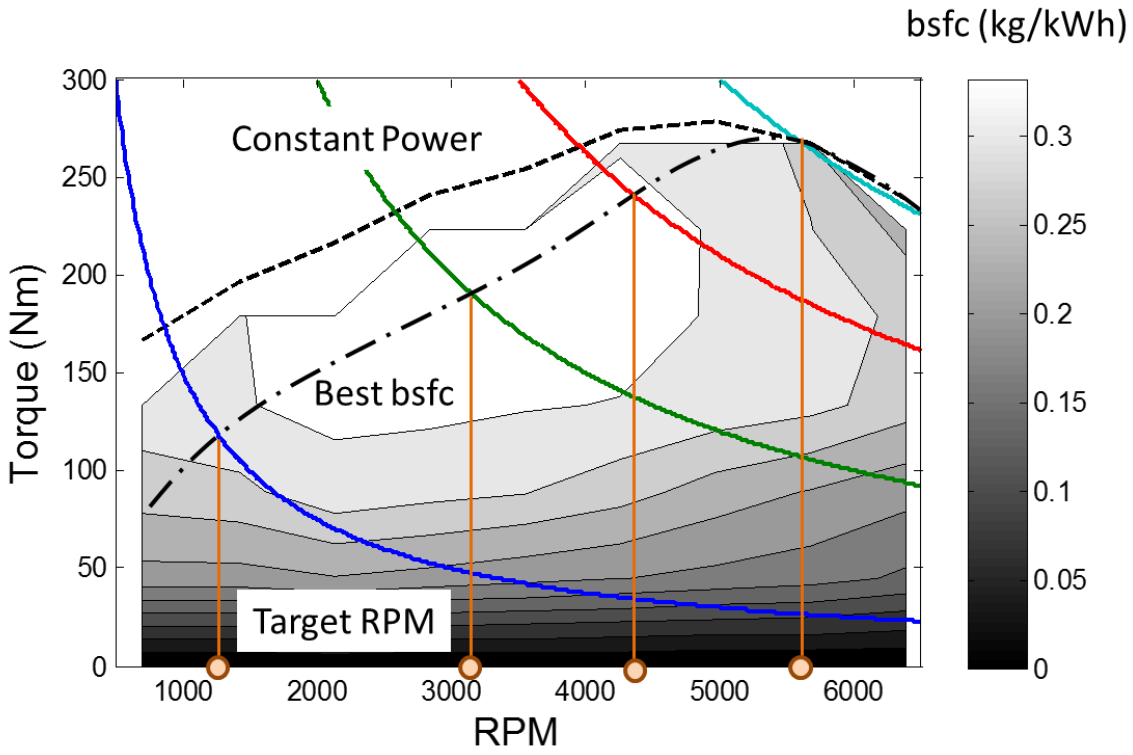

Figure 6.2: Target RPM calculation from power demand and engine BSFC map.

6.2 Simulation Results

Simulations are conducted implementing the proposed MPC strategy within the HIL driving cycle test using the following main parameters.

Table 6.1: Important parameters for the simulation

Engine	Displacement	3.2 L
	Max torque	287 Nm
	Max power	157 kw
Powertrain	Gear ratio	4.1/2.4/1.6/1.2/0.9/0.7
	Final drive	2.8
Vehicle	Mass	1800 kg
	$C_D \times A$	0.25×2.1
FTP Driving Cycle	Max/Average speed	91/34 km/h
	Max accel./decel.	3/-3 m/s^2

The performance of two MPC "drivers" is compared to a PID controller. Figure 6.3 is a snap shot of vehicle speed and normalized driver actuation from a portion of the drive cycle. Both MPC "drivers" demonstrate the ability to optimize control actions according to future reference and constraints. The first MPC (MPC 1 in the figures) has small weighting on the control effort (S_u). Therefore, it tends to change the control actuation aggressively to match the speed profile. The mean speed tracking error (MSTE) is 3.8%. The second "economical" MPC (MPC 2 in the figures) has a larger S_u resulting smooth pedal actions. Although its speed tracking performance (MSTE 6.5%) is slightly worse than the "aggressive" MPC, the "economical" MPC still follows the speed profile better than the PID "driver", whose MSTE is 11.6%.

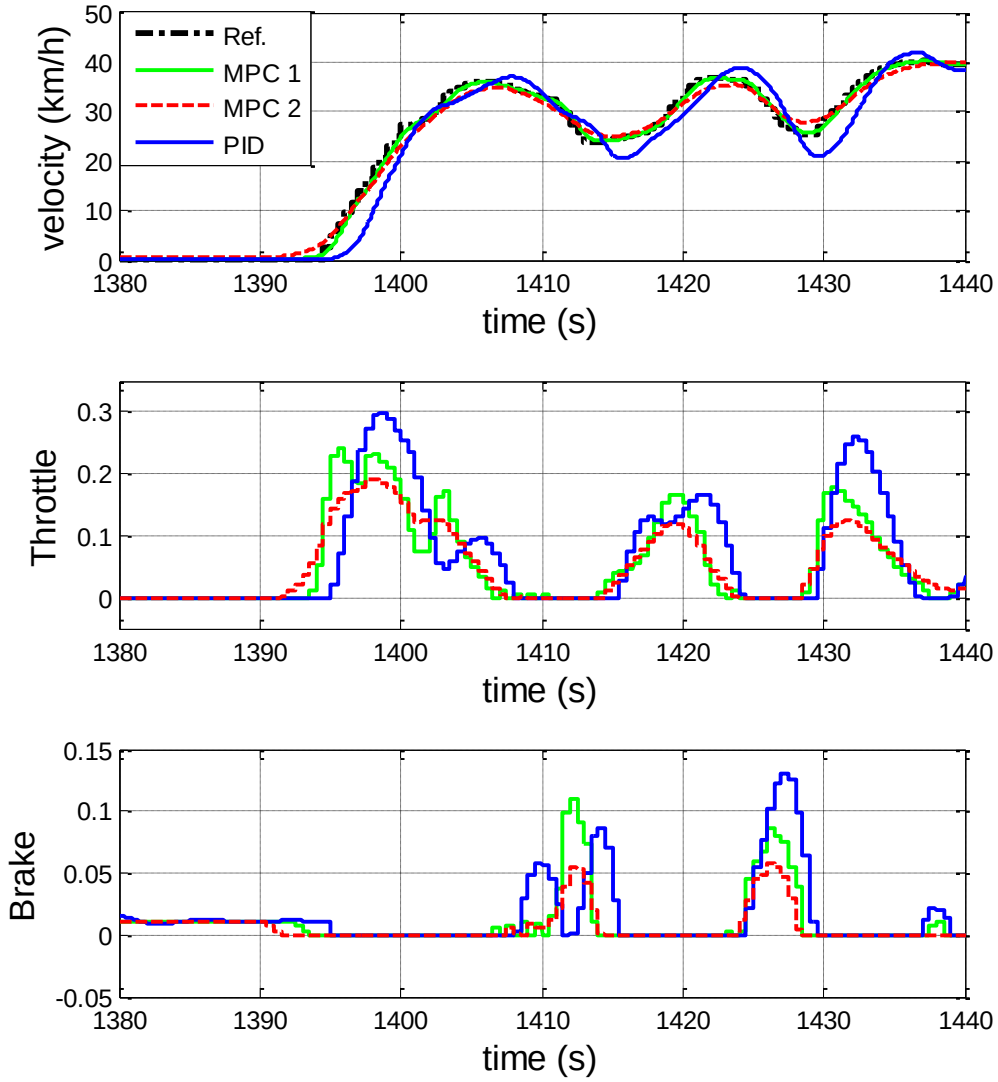

Figure 6.3: Performance comparison between aggressive MPC (MPC1), economical MPC (MPC 2) and PID "drivers"

Figure 6.4 shows the comparison of engine torque, speed and instantaneous fuel flow rate between the three controllers. Since the MPCs generate gas pedal action with lower magnitude, the power demand of MPCs is less than the PID controller. Therefore, the engine speed and torque are lower, with fewer gear changes. This results in lower instantaneous fuel flow rate.

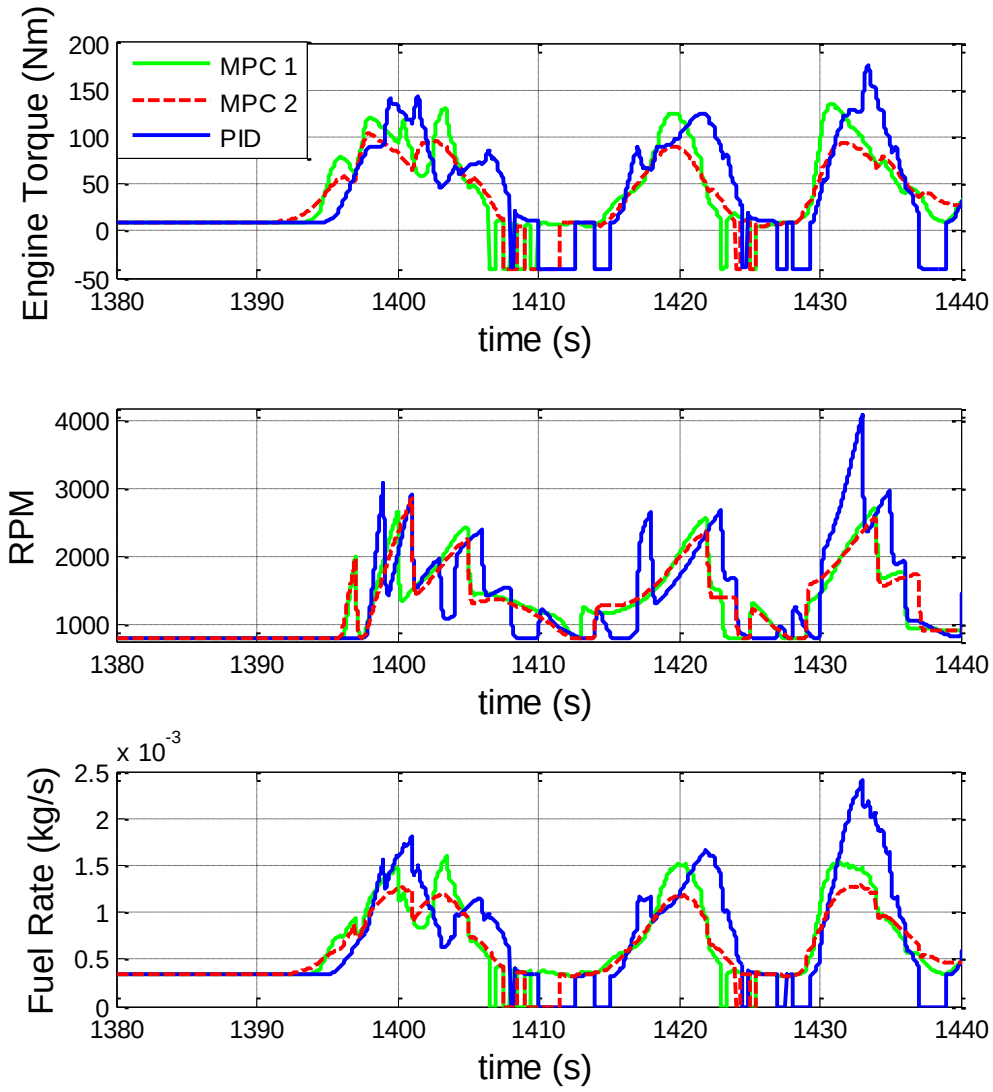

Figure 6.4: Engine behavior comparison between three controllers.

Table 6.2 shows the MPG calculation for three drivers over the entire driving cycle. Although the MPCs are designed to mimic realistic driver reaction, an unintentional result is improved fuel economy of the evaluated vehicle from smooth pedal actuation. The difference in fuel economy may be larger between these three controllers if transient fuel consumption were accurately captured (the engine map is

based on steady-state data), which can be realized with a more detailed engine model or actual hardware testing.

Table 6.2: Fuel economy comparison between the three controllers.

	PID	Aggressive MPC 1	Economical MPC 2
MPG	24.39	25.81	26.62

CHAPTER SEVEN

SUMMARY AND CONCLUSIONS

7.1 Dissertation Summary

This dissertation investigates the challenges of applying model predictive control to SI engine management and testing. Compared to traditional engine control based on feed forward and simple feedback strategies, the model predictive engine control requires much less effort to calibrate, making it favorable for engines with high number of degrees of control freedom. The MPC predicts system behavior for the prediction horizon, making it possible to calculate the optimal control actions that compensate for system delays and incoming constraints. Therefore, the MPC usually has superior transient performance than the classic feedback controllers. However, there are some application issues keeping MPC based engine control from being adopted by automotive industry. This research work focuses on investigating three of them: 1) a new SI engine control framework that can maximize the MPC's potential to optimize engine performance and exploit the control bandwidth of actuators; 2) optimization algorithms that are able to utilize complex engine models to compute optimal control actions; 3) strategies to reduce the computation, calibration and memory demand of the MPC controllers.

The one dimensional model predictive combustion phasing control is challenged by the complexity of the SI engine combustion modeling. The control objective is to find the SPKT that generates close to target combustion phasing without inducing knock and

combustion instability. Although the control objective is very straight forward, achieving this objective requires iterative numeric nonlinear programming algorithms. Three proposed SPKT optimization strategies can find the optimal SPKT with few number of iterations. These three algorithms are proven to be efficient with certain types of combustion models using both simulation and dynamometer tests.

The MIMO SI engine optimal IMEP control increases the control dimensions compare to the combustion phasing control. Although some models developed for the combustion phasing control can be transferred to the IMEP control, the optimization problem formulated to obtain desired control action is much more complicated for the IMEP controller. Chapter four introduces cascaded control structure to simplify the online optimization problem by transferring some nonlinear dynamics to the lower level controllers. LTV and SQP MPC strategies with real time system linearization techniques are applied to solve the nonlinear optimization considering the complex nature of engine models.

Chapter five focuses on reduce the execution time, calibration effort and memory requirement of MPC. This research work proposes to apply pattern recognition techniques to capture the correlation between active set of constraint and system states (and future reference). This technique is able to initialize most LTI and LTV MPC and significantly reduce QP iterations with minimal additional memory demand. The EIL utilizes this LTV MPC strategy to mimic realistic driver actuation on the throttle and brake pedals with preview of the target speed profile. For SQP MPC applications, the MPC can be fully initialized with a decent guess of optimal control actions, which is

approximated by an ANN. Training data of the ANN is generated by offline Monte Carlo simulation of the exact MPC.

The following section of this dissertation lists the most important findings of this research work.

7.2 Significant Conclusions and Findings

7.2.1 Covariance of IMEP Model

The COV of IMEP model is based on flame regime analysis of combustion stability and the thermodynamics of in-cylinder mass. The model was validated with data from steady state engine operation tests. Simulation and experiments were conducted to test the model. The important finds of this section includes:

- The COV of IMEP is used as an indication of combustion instability. However, these two concepts are not exactly equivalent to each other. The synchronization between the combustion process and piston motion should be consider when modeling the COV of IMEP. Therefore, variables related to combustion phasing are included as the inputs to the COV of IMEP model.
- This research work proposes to use the inputs of Leed's diagram to capture the heat release variation during the combustion. These inputs are computed at TDC for two reasons. The first reason is that the instantaneous heat release rate variation peaks around TDC. Furthermore, cylinder volume is the smallest at TDC, making the variation of heat release more influential to cylinder pressure.
- ANN is applied to model the IMEP. A nonlinear conversion model is added before the ANN to reduce the size of the network. This method can reduce the over fitting phenomena, improving extrapolation stability.

7.2.2 Cycle-by-cycle Model Predictive Spark Timing Control

This research work proposes three online optimization methods to search for desired SPKT, which achieves close to target combustion phasing without violation of knock and COV of IMEP constraints. These approaches can be integrated with high-fidelity combustion models. Both simulation and real-time experimental results indicate that these three algorithms can find the optimal SPKT with few number of iterations, making them possible to be implemented with future engine ECUs. The important finds of this section includes:

- The SPKT optimization is a nonlinear programming problem, which cannot be solved analytically. The gradient based optimization methods cannot be applied to this application due the complexity of the combustion models.
- The SPKT optimization is convex for most admissible range of SPKT. Therefore the problem has a unique global optimal solution.
- The direct search methods are favorable to this application since they find the search direction based on function evaluations instead of gradient information. The 2-Phase direct search method applies interior point technique that guarantees feasibility and descending objective function even if the program is terminated prematurely due to lack of computational time. It is the least demanding option among the three proposed SPKT optimization strategies in terms of the continuity of the objective and constraint functions.
- The constraint relaxation method is also a direct search methods that integrates the original constraints into the objective. The most important

advantage of this method is that it is easy to program since it does not handle constraints explicitly. The lack of phase 1 optimization results in fewer number of iterations compared to the 2-Phase. However, the constraint relaxation methods requires the original constraint functions to be convex, making it not compatible with knock and COV of IMEP models of low resolution.

- The proposed RLS polynomial fitting SPKT optimization method finds the optimal SPKT by solving a sub-level optimization during each iteration. The sub-level optimization approximates the original complex objective and constraints functions with low order polynomials using RLS approach. This research work also discusses forgetting factor technique to accelerate the convergence rate of the RLS algorithm, which is particularly important if linear functions are used to approximate nonlinear objective and constraints functions. Simulation and test results shows that the RLS polynomial fitting method has a much less number of iterations than the direct search methods. However, its convergence rate is sensitive to the initial guess of the polynomial function and the continuity of the combustion model output.

7.2.3 Model Based Combustion Phasing Estimation

This research demonstrates an extended Kalman filter based approach to improve the CA50 measurement from cylinder pressure sensor feedback. By employing a CA50 prediction model as a “virtual sensor”, the Kalman Filter effectively solves the conflict of signal processing between responsiveness and accuracy. The proposed CA50 estimation

method was applied to a model based combustion phasing control and validated with both simulation and real-time transient dynamometer tests. The contributions of this section include:

- The KF based approach can respond to CA50 changes within one engine cycle. Because of this unique property, the approach can be applied to different engine types where strong cycle-by-cycle dynamics are present.
- For applications in SI engines where cycle-to-cycle dynamics can be neglected, steady state error is inevitable since the CA50 model is not perfectly accurate. Instead of adapting the model, it is proposed to use a switching mode estimation adapting to whether the engine is in steady-state or transient operation. Negligible steady state error is observed during real-time experiments. Compared to a moving average (10 engine cycles), estimation error RMS of the KF approach is one order of magnitude lower under both transient and steady state situations.
- The application of a forgetting factor in the switching mode KF significantly improves estimation performance when the CA50 prediction model is very inaccurate or fails to capture certain engine dynamics.
- A responsive and reasonably accurate estimation of CA50 makes it possible to employ feedback controllers to regulate combustion phasing. This could potentially reduce amount of calibration work during the development of an IC engine significantly. The estimation results can also be integrated with model based feed forward algorithms to adapt models online.

7.2.4 MIMO SI Engine IMEP Optimal Control

This chapter of the dissertation introduces a model predictive IMEP control frame work and strategy. The proposed frame work can significantly reduce the complexity of the online optimization solving for the optimal control actions. The proposed MPC strategy is able to utilize the complex engine models. The model predictive IMEP control is validated with simulation. The important finds of this chapter includes:

- The cascaded control structure removes orifice flow and combustion phasing models from the MPC loop, significantly reducing the complexity of the online optimization. These dynamics are handled with lower level controllers with faster sampling time and less computational complexity. These controllers maximize the potential of actuators bandwidth. They also provide automotive OEMs the ability to fine tune the control actions to account for un-modelled dynamics.
- The MPC is formulated in engine cycle domain. This approach simplifies the modeling of air-path dynamic by removing its dependency on engine speed. The torque generation modeling is also easier in engine cycle domain since it is not necessary to model the delay between intake and power stroke. Finally, most existing engine combustion models are developed in engine cycle domain. They can be easily integrated with the proposed IMEP control frame work.
- The one dimensional combustion phasing control serves as a lower level controller to the model predictive IMEP control. Since the CA50 target

generated from the MPC has already considered knock and combustion stability constraints, the combustion phasing control have much less number of iterations comparing to the complete version discussed in chapter three.

- The engine is modelled using energy balance approach. This method can accurately model the IMEP output, exhaust gas enthalpy and heat transfer to coolant. This modelling approach makes it easier to expand the model with more actuators. The future expansion of this research work will discuss the model based engine states estimation, which can utilize the proposed engine model to combine information from different sensors.
- The SQP MPC is applied with the optimal IMEP control. In order to utilize the complex engine models, real time linearization technique is employed to compute the Jacobeans of the objective function and constraints. It is demonstrated that the Hessian of the SQP can be easily approximated with the linearized system model in the context of "tracking" MPC. This approximated Hessian is guaranteed to be positive definite and able to ensure global convergence tendency.
- This research work proposes to add increasing control variation penalty to the SQP. This method increases the convergence rate of the SQP. The termination condition of the SQP is also modified by monitoring the objective function value after each iteration. Both these techniques reduces the chance of the SQP stopping at different local minimum points during steady state operation, reducing control chattering issues.

7.2.5 Efficient QP Based MPC Algorithms

In this chapter of the dissertation, efficient strategies to solve QP in the MPC context are discussed. A pattern recognition based active set QP strategy is proposed to solve general MPC problems. The similar concept is expanded to the SQP MPC applications. Instead of guessing the active set constraints, an ANN is used to directly estimate the optimal control action, which is then used to initialize the sub-QP problem. These MPC strategies were compared with traditional active set QP algorithm using simulation. The important finds of this chapter includes:

- The Hildreth dual active set algorithm is applied to solve the QP problems. Without matrix inversions during each iteration, this algorithm is fast and reliable.
- The active constraints set can be described with a binary pattern vector. The correlation between these vectors and corresponding system states are treated as a function identified by pattern recognition techniques. ANN is used in this research work. But it does not exclude possibilities of other pattern recognition techniques to be applied to this application. The ANN pattern function can accurately predict the active constraints set. Compared to PWA methods, the proposed QP strategy is able to handle LTV MPCs. It also requires much less memory space, making it possible to be applied with MPCs of long horizons.
- It is identified that the SQP MPC cannot be fully initialized with information of active set of constraints. A decent initial guess of the optimal control action

is necessary to reduce the number of major iterations. It is proposed to use ANN to approximate the optimal control actions with the current system states and future reference. Simulation results show that the ANN assisted SQP has much less number of major and minor iterations than the traditional SQP. This method significantly reduces the execution time of the model predictive IMEP control.

- The proposed QP strategies utilizes ANN to generate a start of search point that is very close to optimal solution. As a result of this warm start approach, the effort to search for the optimal control action is greatly reduced. Since the ANN results are not directly used to compute control action, the MPC is free from the stability and robustness issues caused by fitting errors of the ANN.

7.2.6 Engine –in – Loop Driving Cycle Test with MPC Driver Model

This chapter introduces an EIL test setup with MPC driver model based on the proposed pattern recognition QP strategy. The system is validated with simulation. The important finds of this chapter includes:

- The MPC successfully mimics the pedal actuation of a real human driver, who foresees the incoming traffic conditions and adjust pedal actions predictively. For this reason, the MPC tracks the speed profile much than the PID “driver”. Compared to real human driver, the MPC can generate repeatable driving cycle test results.
- The MPC can simulate different driving styles of human drivers by simply changing the weighting on tracking performance and control effort.

Simulation results show that an “aggressive” MPC driver can track the speed profile better than the “economical” MPC driver with more fuel consumption.

7.3 Future Work

This research work provides a frame work of model predictive SI engine management system. It demonstrates great pragmatic potentials of MPC to be implement with modern SI engine controls. The future expansions of this frame work are suggested as follows:

- Development of the model based engine state estimation of the proposed IMEP controller. This estimation will utilize the cycle-by-cycle engine model and their real time linearization results to converge sensor errors and estimate unmeasurable engine states. Since the proposed engine model integrates air-path dynamics, IMEP, exhaust gas enthalpy and heat transfer to coolant together, it is possible to utilize most of the sensors available on modern SI engines to estimate the engine states comprehensively.
- The model predictive engine control frame work can be expanded with other actuators, including VVT, AFR and turbo charger. The fact that the MPC is formulated in engine cycle domain means that the frame work can also be expanded to engines with advanced combustion mode like HCCI.

APPENDICES

Appendix A

F_N and G_N in equation (5.2)

$$F_N = \begin{bmatrix} C(k)A(k) \\ C(k+1)A(k+1)A(k) \\ C(k+2)A(k+2)A(k+1)A(k) \\ \vdots \\ C\left(k+N_p\right)A\left(k+N_p\right)\dots A(k) \end{bmatrix}$$

$$G_N = \begin{bmatrix} C(k+1)B(k) & 0 & \cdots & 0 \\ C(k+2)A(k+1)B(k) & C(k+2)B(k+1) & \cdots & 0 \\ C(k+3)A(k+2)A(k+1)B(k) & C(k+2)A(k+2)B(k+1) & \cdots & 0 \\ \vdots & \vdots & \vdots & \vdots \\ C(k+N_c)A(k+N_c-1)\dots A(k+1)B(k) & \cdots & \cdots & C(k+N_c)B(k+N_c-1) \\ C(k+N_c+1)A(k+N_c)\dots A(k+1)B(k) & \cdots & \cdots & C(k+N_c+1)A(k+N_c)B(k+N_c-1) \\ \vdots & \vdots & \vdots & \vdots \\ C\left(k+N_p\right)A\left(k+N_p-1\right)\dots A(k+1)B(k) & \cdots & \cdots & C\left(k+N_p\right)A\left(k+N_p-1\right)\dots A(k+N_c)B(k+N_c-1) \end{bmatrix}$$

Appendix B

Important abbreviations and variables

A	State transition matrix Area
$A, B, C\ and\ D$	State space matrices
AFR	Air-to-fuel ratio
A_{flame}	Flame front area
A_G	Knock model fitting constant
α	Forgetting factor
ANN	Artificial Neural Network
α	Forgetting factor
b	Linear interception term of QP constraints
B_G	Knock model constant for activation energy
$BSFC$	Brake specific fuel consumption
$CA10, CA50$ ...	Crank angle at 10%, 50%,… mass burnt fraction
C_D	Discharge coefficient
COV	Covariance (of IMEP)
c_V, c_P	Constant volume/pressure heat capacity
D	Diameter
δ	Variation
δ_L	Flame thickness
e	Slope terms of Willians approximation
ECL	Exhaust camshaft location
EKF	Extended Kalman Filter
η_V	Volumetric efficiency

EVC	Crank angle of exhaust valve close
F	Linear matrix of QP Force
F_N	Appendix A
γ	Heat capacity ratio
G_N	Appendix A
H	Quadratic matrix of QP
ICL	Intake camshaft location
$IMEP$	Indicated mean effective pressure
IVO	Crank angle of intake valve open
J	Objective function of optimization problems
$K_0, K_X\ and\ K_R$	Gain matrices of PWA MPC algorithm
Ka	Karlovitz number
KF	Kalman Filter
KI	L-W knock integral Knock intensity (normalized)
K_k	Estimation gain at k^{th} iteration
L	Turbulence integral length scale CA50 estimation gain Valve lift
λ	Taylor micro scale Lagrange multiplier
LHV	Lower heating value
LTI	Linear time invariant
LTV	Linear time variant

M	Linear gain of QP constraints
m	Mass
MAP	Manifold pressure
m_b	Burnt mass
m_e	Entrained mass by flame
MPC	Model predictive Control
μ	Friction coefficient
n	Knock model pressure fitting constant System order
OLC	Crank angle where intake and exhaust valves have the same lift
OLV	Overlap volume
ω_e	Engine speed in rad/s
P	Pressure CA50 estimation error covariance
P_k	Estimation error covariance at k^{th} iteration
ϕ	Sensitivity matrix of performance
Q	Heat Variance of CA50 modeling error
QP	Quadratic Programming
ρ	Density
R	Gas constant Variance of CA50 measurement noise
r	MPC weighting on tracking performance Weighting factor
R_e	Reynolds number

RGF	Residual gas faction
RGM	Residual gas mass
S	MPC weighting on control effort
s	Weighting factor
S_L	Laminar flame speed
$SPKT$	Spark timing (deg bTDC)
SQP	Sequential quadratic programming
σ_0	Stoich air-to-fuel ratio
T	Temperature Torque
θ	Coefficient vector in RLS. Throttle/EGR valve angle Crank angle
ϑ	Ratio of heat coolant transfer in terms of rejected heat
τ	Time constant
τ_G	Ignition delay
u'	Turbulence intensity
V	Volume Velocity
v	Kinematic viscosity CA50 measurement noise
W	Work
w	CA50 model error
$[x]$	Quantification of combustion reactant
x_b	Mass burnt fraction

ξ	Active constraints set index vector
ζ	Combustion phasing

REFERENCES

Abdel-Gayed, R.G., Bradley, D. and Lung, F.K.-K., "Combustion Regimes and the Straining of Turbulent Premixed Flames," *Combustion and Flame* 76: 213-218 (1989)

Abdi Aghdam, E., Burluka, A.A., Hattrell, T., Liu, K., Sheppard, C.G.W., Neumeister, J. and Crundwell, N. "Study of cyclic variation in an SI engine using quasi-dimensional combustion model", *in Proc. of 2007 SAE World Congress*, no. 2007-01-0939, April, 2007.

Abraham, J., Williams, F.A. and Bracco, F.V., "A Discussion of Turbulent Flame Structure in Premixed Charges," *SAE Technical* Paper no. 850345, 1985.

Alberer, D., Ranzmaier, M., del Re, L. and Huschenbett, M. "MIMO model predictive control for integral gas engines under switching disturbances", *in Proc. of 17th IEEE International Conference on Control Applications Part of 2008 IEEE Multi-conference on Systems and Control*, pp. 317-322, Sep., 2008, San Antonio, USA.

Aleiferis, P.G Hardalupas, Y. Taylor, A.M.K.P., Lshii, K., and Urata, Y., "Flame chemiluminescence studies of cyclic combustion variations and air-to-fuel ratio of the reacting mixture in a lean-bun stratified-charge spark-ignition engine", *Cobustion and Flame*, vol. 136, no. 1-2, pp. 72-90, Jan., 2004.

Ali, A., and Blath, P. "Application of modern techniques to SI-engine torque control", *in Proc. of 2006 IEEE International Conference on Control Applications*, pp. 2405-2410,Oct., 2006, Munich, Germany.

Arici, O., Johnson, J.H. and Kulkarni A.J., “Cooling system simulation; Part 1 – model development”, *SAE Paper*, no. 1999-01-0240, 1999.

Arsie, I., Di Leo, R., Falco, S., Pianese, C. and Cesare, M.D., “Estimation of the engine thermal state by in-cylinder pressure measurement in automotive diesel engines”, *SAE Technical Paper*, no. 2015-01-1623, 2015.

Assanis D. N., Filipi Z. S., Fiveland S. B., Syrimis M., “A predictive ignition delay correlation under steady-state and transient operation of a direct injection diesel engine.” , *Transactions of the ASME Journal of Engineering for Gas Turbines and Power*, vol.125, no. 2, pp. 450-457, 2003.

Banavar, R. N. “Extremum seeking loops with quadratic functions: Estimation and control,” Int. J. Control, vol. 76, no. 14, pp. 1475–1482, 2003.

Banks, A., Vincent J. and Anyakoha, C. “A review of particle swarm optimization. Part I. Background and development”, *Natural Computing*, vol. 6, no. 4, pp. 467-484, Dec., 2007.

Balau, A. and C. Lazar, “One step ahead MPC for an automotive control application”, *in Proc. of 2nd Eastern European Regional Conference on the Engineering of Computer Based Systems*, pp. 61-70, Sep., 2011, Bratislava.

Bartlett, R.A. and Biegler, L.T. “QPSchur: a dual, active set, Schur complement method for large-scale and structured convex quadratic programming algorithm”, *Optimization and Engineering*, vol. 7, pp. 5-32, 2006

Bemporad, A., Morari, M., Dua,V. and Pistikopoulos, E.N. “The explicit linear quadratic regulator for constrained systems”, *Automatic*, vol. 38, no. 1, pp. 3-20, Jan. 2002.

Bengtsson, J., Strandh, P., Johansson, R., Tunestál, P. and Johansson, B., “Multi-output control of a heavy duty HCCI engine using variable valve actuation and model predictive control,” *SAE Int.*, Warrendale, PA, 2006-01-0873, 2006.

Benson, D.A., Huntington, G.T., Thorvaldsen, T.P. and Rao, A.V., “Direct trajectory optimization and costate estimation via an orthogonal collocation method”, *Journal of Guidance, Control, and Dynamics*, vol. 29, no. 6, pp. 1435-1440, Nov., 2006.

Bertola, A., Dolt, R. and Höwing, J., “The use of spark plug pressure transducers for engine indication measurements – possibilities and limits”, *SAE Technical Paper*, no. 2015-26-0041, 2015.

Bertsekas, D.P., *Constrained Optimization and Lagrange Multiplier Methods*, Academic Press, London and New York, 1982.

Bezdek, J.C., Keller, J., Krisnapuram, R. and Pal, N.R. *Fuzzy Models and Algorithms for Pattern Recognition and Image Processing*, Springer US, New York, 1999.

Bicer, C., Babacan, E.K. and Ozbek, L., "Stability of the adaptive fading extended Kalman filter with the matrix forgetting factor", *Turkish Journal Electrical Engineering and Computer Sciences*, 20(5): 819-833, 2012.

Bishop, C.M. *Neural Networks for Pattern Recognition*, Clarendon Press, Oxford, 1995.

Blackman, P. F. "Extremum-seeking Regulators," *in An Exposition of Adaptive Control*, J. H. Westcott, Ed. Pergamon Press, New York, 1962, pp. 36–50.

Blizard, N. and Keck, J., "Experimental and Theoretical Investigation of Turbulent Burning Model for Internal Combustion Engines," *SAE Paper*, No. 740191, SAE Transactions 86, 1974.

Bonatesia, F., Waters, B. and Shayler, P.J., "Burn angles and form factors for Wiebe function fits to mass fraction burned curves of a spark ignition engine with variable valve timing", *International Journal of Engine Research*, vol. 11, no. 2, pp. 177-186, 2010.

Bougrine, A., Richard, S. and Veynante, D. "Modelling and simulation of the combustion of ethanol blended fuels in a si engine using a 0d coherent flame model," *SAE Technical Paper*, no. 2009-24-0016, 2009.

Boser, B.E., Guyon, I.M. and Vapnik,V.N. "A training algorithm for optimal margin classifiers", *in Proc. of the Fifth ACM Workshop on Computational Learning Theory*, pp. 144-152, 1992.

Bougrine, A., Richard, S. and Veynante, D. “Modelling and simulation of the combustion of ethanol blended fuels in a si engine using a 0d coherent flame model,” *SAE Technical Paper*, no. 2009-24-0016, 2009.

Bozza, F, De Bellis, V., and Siano, D, “A Knock Model for 1D Simulations Accounting for Cyclic Dispersion Phenomena”, *SAE Technical Paper* 2014-01-2554, 2014, doi: 10.4271/2014-01-2554.

Brehob, D.D., and Newman, C.E., "Monte Carlo Simulation of Cycle-to-Cycle Variability," *SAE Technical Paper* 922165, 1992.

Broyden, C.G., “The convergence of a class of double-rank minimization algorithms, parts I and II”, *J. Inst. Math. Applics.*, vol. 6, pp. 76-90 and 222-236, 1970.

Cairano, S. Di, Doering, J., Kolmanovsky, I.V. and Hrovat, D. “MPC-based control of engine deceleration with open torque converter”, *in Proc. of 51st IEEE Conference on Decision and Control*, pp. 3753-3758, Dec., 2012, Maui, USA.

Camacho, E.F. and Bordons, C. *Model Predictive Control*, Springer, 2nd ed., 2007, pp. 5-6

Caruntu, C.F., Onu, D. and Lazar, C. “Real-time simulation of a vehicle drivetrain controlled through CAN using a robust MPC strategy”, *in Proc. of 15th International Conference on System Theory*, Control, and Computing, pp. 1-7, Oct., 2011, Sinaia.

Caton, J.A., “Combustion phasing for maximum efficiency for conventional and high efficiency engines”, *Energy Conversion and Management*, 77: 564-576, 2014.

Cartellieri, W., Chmela, F.G., Kapus, P.E. and Tatschl,R.M., “Mechanisms leading to stable and efficient combustion in learn burn gas engines”, *Proceedings of International Symposium COMODIA, 1994*.

Caruntu, C.F., Onu, D. and Lazar, C. “Real-time simulation of a vehicle drivetrain controlled through CAN using a robust MPC strategy”, *in Proc. of 15th International Conference on System Theory, Control, and Computing*, pp. 1-7, Oct., 2011, Sinaia.

Chiang, C.J. and Stefanopoulou, A.G. “Control of thermal ignition in gasoline engines”, *in Proc. of American Control Conference*, 2005, pp. 3871-3876.

Colin, G., Chamaillard, Y., Bloch, G. and Corde, G. “Neural control of fast nonlinear systems-application to a turbocharged SI engine with VCT”, *IEEE Transactions on Neural Networks*, vol. 18, no. 4, pp. 1101-1114, Jul., 2007.

Colin, G., Chamaillard, Y., Charlet, A., Bloch, G. and Corde, G. “Linearized neural predictive control a turbocharged SI engine application”, *SAE Technical Paper*, 2005-01-0046, 2005.

Corona, D. and Schutter, B.D. “Adaptive cruise control for a SMART car: a comparison benchmark for MPC-PWA control methods”, *IEEE Transactions on Control Systems Technology*, vol. 16, no. 2, pp. 365-372, Mar., 2008.

Cortona, E., Onder, Ch.H. and Guzzella L., "Engine thermal management with components for fuel consumption reduction", *International Journal of Engine Research, IMechE*, vol. 3, no. 3, pp. 157-170, 2002.

Cristofaro, F.D., Funel, A. and Scala, S. "Development of calibration tools for model based engine control strategies", *in Proc. of IEEE Conference on Control Applications*, vol. 1, pp. 146-148, Jun., 2003.

Dai, W, Russ, S.G., Trigui, N. and Tallio, K.V., "Regimes of premixed turbulent combustion and misfire modeling in SI engines", *SAE Technical Paper*, no. 982611, 1998.

Dai W., Trigui, N. and Lu, Y., "Modeling of cyclic variations in spark-ignition engines", *SAE Technical Paper*, no. 2000-01-2036, 2000.

Dennis, J.E. and Schnabel, R.B., *Numerical Methods for Unconstrained Optimization and Nonlinear Equations*, Prentice-Hall, Inc., Englewood Cliffs, New Jersey, 1983.

Di Cairano, S., Bemporad, A. and Kolmanovsky, I.V. "Stochastic MPC with learning for driver-predictive vehicle control and its application to HEV energy management", *IEEE Transactions on Control Systems Technology*, vol. PP, no. 99, pp. 1- 14, Jul., 2013.

Di Cairano, S., Doering, J., Kolmanovsky, I.V. and Hrovat, D. "MPC-based control of engine deceleration with open torque converter", *in Proc. of 51st IEEE Conference on Decision and Control*, pp. 3753-3758, Dec., 2012, Maui, USA.

Di Cairano, S., Yanakiev, D., Bemporad, A., Kolmanovsky, I.V. and Hrovat, D. "Model predictive idle speed control: design, analysis and experimental evaluation", *IEEE Transactions on Control Systems technology*, vol. 20, no. 1, pp. 84-97, Jan., 2012.

Dorey, R. E. and Stuart, G. "Self-tuning control applied to the in-vehicle calibration of a spark ignition engine," *in Proc. IEEE Int. Conf. Control Appl*. pp. 121–126, Glasgow, U.K., 1994.

Douaud, A. and Eyzat, P., "Four-Octane-Number Method for Predicting the Anti-Knock Behavior of Fuels and Engines," *SAE Technical Paper,* No. 780080, 1978.

Draper, C.S. and Li, Y. "Principles of Optimizing Control Systems", *ASME Publications*, 1954.

Karnik, A.Y., Buckland, J.H. and Freudenberg, J.S. "Electronic throttle and wastegate control for turbocharged gasoline engines", *in Proc. of 2005 American Control Conference*, pp. 4435-4439,Jun., 2012, Portland, USA.

Ferreau, H.J., Bock, H.G. and Diehl, M. "An online active set strategy to overcome the limitations of explicit MPC", *Int. J. of Robust and Nonlinear Control*, vol. 18, no. 8, pp. 816-830, May 2008.

Ferreau, H.J., Bock, H.G. and Diehl, M. “An online active set strategy for fast parametric quadratic programming in MPC application”, *in Proc. of the IFAC Workshop on Nonlinear Model Predictive Control for Fast Systems*, Grenoble, 2006.

Ferreau, H.J., Ortner, P., Langthaler, P., del Re, L. “Predictive control of a real-world diesel engine using an extended online active set strategy”, *Annual Reviews in Control*, vol. 31, no. 2, pp. 293-307, 2007.

Feru, E., Lazar, M., Gielen, R.H., Kolmanovsky, I.V. and Di Cairano, S. “Lyapunov-based constrained engine torque control using electronic throttle and variable cam timing”, *in Proc. of 2012 American Control Conference*, pp. 2866-2871,Jun., 2012, Fairmont Queen Elizabeth, Canada.

Fiacco, A.V., *Introduction to Sensitivity and Stability Analysis in Nonlinear Programming*, Mathematics in science and engineering, vol. 165, 1983

Filipi, Z.S., Assanis, D., “The Effect of the Stroke-to-Bore Ratio on Combustion, Heat Transfer and Efficiency of a Homogenous Charge Spark Ignition Engine of Given Displacement,” *Int. Journal of Engine Research*, Vol. 1, No. 2, 191-208, 2000.

Filipi, Z.S., Fathy, H., Hagena, J., Knafl, A., Ahlawat, R., Liu, J., Jung, D., Assanis, D., Peng, H. and Stein, J. “Engine-in-the-loop testing for evaluating hybrid propulsion concepts and transient emissions –HMMWV case study’, *SAE Technical Papers*, no. 2006-01-0443, 2006.

Fletcher, R., “Methods related o Lagrangian functions”, in P.E. Gill and W. Murray, editors, *Numerical Methods for Constrained Optimization*, pp. 228-234. Academic Press, London and New York, 1974.

Fletcher, R., *Practical Methods of Optimization*, John Wiley and Sons, Chichester and New York, Brisbane, Toronto and Singapore, second edition, 1987.

Fox, J., Cheng, W. and Heywood, J., “A model for predicting residual gas fraction in spark-ignition engines”, *SAE Technical paper*, no. 931025, 1993.

Gaetner, L. and Ebenhoch, M. “The ZF automatic transmission 9HP48 transmission system, design and mechanical parts”, *SAE Technical Paper*, no. 2013-01-1276, April, 2013.

Galloni E., “Analyses about parameters that affect cyclic variation in a spark ignition engine”, *Applied Thermal Engineering*, vol. 29, pp. 1131-1137, 2009

Garcia, C., Prett, D., and Morari, M. “Model predictive control: theory and practice – a survey”, *Automatica (Oxford)*, vol. 25, no. 3, pp. 335-348, 1989.

Ghazimirsaied, A., Shahbakhti, M. and Koch, C.R., “Nonlinear dynamics in cyclic variations of combustion phasing in an HCCI engine”, *in Proc. of the ASME Internal Combustion Engine Division 2009 Spring Conference*, Milwaukee, Wisconsin, USA, May, 2009.

Ghojel, J.I. “Review of the development and applications of the Wiebe function: a tribute to the contribution of ivan wiebe to engine research”, *Int. J. Engine Res.*, vol. 11, no. 4, pp. 297-312, August, 2010.

Gill, P.E., Gould, N.IM., Murray, W., Saunders, M.A. and Wright, M.H. “A weighted Gram-Schmidt method for convex quadratic programming”, *Mathematical Programming*, vol. 30, pp. 176-195, 1984.

Gill, P.E., Murray, W., Saunders, M.A. and Wright, M.H. “Procedures for optimization problems with a mixture of bounds and general linear constraints”, *ACM Transactions on Mathematical Software*, vol. 10, no. 3, pp. 282-298, 1984.

Giorgetti, N., Ripaccioli, G., Bemporad, A., Kolmensovsky, I.V. and Hrovat, D. “Hybrid model predictive control of direct injection stratified charge engines”, *IEEE/ASME Transactions on Mechatronics*, vol. 11, no. 5, Oct., 2006.

Glassman, I., “Combustion”, *Academic Press*, 1977.

Goldfarb, D. and Idnani, A. “A numerically stable method for solving strictly convex quadratic programs”, *Mathematical Programming*, vol. 27, pp. 1-33, 1983.

Goldsmith, M.J., *Sequential Quadratic Programming Methods Based on Indefinite Hessian Approximations*, PhD dissertation, Stanford University, 1999.

Goncalves, A.S. “A primal-dual method for quadratic programming with bounded variables”, *Numerical Methods for Nonlinear Optimization*, Academic Press, London, 1972, pp. 255-263.

Gómez, J. and Camacho, E.F., “Neural network MBPC for mobile robots path tracking”, *Robotics and Computer Integrated Manufacturing Journal*, vol. 11, no. 4, pp. 271-278, Dec., 1994.

Goodman, J., “Newton’s method for constrained optimization”, *Math. Prog.*, vol.33, pp. 162-171, 1985.

Greene, A.B. and Lucas, G.G., *The Testing of Internal Combustion Engines*, English University Press Ltd, 1969.

Griewank, A. and Walther, A., *Evaluating Derivatives*, in SIAM, 2008.

Grünbacher, E., Kefer, P. and del Re, L. “Estimation of the mean value engine torque using an extended Kalman filter”, *SAE Technical Paper*, no. 2005-01-0063, Apr., 2005.

Guzzella, L. and Onder, C.H., *Introduction to modeling and control of internal combustion engine systems*, 2nd ed., Springer, 2009.

Hall, C.M., Shaver, G.M., Chauvin, J. and Petit, N., “Combustion phasing model for control of a gasoline-ethanol fueled SI engine with variable valve timing”, *in Proc. of 2012 American Control Conference*, pp. 1271-1277, Montreal, QC, June, 2012.

Hall, C.M., Shaver, G.M., Chauvin J. and Petit, N "Control-oriented modelling of combustion phasing for a fuel-flexible spark-ignited engine with variable valve timing", *International Journal of Engine Research*, vol. 13, no. 5, pp. 488-463, Oct., 2012.

Haskara, I., Zhu, G.G. and Winkelman, J. "Multivariable EGR/Spark Timing Control for IC Engines via Extremum Seeking", *in Proc. of the 2006 American Control Conference*, Minneapolis, USA, Jun., 2006.

Hellström, E., Lee, D., Jiang, L., Stefanopoulou, A.G. and Yilmaz, H. "On-Board Calibration of Spark Timing by Extremum Seeking for Flex-Fuel Engines", *IEEE Transactions on Control Systems Technology*, vol. 21, no. 6, pp. 2273-2279, 2013

Herceg, M., Raff, T., Findeisen, R. and Allgöwer, F. "Nonlinear model predictive control of a turbo-charged diesel engine", *in Proc. of IEEE International Conference on Control Applications*, pp. 2766-2771, Oct., 2006, Munich, Germany.

Heywood, J.B. *Internal Combustion Engine Fundamentals*, 1st ed., McGraw-Hill, 1988.

Hill, P.G., "Cyclic variation and turbulence structure in spark-ignition engines", *ombustion and Flame*, vol. 72, no. 1, pp. 73-89, Apr., 1988.

Hooke, R. and Jeeves, T.A. "'Direct search' solutions of numerical and statistical problems", *Journal of the Association for Computing Machinery (ACM)*, vol. 8, no. 2, pp. 212-229, 1961.

Hrovat, D. “MPC-based idle speed control for IC engine”, *in Proc. of FISITA conference*, 1996, Prague, Czech Rep.

Hrovat, D., Di Cairano, S., Tseng, H.E. and Kolmanovsky, I.V. “The development of model predictive control in automotive industry: a survey”, *in Proc. of 2012 IEEE International Conference on Control Applications (CCA)*, pp. 295-302, Oct. 2012.

Hrovat, D. and Sun, J. “Models and control methodologies for IC engine idle speed control design”, *Control Engineering Practice*, vol. 5, no. 8, pp. 1093-1100, 1997.

Huang, M., Nakada, H., Polavarapu, S., Choroszucha, R., Butts, K. and Kolmanovsky, I.V. “Towards combining nonlinear and predictive control of diesel engines”, *in Proc. of 2013 American Control Conference*, pp.2846-2853 , Jun., 2013, Washington DC, USA.

International Energy Agency, “Global EV Outlook-Understanding the Electric Vehicle Landscape to 2020”, [http://www.iea.org/ topics /transport/ electricvehiclesinitiative/ publications/], *accessed in Feb. 26, 2014.*

Kalman, R.E., “A New Approach to Linear Filtering and Prediction Problems”, *Journal of Basic Engineering*, 82D: 35-45, 1960.

Kasseris, E., “Knock Limits in Spark Ignited Direct Injected Engines Using Gasoline/Ethanol Blends”, PhD dissertation, Massachusetts Institute of Technology, 2011.

Kee, R. J.; Rupley, F. M.; Miller, J. A. "CHEMKIN-II: A Fortran Chemical Kinetics Package for the Analysis of Gas Phase Chemical Kinetics" *Sandia Report no. SAND 89-8009B*; Sandia National Laboratories, 1989.

Kim, B.A., Lee, S. H., Lee, Y.O., and Chung, C.C. "Comparative study of approximate, proximate, and fast model predictive control with applications to autonomous vehicles", *in Proc. of Control, Automation and Systems*, pp.479-484, 2012.

Krsti ć, M. and Wang, H. "Stability of extremum seeking feedback for general nonlinear dynamic systems," *Automatica*, vol. 36, no. 4, pp. 595–601, 2000.

Lacour, C. and Pera, C., "An experimental database dedicated to the study and modelling of cyclic variability in spark-ignition engines with LES", *SAE Technical Paper*, no. 2011-01-1282, 2011.

Lafossas, F., Colin, O., Berr, F. L. and Menegassi, P. "Application of a new 1d combustion model to gasoline transient engine operation," *SAE 2005-01-2107*, 2005.

Langthaler, P. and del Re, L. "Fast predictive oxygen charge control of a diesel engine", *in Proc. of 2007 American Control Conference*, pp.4388-4393 , Jul., 2007, New York, USA.

Larsson, S. and Andersson, I. "Self-optimising control of an Si-engine using a torque sensor," Control Eng. Pract., vol. 16, no. 5, pp. 505–514, 2008.

Le Berr, F., Miche, M., Solliec, G. L., Lafossas, F.-A., and Colin, G. "Modelling of a turbocharged SI engine with variable camshaft timing for engine control purposes," *SAE 2006-01-3264*, 2006.

Le Coz, J.F. "Cycle-to-cycle correlations between flow field and combustion initiation in an SI. Engine", *SAE Paper* no. 920517, 1992.

Lee, K.H. and Kim. K., "Influence of initial combustion in SI engine on following combustion stage and cycle-by-cycle variations in combustion process", *International Journal of Automotive Technology*, 2(1): 25-31, 2001.

Lee,T.K., and Filipi, Z.S. "Nonlinear model predictive control of a dual-independent variable valve timing engine with electronic throttle control", *in Proc. of the Institution of Mechanical Engineers, Part D: Journal of Automobile Engineering*, vol. 225, no. 9, pp.1221-1234, Sep., 2011.

Lee,T.K., Kramer, D. and Filipi, Z.S., "High-degree-of-freedom engine modelling for control design using a crank-angle-resolved flame propagation simulation and artificial neural network surrogate models," *Journal of Systems and Control Engineering*, vol. 224, no. 16, pp. 747-761, 2010.

Lee, T.K., Prucka, R.G. and Filipi, Z.S., "Real-time estimation of combustion variability for model-based control and optimal calibration of spark ignition engines", *in Proc. of the*

Institution of Mechanical Engineers, Part D (Journal of Automobile Engineering), vol. 223, no. D11, pp. 1361-1372, Nov., 2009.

Li, J. and Rhinehart, R.R. "Heuristic random optimization", *Computers & Chemical Engineering*, vol. 22, no. 3, pp. 427-444, 1995.

Li, P., Shen, T. and Liu, D. "Unknown offset free MPC for air-fuel ratio balancing control in multi-cylinder SI engines", *in Proc. of 2010 8th IEEE International Conference on Control and Automation*, pp.1385-1390 , Jun., 2010, Xiamen, China.

Livengood, J.C. and Wu, P.C. "Correlation of auto-ignition phenomena in internal combustion engines and rapid compression machines", *Symposium (International) on Combustion*, vol. 5, no. 1, pp. 347-355, 1955.

Livshiz, M., Kao, M. and Will, A. "Validation and calibration process of powertrain model for engine torque control development", *SAE Technical Paper*, 2004-01-0902, 2004.

Ljung, L. *System Identification: Theory for the User*, Second Edition, Prentice-Hall, 1999, pp. 363-368.

Long, E.J., Rimmer, J.E.T., Justham, T., Garner,C.P., Hargrave, G.K., Richardson, D. and Wallace, S. "The influence of in-cylinder turbulence upon engine performance within a direct injection IC engine", *in Proc. of the 7th International Conference on Modeling and Diagnostics for Advanced Engine Systems*, pp.213-220, 2008.

Luenberger, D.G. *Optimization by Vector Space Methods*, John Wiley and Sons, New York, 1969.

Mantel, T., "Three dimensional sudy of flame kernel formation around a spark plug", *SAE Technical Paper*, no. 920587, 1992.

Maruyama, T., Ejiri, A., Ikai,Y. and Shimotani, K. "Model predictive control considering disturbances in diesel engine air intake systems", *in Proc. of 2012 IEEE International Conference on Control Applications Part of 2012 IEEE Multi-Conference on Systems and Control*, pp. 401-408, Oct., 2012, Dubrovnik, Croatia.

Matthews, R.D., Sarwar, M.G., Hall, M.J., etc., "Predictions of Cyclic Variability in an SI Engine and Comparisons with Experimental Data," *in Proc. of SAE International Fuels and Lubricants Conference*, Toronto, Canada, 1991

Meyer, R. and Thring, R.H., "Mixture preparation measurements", *SAE Technical Paper* 950069, 1995. Doi: 10.4271/950069

Murayama, A. and Yamakita, M. "Speed control of vehicles with variable valve lift engine by nonlinear MPC", *in Proc. of ICROS-SICE International Joint Conference 2009*, pp. 4128-4133, Aug., 2009, Nagoya, Japan.

Nabi, S., Balike, M., Allen, J. and Rzemien, K. "An overview of hardware-in-the-loop testing systems at Visteon", *SAE Technical Papers*, no. 2004-01-1240, 2004.

Nakajima, S., Saiki, R. and Goryozono, Y. “Development of an engine for flexible fuel vehicles (FFV)”, *SAE Technical Paper*, 2007-01-3616, 2007.

Nocedal, J. and Wright, S., *Numerical Optimization*, Springer-Verlag, 2000.

Ortner, P., Langthaler, P., Vicente, J., Ortiz, G. and del Re, L. “MPC for a diesel engine air path using an explicit approach for constraint systems”, *in Proc. of 2006 IEEE International Conference on Control Applications*, pp. 2760-2765, Oct., 2006, Munich, Germany.

Ozdor, N., Dulger, M., and Sher, E., “Cyclic Variability in Spark Ignition Engines A Literature Survey,” *SAE Technical Paper 940987*, 1994.

Pistikopoulos, E.N., Georgiadis, M.C. and Dua, V., *Multi-Parametric Programming Volume 1*, WILEY-VCH Verlag GmbH & Co. KGaA, Weinheim, 2007

Popovic, D., Jankovic, M., Magner, S. and Teel, A. R. “Extremum seeking methods for optimization of variable cam timing engine operation,” *IEEE Trans. Control Syst. Technol.*, vol. 14, no. 3, pp. 398–407, May 2006.

Quirynen, R., Houska, B., Vallerio, M., Telen, D. and et al., “Symmetric algorithmic differentiation based exact Hessian SQP method and software for Economic MPC”, *in Proc. of 2014 Annual Conference on Decision and Control*, Los Angeles, CA, Dec., 2014.

Patterson, G. and Davis, R., “Geometric and Topological Considerations to Maximize Remotely Mounted Cylinder Pressure Transducer Data Quality”, *SAE Technical Paper* No. 2009-01-0644, 2009.

Peters, N., "Laminar Flamelet Concepts in Turbulent Combustion,", 21st Symposium (International) on Combustion, The Combustion Institute, pp 1231-1250, 1986.

Pfeifer, A., Krueger, M., Gruetering, U. and Tomazic, D. “U.S. 2007 – Which way to go? Possible technical solutions”, *SAE Technical Paper*, 2003-01-0770, 2003.

Piche, S., Sayyarr-Rodsari, B. Johnson, D. and Gerules, M. “Nonlinear model predictive control using neural networks”, *IEEE Control Systems Magazine*, vol. 20, no. 3, pp. 53-62, 2000.

Pischinger, S. and Heywood, J.B. “How heat losses to the spark plug affect flame kernel development in an SI engine”, *SAE Paper* no. 900021, 1990.

Raffo, G.V., Gomes, G.K., Normey-Rico, J.E., Kelber, C.R. and Becker, L.B. “A predictive controller for autonomous vehicle path tracking”, *IEEE Transaction on Intelligent Transportation System*, vol. 10, no. 1, pp. 92–102, Mar. 2009.

Rao, S.S., *Engineering Optimization*, John Wiley Sons, Inc., 1996.

Rassweiler, G.M. and Withrow, L., “Motion pictures of engine flames correlated with pressure cards”, *SAE Trans.*, 42(5):185-204, 1938.

Ravi, N., Roelle, M.J. and Gerdes, J. C. “Controller-observer implementation for cycle-by-cycle control of an HCCI engine”, *in Proc. of 2007 ASME International Mechanical Engineering Congress and Exposition*, Seattle, Washington, USA, Nov., 2007.

Ravi, N., Roelle, M.J., Jungkunz, A.F. and Gerdes, J.C., “A physically based two state model for controlling exhaust recompression HCCI in gasoline engines”, *in Proc. of the 2006 ASME International Mechanical Engineering Congress and Exposition*, Chicago, Illinois, USA, Nov., 2006.

Rhinehart, R.R., Su, M. and Manimegalai-Sridhar, U. “Leapfrogging and synoptic Leapfrogging: a new optimization approach”, *Computer & Chemical Engineering*, vol. 40, pp. 67-81, May, 2012.

Richalet, J., Rault, A., Testud, J.L. and Papon, J. “Algorithmic control of industrial process”, *in Proc. of 4th IFAC Symposium on Identification and System Parameter Estimation*, Tbilisi, USSR, 1976.

Richalet, J., Rault, A., Testud, J.L. and Papon, J. “Model predictive heuristic control: application to industrial process”, *Automatica*, vol. 14, no. 2, pp. 413-428, 1978.

Richard, S., Bougrine, S., Font, Lafossas, G. F. and Berr, F. L., “On the reduction of a 3d cfd combustion model to build a physical 0d model for simulating heat release, knock and pollutants in SI engines,” *Oil Gas Science Technology - Rev. IFP*, 64(3): 223–242, 2009.

Russ, S.G., Lavoie, G. and Dai, W., "SI engine operation with retarded ignition: Part 1 – cyclic variations", *SAE Technical Paper*, no. 1999-01-3506, 1999.

Santillo, M. and Karnik, A. "Model predictive controller design for throttle and wastegate control of a turbocharged engine", *in Proc. of 2013 American Control Conference, pp. 2183-2188*, Jun. 2013, Washington DC, USA.

Sardarmehni, T., Menhaj, M.B., Safarizade, N. and Rahmani, H. "Robust neural predictive control of normalized air-to-fuel ratio in internal combustion engines", *in Proc. of 13th Iranian Conference on Fuzzy Systems*, pp. 1-4, 2013.

Schmid, C. and Biegler, L.T. "Quadratic programming methods for reduced hessian SQP", *Computers & Chemical Engineering*, vol. 18, no. 9, pp. 817-832, 1994

Schten, K., Ripley, G., Punater, A. and Erickson, C., "Design of an automotive grade controller for in-cylinder pressure based engine control development", *SAE Technical Paper*, No. 2007-01-0774, 2007.

Scotson, P.G. and Wellstead, P. E. "Self-tuning optimization of spark ignition automotive engines," *IEEE Control Syst. Mag.*, vol. 3, no. 10, pp. 94–101, Apr. 1990.

Shakouri, P. and Ordys, A. "Application of the state-dependent nonlinear model predictive control in adaptive cruise control system", *in Proc. of 14th International IEEE*

Conference on Intelligent Transportation Systems, pp. 686-691, Oct., 2011, Washington DC, USA.

Sharma, R., Nešic, D. and Manzie, C. "Idle speed control using linear time varying model predictive control and discrete time approximations", *in Proc. of 210 IEEE International Conference on Control Applications*, pp. 1140-1145, Yokohama, Japan, Sep., 2010.

Shaver, G., Roelle, M. and Gerdes, J. "Decoupled control of combustion timing and work output in residual-affected HCCI engines," *in Proc. Amer. Control Conf.*, 2005, pp. 3871–3876.

Shibata, Y., Shimonosono, H. and Yamai, Y., "New design of cooling system with computer simulation and engine compartment simulator", *SAE Paper*, no. 931075, 1993.

Shidore, N. and Pasquier, M. "Interdependence of system control and component sizing for a Hydrogen-fueled hybrid vehicle", *SAE Technical Papers*, no. 2005-01-3457, 2005.

Shrestha, S. B. and Karim, G. A., "A predictive model for gas fueled spark ignition engine applications," *SAE 1999-01-3482*, 1999.

Sjeric, M., Kozarac, D. and Taritas, I., "Experimentally supported modeling of cycle-to-cycle variations of SI engine using cycle-simulation model", *SAE Technical Paper*, no 2014-01-1069, 2014, doi: 10.4371/2014-01-1069.

Song, J. and Sunwoo, M., "Flame kernel formation and propagation modelling in spark ignition engines," *Proceedings of the Institution of Mechanical Engineers,* Part D: Journal of Automobile Engineering, 2001.

Stanglmaier, R.H. and Roberts, C.E. "Homogeneous Charge Compression Ignition (HCCI): benefits, compromises, and future engine applications", *SAE Technical Paper,* 1999-01-3682, 1999.

Stefanopoulou, A.G., Cook, J.A., Grizzle, J.W. and Freudenberg, J.S. "Control-oriented model of a dual equal variable cam timing spark ignition engine", *Transactions of the ASME. Journal of Dynamic Systems, Measurement and Control*, vol. 120, no. 2, pp. 257-266, Jun., 1998.

Tabaczynski, R., Ferguson, C., Radhakrishnan, K., "A Turbulent Entrainment Model for Spark-Ignition Engine Combustion," *SAE Paper,* No. 770647, 1977

Tabaczynski, R., Trinker, F., Shannon, B., "Further Refinement and Validation of a Turbulent Flame Propagation Model for Spark Ignition Engines," *Combustion and Flame*, vol. 39, pp. 111-121, 1980.

Teel, A. R. and Popovic, D. "Solving smooth and nonsmooth multivariable extremum seeking problems by the methods of nonlinear programming," *in Proc. Amer. Control Conf.*, pp. 2394–2399, 2001.

Thang Truong, D.V., Meywerk, M. and Tomaske, W. “Torque vectoring for rear axle using adaptive sliding mode control”, *in Proc. of 2013 International Conference on Control, Automation and Information Science*, pp. 328-333, Nov., 2013, Nha, Trang.

The Analytic Sciences Corporation, Gelb, A. *Applied Optimal Estimation*, the M.I.T. Press, Cambridge, Massachusetts and London, 1974.

Vermillion, C., Butts, K. and Reidy, K. “Model predictive engine torque control with real-time driver-in-the-loop simulation results”, *in Proc. of 2010 American Control Conference*, pp.1459-1464, Baltimore, USA, Jun. 2010.

Viljoen, C., Yates, A., Swarts, A., Balfour, G. et al., “An Investigation of the Ignition Delay Character of Different Fuel Components and an Assessment of Various Auto-ignition Modelling Approaches,” *SAE Technical Paper*, No. 2005-01-2084, 2005.

Wahlström, J. and Eriksson, L. “Output selection and its implications for MPC of EGR and VGT in disel engines”, *IEEE Transactions on Control Systems Technology*, vol. 21, no. 3, pp. 932-940, May., 2013.

Wang, L. *Model Predictive Control System Design and Implementation Using MATLAB*, Springer, London, 2009, pp. 63-68.

Wang, S., Prucka, R., Prucka, M. and Dourra, H., “Control-oriented residual gas mass prediction for spark ignition engines”, *International J. of Engine Research*, doi: 10.1177/1468087414555732

Wellstead, P. E. and Scotson, P. G. “Self-tuning extremum control,” *IEEE Control Theory Appl.*, D, vol. 137, no. 3, pp. 165–175, 1990.

Wilson, R.B., *A Simplicial Method for Convex Programming*, PhD dissertation, Harvard University, 1963.

Westbrook, C.K., Warnatz, J., and Pitz, W.J., “A detailed chemical kinetic reaction mechanism for the oxidation of iso-octane and nheptane over an extended temperature range and its application to analysis of engine knock”, *Twenty-second Symposium (Int.) on Combustion, The Combustion Institute,* p.893-901, 1988.

Widd, A., Ekholm, K., Tunestål, P. and Johansson, R. “Physics-based model predictive control of HCCI combustion phasing using fast thermal management and VVA”, *IEEE Transactions on Control Systems Technology*, vol. 20, no. 3, pp. 688-699, May, 2013.

Wismer D.A. and Chattergy, R. *Introduction to Nonlinear Optimization, a Problem solving Approach,* North-Holland, New York, 1978, pp. 254-258.

Wo, S. K., “The Effects of Pressure, Temperature and Concentration on the Reactivity of Alkanes: Experiments and Modeling in a Rapid Compression Machine” *27th International Symposium on Combustion,* University of Colorado at Boulder, September 2-7,1998

Wright, S.J. *Primal-dual Interior-point Methods*, SIAM: Philadelphia, PA, 1997.

Xiao, B., Wang, S. and Prucka, R. “Virtual combustion phasing target correction in the knock region for model-based control of multi-fuel SI engines”, *SAE Int. J. Engines*, vol. 6, no. 1, 2013.

Yan, F., Wang, J. and Huang, K. “Hybrid electric vehicle model predictive control torque-split strategy incorporating engine transient characteristics”, *IEEE Transactions on Vehicular Technology*, vol. 61, no. 6, pp.2458-2467, 2012.

Yi, J., Wooldridge, S., Coulson, G., Hilditch, J. and et al., "Development and optimization of the Ford 3.5L V6 EcoBoost combustion system," *SAE Int. J. Engines*, vol. 2, no. 1:1388-1407, 2009.

Young, M., “Cyclic Dispersion - Some Quantitative Cause-and-Effect Relationships,” *SAE Technical Paper 800459*, 1980.

Zhai, Y.J., Yu, D.L., Tafreshi, R. and Al-Hamidi, Y. “Fast predictive control for air-fuel ratio of SI engines using a nonlinear internal model”, *International Journal of Engineering, Science and Technology*, vol. 3, no. 6, pp. 1-17, 2011.

Zhou, J.S., Liu, Z.Y. and Pei, R. “A new nonlinear model predictive control scheme for discrete-time system based on sliding mode control”, *in Proc. of American Control Conference*, pp. 3079-3084, Jun., 2001, Arlington, USA.

Zhu, G.G., Daniels, C.F. and Winkelman, J., “MBT timing detection and its closed-loop control using in-cylinder pressure signal”, *SAE Technical Paper*, 2003-01-3266.

Zhu, Q. and Ayalew, B. “Predictive roll, handling and ride control of vehicles with solid axles via active suspensions”, *in Proc of 2014 American Control Conference*, pp. 2102-2107, Jue. 2014.

Zhu, Q., Onori, S., and Prucka, R., “Pattern recognition technique based active set QP strategy applied to MPC for a driving cycle test”, *in Proc. of 2015 ACC*, Chicago, IL, Jul., 2015.

Zhu, Q., Wang, S., Prucka, R., Prucka, M. and Dourra, H., “Model-based control-oriented combustion phasing feedback for fast CA50 estimation”, *SAE Technical Paper*, no. 2015-01-0868, 2015.

Zhu, Y. “Efficient recursive state estimator for dynamic systems without knowledge of noise covariances”, *IEEE Transactions on Aerospace and Electronic Systems*, 35(1): 102-114, 1999.